Summer 7-2018

Compartmentalization of DNA-Based Molecular Computing Elements Using Lipid Bilayers

Aurora Fabry-Wood
University of New Mexico

Aurora Fabry-Wood

Candidate

Biomedical Engineering

Department

This dissertation is approved, and it is acceptable in quality and form for publication:

Approved by the Dissertation Committee:

Steven W. Graves, PhD, Chairperson

Darko Stefanovic, PhD

Matthew R. Lakin, PhD

Nick J. Carroll, PhD

Menake Piyasena, PhD

Compartmentalization of DNA-Based Molecular Computing Elements Using Lipid Bilayers

By
Aurora Fabry-Wood

BS, Biology, University of Arizona, 2004
MS, Biomedical Engineering, University of New Mexico, 2015

DISSERTATION

Submitted in Partial Fulfillment of the
Requirements for the Degree of

Doctor of Philosophy
Engineering

The University of New Mexico
Albuquerque, New Mexico
July 2018

ACKNOWLEDGEMENTS

I would first like to thank my committee for their support and the knowledge they shared along the way. Professor Steven W. Graves, who served as chairman of the committee, was always there to remind me of my ultimate goal. He managed me like a champion and I will forever appreciate that. My co-advisor Professor Darko Stefanovic continuously expected excellence, which drove me to succeed. His requests for big picture objectives helped me to keep a broader audience in mind. Professor Matthew R. Lakin working with you has improved my technical writing skills, by orders of magnitude. “The United States and Great Britain are two countries separated by a common language,” said George Bernard Shaw. Thank you, Matt, for imparting some of your British eloquence on this American chick. Professor Nick J. Carroll I greatly appreciate your presence in the lab, I hope you never forget the value of that. Also, you always recognize my various skills in the lab – thank you so much for that. Finally, thank you Professor Menake Piyasena, of New Mexico Tech, for your valuable research. Silica microspheres would not have been a part of my dissertation without your publications on the topic. I consider myself very lucky to have had such an exceptional group of mentors.

Professor Milan Stojanovic, Dr. Stevan Pecic and Dr. Kyung-Ae (Kasi) Yang at Columbia University also contributed significantly to this work. Prof. Stojanovic provided continuous advice and was always a pleasure to work. Dr. Pecic synthesized the OPV compound described in Chapter 6 and provided very useful feedback regarding the click chemistry. Dr. Yang advised on the aptamers presented in Chapter 7.

Additionally, there were a number of professors that did not serve on my committee, but whose support deserves acknowledgement. Professor Andrew P. Shreve whose dedication as an instructor and overall knowledge base is very inspiring. Professor Eva Chi for being such an intelligent and composed mentor. Professor David G. Whitten for his wealth of experience and publishing expertise.

I had the privilege of working with a number of exceptional undergraduates and I would like to take a moment to appreciate their dedication and hard work. Nick A. Baker, who worked with our group for 2 years, you made my first couple of years as a undergrad mentor super fun. Madalyn E. Fetrow, who has been with the lab for the last 3 years, we are lucky to have you. Ayomide Oloyede, who has been with the group for the last year, you are a joy to work with.

I would also like to acknowledge the amazing group of graduate students who were with me along the way. Thank you, Katie Schroeder (not technically a grad student but with us along the way), Heather Mendez, Jennifer Fetzer and Dr. Nadiezda Fernandez-Oropeza for being such amazing ladies and for all the kindness you brought to our group. Thank you, Frank Fencl for being my graduate school twin and for all the laughter you bring. Thank you, Adan Myers y Gutierrez for countless discussions and being such a great travel buddy. Thanks also to Dr. Albert Perry III, Dr. Harry Pappas, Dr. Loreen Stromberg, Dr. Kent Coombs, Dr. Matthew Rush, Adeline Fanni, and Kiersten Lenz for general awesomeness.

DEDICATION

This body of work is dedicated to my parents Larry Wood, Elizabeth Fabry and my Official Step-Pop James Mahoney. My mother whose support and love is unparalleled. My father who diligently taught me the physics of this planet and solar system. And Jim for his endless commitment to his family and to this planet we all call home. To all three of them for brining me up in the Grand Canyon, on the Mogollon Rim, and in the midst of the loving, intelligent and adventurous Homeward Bound community. A community which to this day inspires me and keeps me honest.

I would also like to dedicate this to my sisters, brothers and many friends. Sagi your compassion deserves a Nobel Prize and I absolutely respect you. Dawn you are an amazing sister and a better mother, love you big sis'. Kyra I am so lucky to have your enduring friendship. Tevis your curiosity is inspiring. Donovan you have the biggest heart, and sweetest family. Finally, I dedicate this work to the many amazing people who have graced my life.

Compartmentalization of DNA-Based Molecular Computing Elements Using Lipid Bilayers

By Aurora Fabry-Wood

BS, Biology, University of Arizona, 2004
MS, Biomedical Engineering, University of New Mexico, 2015
PhD, Biomedical Engineering, University of New Mexico, 2018

ABSTRACT

This dissertation will present a progression from the detection of double-stranded DNA using a combination of toehold-mediated strand displacement and DNAzyme reactions in dilute saline solutions, to the generation of separate compartments to allow standardization of DNA computing elements, by protecting from complementary strands. In well-mixed solutions complementary regions

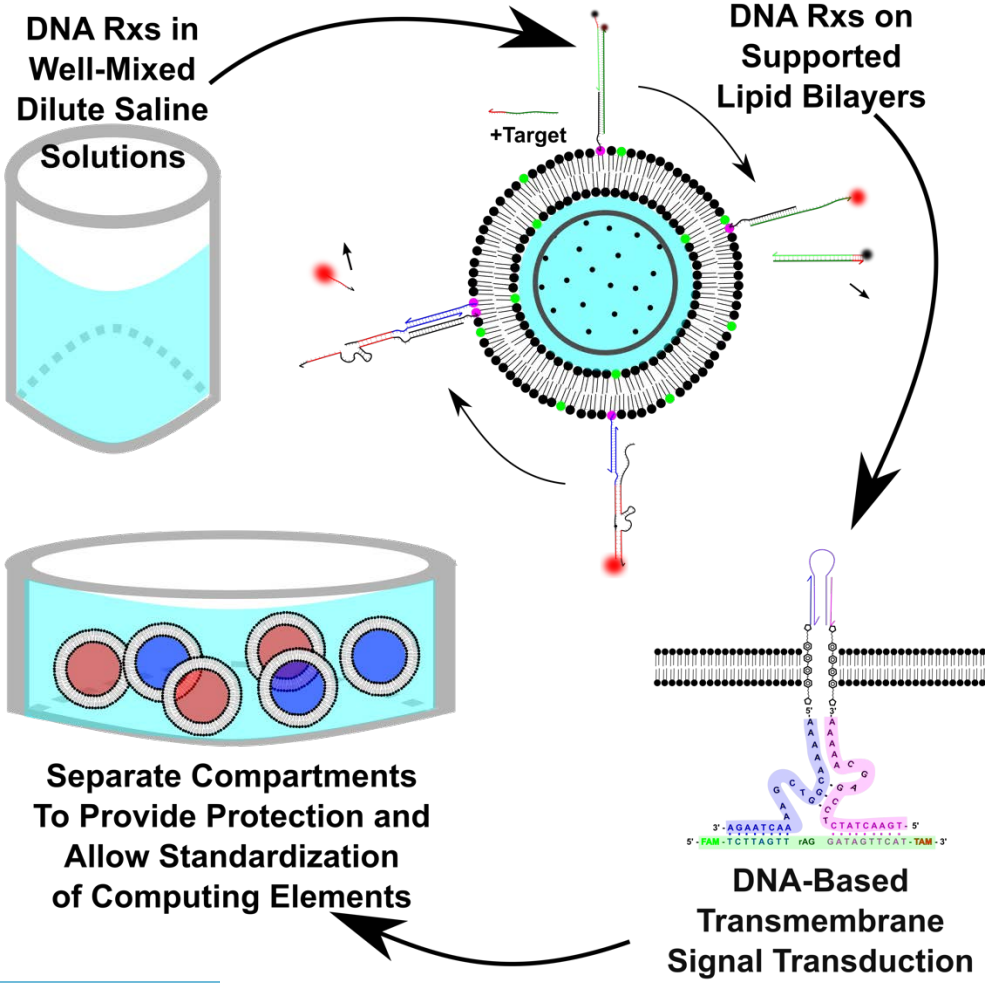

cause spurious interactions. Importantly, these compartments also provide protection from nucleases. Along the way we will also explore the use of silica microsphere supported lipid bilayers to run compartmentalized DNA reactions on a fluid surface and the design of a molecule capable of DNA-based transmembrane signal transduction.

Table of Contents

TABLE OF FIGURES

TABLE OF FIGURES (cont.)

TABLE OF TABLES

CHAPTER 1 - INTRODUCTION

1.1 A Need for Improved Arbovirus Diagnostics

We live in a rapidly changing world, full of impressive technological advances. From airplanes and diesel-powered freighters, which move people and cargo across the globe at astounding rates, to computers, which control our medical devices, automobiles and satellites, the world of today is vastly different than the world of 1918. The advances made over the last 100 years have greatly enriched the standard of living for citizens of the developed world, and to some extent for all of humanity. However, this enrichment is balanced by considerable threats to life, as we know it. With globalization, increased trade and travel, comes the spread of disease. In addition, human activities over the last century have significantly increased greenhouse gases, while simultaneously depleting oxygen-producing vegetation. According to the Intergovernmental Panel on Climate Change, corroborated by scientific communities across the globe and zealously denied by a select minority, the global average temperature is predicted to increase steadily over the next century.[1,2]

Consequently, infectious tropical diseases, such as the arbovirus Dengue virus (DENV), are an emerging threat to developed nations found in temperate zones. The number of DENV cases has increased by 30-fold over the last 50 years,[3] and as of 2013 there were an estimated 390 million DENV infections annually;[4] endangering 40% of the world's population according to the World Health Organization and making DENV the most frequent arboviral infection. DENV has two mosquito vectors, *Aedes aegypti* and *Ae. albopictus*, which in the

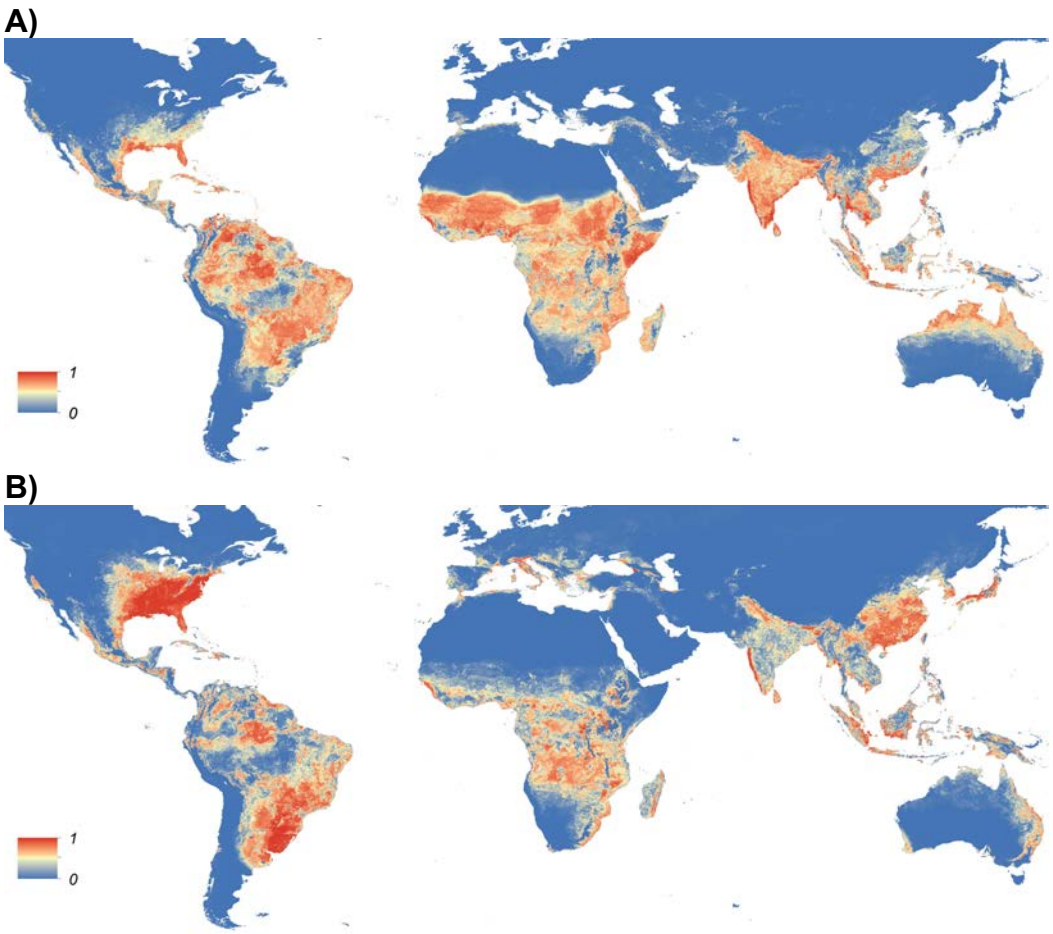

Figure 1.1 - Predicted Range of *Ae. Aegypti* and *Ae. Albopictus*. Global map of the predicted distribution of *Ae. aegypti* **A**) and *Ae. albopictus* **B**). The map depicts the probability of occurrence (from 0 blue to 1 red) at a spatial resolution of 5 km x 5 km. *Reprinted as public domain.*[5]

past were endemic to warm and moist tropical and subtropical regions. However, increased temperatures, coupled with changing weather patterns, have expanded, and are projected to continue expanding, the range of these vectors.[5,6] The predicted range of *Ae. aegypti* and *Ae. albopictus* was recently determined using a probabilistic species distribution model, which incorporated both climatic and anthropogenic factors (**Figure 1.1**). To mitigate this threat detection platforms are needed. Rapid, accurate and low-cost diagnostics are required for effective treatment and to decrease the spread of DENV and similar arboviruses.

Accurately diagnosing and serotyping DENV infections is critical because a patient infected by multiple serotypes is at elevated risk for dengue hemorrhagic fever and dengue shock syndrome, which increases the risk of fatality.[7] However, there are four DENV serotypes (DENV-1, DENV-2, DENV-3 and DENV-4), which are genetically and for the most part antigenically distinct.[8] There are also different genotypes within each serotype and DENV has a high mutation rate; due to large populations, achieved through rapid reproduction, that is often accompanied by inaccurate genome replication.[8] This makes DENV, and pathogens with similar genetic make-ups, difficult to diagnose and serotype.

Currently, antigenic methods do not precisely distinguish between serotypes, which determine disease progression, response to vaccines, the size of the epidemic and continued viral evolution.[9] Also, as the DENV genome evolves diagnostic methods must be updated. A solution to this problem is to design modularized bioassay platforms that target nucleic acid signatures and are capable of rapid modification.[10,11] The current gold standard for the detection of nucleic acid signatures is polymerase chain reaction (PCR), which amplifies specific nucleic acid signatures well above background levels and as a result can detect pathogens that are present at concentrations as low as 100 copies/mL.[12]. In biosensing applications[13,14] it is often necessary to detect pathogens at this concentration. However, PCR requires thermal cycling, proteins and highly trained technicians, as such new isothermal biosensing technologies would prove beneficial; especially in resource-poor areas. Molecular scale computers, built using biopolymers (i.e. nucleic acids), are capable of isothermal biosensing and allow more complex

decision making than PCR. These systems are also able to target multiple pathogenic signatures, integrated into a single diagnostic decision. Targeting multiple nucleic acid signatures will increase specificity and improve differential diagnosis in the early stages of disease states with complex genomic overlaps and/or disease states that exhibit similar symptoms.[15]

1.2 Molecular Scale Computers as a Solution

Molecular scale computers can potentially improve the specificity, and decrease the time and cost associated with the diagnosis and serotyping of diseases, such as DENV. DNA, due to its highly predictable thermodynamic and mechanical properties, is an ideal building material for molecular scale computers. DNA is also programmable and inherently biocompatible. Thus, DNA-based molecular computation has great potential as a diagnostic tool.

Nadrian Seeman recognized nucleic acids as programmable molecules in the early 1980s[16], and published more than 60 journal articles over the next decade. By the late 1990s Seeman was demonstrating the self-assembly of two-dimensional DNA crystals.[17] In 1994, inspired by Richard Feynman's 1959 Miniaturization talk on submicroscopic computer, Leonard Adleman computed a Hamiltonian path using DNA.[18] These advancements meant that by the turn of the millennium DNA nanotechnologists were able to direct the assembly of nanoscale molecular structures, and to compute complex mathematical algorithms using the predictability of DNA complementarity.

Building on Seeman and Adelman's discoveries, enzyme-based computational systems were developed. These systems relied on catalytic DNA

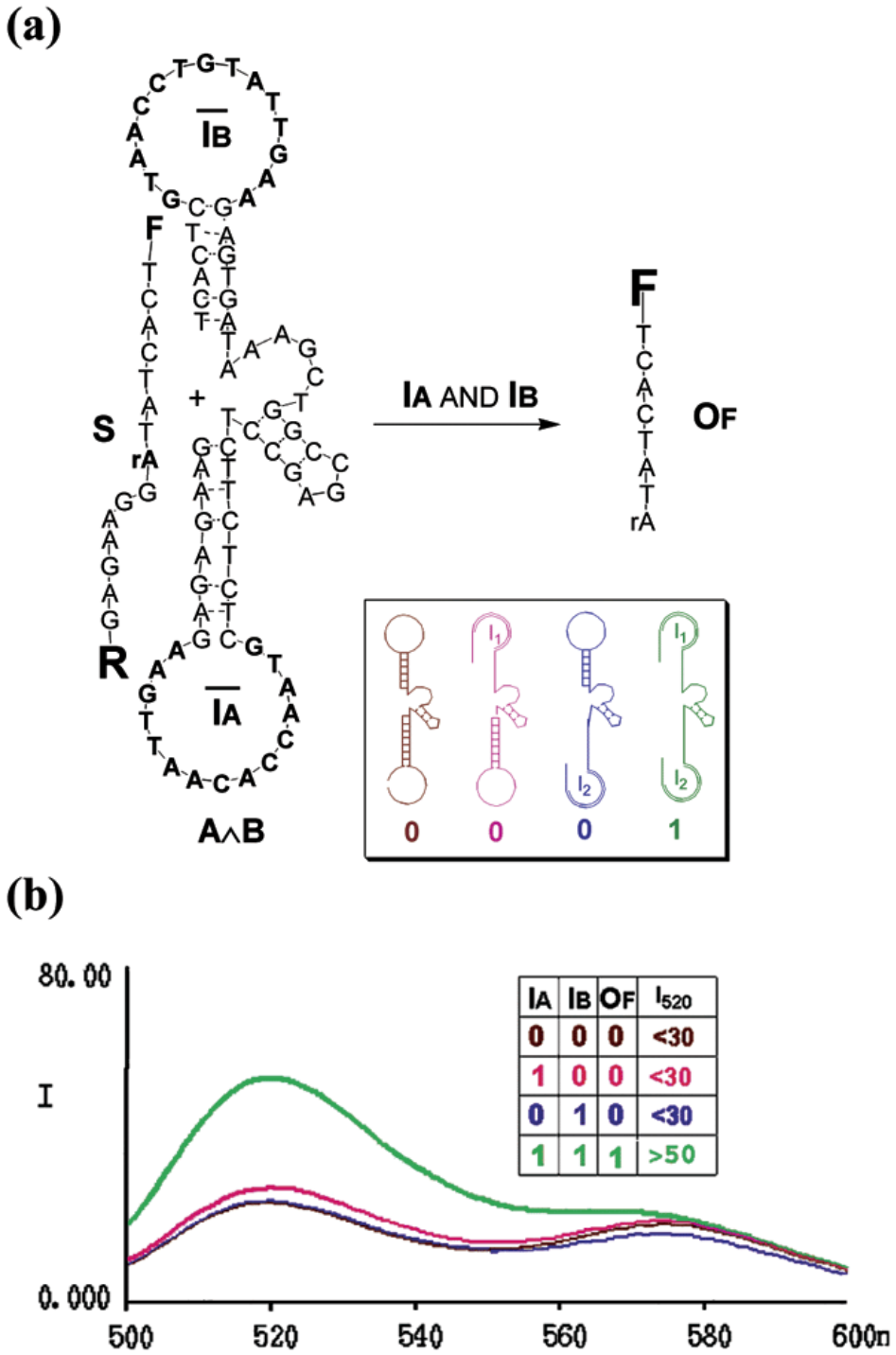

Figure 1.2 – DNAzyme Based Molecular Computation. **(a)** AND gate (**A∧B**) is constructed through attachment of two loops complementary to input oligonucleotides to the 5'- and 3'-ends of the deoxyribozyme; deoxyribozyme is active only if both inputs are present; insert schematically presents inactive gate (output 0) with closed one (magenta and blue) or both loops (brown) and active gate with both loops open (output 1, green). **(b)** Fluorescence spectra (relative intensity vs emission wavelength, λ_{exc} = 480 nm, t = 4 h) of the solution containing **A∧B**, **S**, and (from top to bottom): I_A and I_B (output 1, green line), only I_B, only I_A, or no input oligonucleotides. (Insert) Truth table for AND gate. *Reprinted with permission from Stojanovic et al.*[19] *Copyright 2002 American Chemical Society.*

strands (DNAzymes), which are single stranded DNA oligonucleotides that catalyze a variety of chemical reactions in the presence of divalent metal ions.[20,21] For DNA-based molecular computation, DNAzymes catalyze the cleavage of a partially complementary chimeric DNA substrate molecule at a single RNA base.[10,22-26] The initial DNAzyme logic gates relied on a conformational change that selectively produced an output when the correct combination of inputs were present. An example of an AND gate is shown in **Figure 1.2**, where the DNAzyme is only activated when input A and input B are both present, at which point the DNAzyme is able to bind the chimeric substrate molecule and cleave it. This process results in an increase in fluorescence only when the correct combination of inputs is present. Every logic gate has a corresponding truth table, which is referenced to a fluorescent readout that must be above a set threshold to be counted as true (**Figure 1.2b**). Based on predicted secondary structures, the authors were able to implement a functionally complete set of Boolean logic gates. Boolean logic is a branch of algebra where the values of variables are reduced to true or false, which can be further simplified to 1 or 0. Digital electronic computers use Boolean logic to make decisions. Using this set up, biosensors were designed to sense multiple disease markers, which could potentially deliver drug cargos based on the Boolean output.[19] The complexity of these systems was rapidly increased, with the demonstration of a molecular tic-tac-toe opponent,[23] followed by half adder[27] and full adder systems.[28] DNAzymes were also used to develop molecular walkers, or spiders, which could autonomously navigate a path.[29] These technologies contributed predictable mechanical control, via pre-determined

secondary structures, to the DNA-based molecular computing toolbox. These technologies also increased the computational complexity of DNA based molecular computing systems.

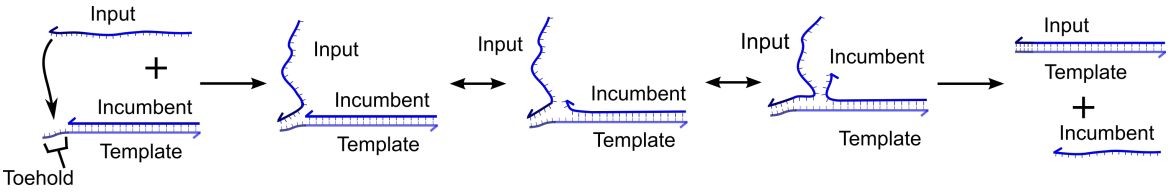

Figure 1.3 - Toehold-Mediated Strand Displacement (TMSD). An input strand binds to the toehold region of a logic gate complex, which is comprised of a shorted incumbent strand and a longer template strand. After binding the input begins to displace the incumbent strand via branch migration. Ultimately, the incumbent is fully displaced resulting is a more thermodynamically stable input/template complex.

Computational strand displacement systems were developed around the same time as the first DNAzyme papers, and also built on Seeman and Adelman's works. The initial enzyme-free systems represented nanoscale machines, constructed of and fueled by DNA.[30,31] These systems were followed by molecular circuits,[32] the kinetics of which could be controlled by the length of a toehold.[33] A toehold serves as a nucleation site for the binding of an input strand to a logic gate complex that comprises an incumbent strand, which is fully complementary to a longer strand called the template strand (**Figure 1.3**). The toehold is a single stranded DNA (ssDNA) overhang of the template strand that extends beyond the incumbent strand. Once the ssDNA input strand binds to the toehold, breathing of the double stranded DNA (dsDNA) causes a branch migration process to take place, as the base pairs of the gate spontaneously open and hence the input strand is able to gradually displace the incumbent strand of the gate. Once the input strand fully hybridizes to the template, the incumbent strand is released. Formation of the resulting input/template complex

is thermodynamically favored owing to the net increase in the number of base pairs. These early toehold-mediated strand displacement (TMSD) systems brought thermodynamic and kinetic control to DNA-based molecular computing systems.

In 2006, Paul Rothemund introduced DNA origami,[34] whereby staple strands bind to a template strand to form precise structures. The sophistication of DNA origami was recognized almost immediately, has been incorporated into almost four thousand publications, ranging from the construction of complex three-dimensional nanoscale structures[35] to the placement of molecules with localization of molecules with Bohr radius resolution[36]. The most remarkable contribution of DNA origami is not the visually impressive two and three-dimensional nanoscale structures, but instead the ability to self-assemble molecular systems with precise control over molecular orientations and locations. This is possible because of DNA's incredibly precise structure, with highly predictable length and hybridization properties.[37] With the help of well-established software packages, such as cadnano, which generate reliable sequences, scientists are able to design desired structures, such as DNA origami tiles, and incorporate appropriate addressing systems by including extensions in the staple strand sequences. Eleven years after Rothemund introduced DNA origami, structures on the microscale were achieved.[38] Now DNA nanotechnologists are able to direct the assembly of microscale DNA-based structures, and send molecules to specific addresses on these structures.

In addition to being excellent tools for developing diagnostics, DNA-based molecular computing systems have been: carried out *in vivo*,[39-41] used to mimic protein structures,[42] and used to model biological processes.[43,44] Once a number of limitations have been addressed, DNA-based molecular computation could be used in the development of theranostics, reduce costs associated with clinical trials, and elucidate elements of biomolecular circuitry that are still not well understood.

1.3 Limitations Associated with Solution Phase DNA-Based Molecular Computing Systems

As remarkable as DNA nanotechnology systems are, with their predictable thermodynamic and mechanical properties that allow for complex computation and precise molecular orientation and localization, they are difficult to scale up. To date the largest circuit, reported in 2011, was a four-bit square-root circuit, requiring 130 strands.[45] In addition, the most logical and valuable applications require these systems to operate at high levels in biological samples or *in vivo*. There are three major limitations to scaling up DNA computation circuits – spurious interactions, signal attenuation as circuit size increases, and methods of analysis. These factors along with exposure to nucleases, a requirement for ssDNA inputs and significantly increased sequence complexity in biological systems significantly limit computational operation.

In solution phase reactions systems all components must be non-interfering to prevent spurious interactions, which can overwhelm output signals resulting in decreased signal to noise ratios. Spurious interactions often referred to as leakage, occur when output signals are generated in the absence of activating input signals.

One of the first efforts to decrease leakage was thresholding,[32] which required a specific level of output for signal transduction. Careful sequence design, such as the incorporation of mismatches to destabilize leakage prone regions, can significantly reduce leakage.[10,46] Additionally, structural designs, which protect sequences vulnerable to leakage, have also been shown to reduce leakage.[45,47] Finally domain level motifs, which prevent leakage by increasing the number of spurious events required for leakage to occur, have been demonstrated.[48] Again, many elegant designs that effectively reduce leakage have been demonstrated, but as circuits are layered into more complex cascades or introduced to large biological sequence spaces, the background produced by leakage's shadow overwhelms signals.

The DNA-based molecular computing systems described thus far have been designed to target simple ssDNA oligonucleotides in solutions that are relatively simple, as compared to biological systems. However, when developing diagnostics that target pathogenic genomes, or implementing molecular circuits *in vivo,* synthetic systems must be designed to function in a highly complex sequence space. Twenty base genomic signatures are often sufficient to identify a specific pathogen (**Figure 1.4A**). However, pathogenic genomes often contain 10^4 – 10^6 bases, and in the case of dsDNA genomes this number represent only half of the total number of bases present. For example, the DENV serotype 1 genome has 10,735 bases (Dengue 1, from GenBank sequence accession number NC_001477.1), and this ssRNA viral genome is small compared to bacterial pathogens such as *Escherichia coli* with ~5.53×10^6 bases (1.11×10^7 total bases as

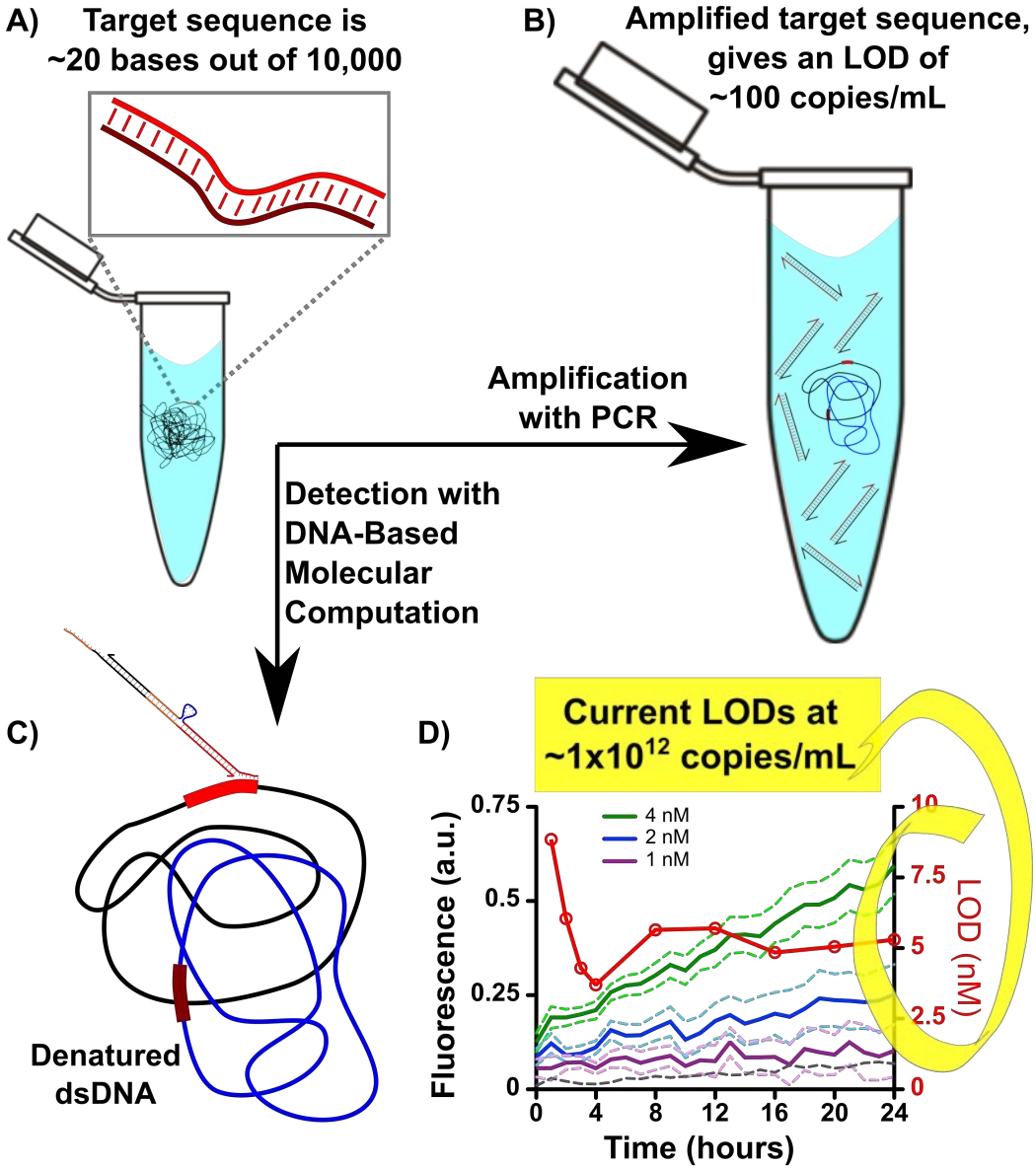

Figure 1.4 – LODs for PCR and DNA-Based Molecular Computation. A) The genomic material of pathogens is very complex, with tens of thousands of bases in a typical genome. There are signatures (sequences that are only found in specific species) and commonalities (sequences that are found across many species) throughout genomes. Nucleic acid-based diagnostics are frequently designed to target signatures of ~20 bases. **B)** PCR is the gold standard among detection platforms, as the amplification process increases the 20-base target sequence to concentrations well above the genomic material. This process results in limits of detection (LODs) as low as 100 copies/mL. **C)** Most DNA-based molecular computation systems are designed to interface with single strand nucleic acids, and when targeting dsDNA genomes denaturation protocols are required. Once the genomic material has been denatured toeholds on molecular logic gates bind the genomic signature and the logic gate is activated. **D)** Activated logic gates then produce fluorescent signals that can be used to calculate LOD values, such as this hypothetical LOD plot. Current LODs for DNA-based molecular computation are at ~3x10^{12} copies/mL, making it far less sensitive than PCR.

this genome is dsDNA) (Escherichia coli O157:H7, from GenBank sequence accession number AE005174.2). Designs that are robust to non-specific interactions that may arise from regions of the genome that are not being specifically targeted are still needed.

A wide variety of techniques have been employed to amplify signals for DNA computation, and still signal attenuation limits circuit size. Signal loss is a natural consequence of signal transduction and must be accounted for. In systems that lack amplification, each input signal activates only one logic gate and at low signal concentrations detection becomes infeasible. In 2004, hybridization chain reaction (HCR) was introduced as an initial means of isothermal amplification.[49] In HCR systems input strands initiate a polymerization of DNA hairpin logic gates that would otherwise be kinetically trapped. However, once the reaction is initiated the hairpins continue to polymerize until they are fully consumed, making these systems difficult to incorporate into cascades. In strand displacement systems, signals are amplified via metastable fuel complexes[32,50] or alternately with a reversible toehold exchange seesaw gate.[45,51] In DNAzyme-driven molecular computation, input signals activate DNAzymes, each of which can cleave multiple substrate molecules, enabling signal amplification via enzymatic catalysis.[24] Both biomolecular and silicon based circuits have methods for restoring attenuated signals, and although many elegant designs have been implemented signal attenuation continues to limit DNA-based molecular computing circuits.

Amplification is also required to improve circuit performance at physiologically relevant concentrations. Again, PCR amplifies the target sequence

to concentrations far above genomic concentrations and this amplification process results in limit of detection (LODs) as low as 100 genome copies/mL (**Figure 1.4B**). However, with isothermal DNAzyme amplification, a limit of detection of ~25 picomolar has been demonstrated for simple ssDNA molecules, and when the complexity of the sample increases the limit of detection goes up to ~5 nanomolar ($3x10^{12}$ molecules/mL, **Figures 1.4C and 1.4D**).[10] These systems must also incorporate methods for accessing dsDNA pathogenic genomes, as current techniques require single stranded nucleic acid inputs (**Figure 1.4C**).

Current methods of analysis either provide strictly qualitative data or require fluorophores and as circuit size increases the number of fluorophores required becomes cost prohibitive. As such, new methods of analysis are required. Microscopy is an excellent way to visualize static and dynamic systems, but does not provide highly quantitative data, nor is it a high throughput method of analysis. Still, atomic force microscopy (AFM), or transmission electron microscopy (TEM), is used to characterize most origami structures,[37,52] while fluorescent microscopy is used to track larger DNA based systems.[42,44] A promising alternative is flow cytometry, which provides highly quantitative and high-throughput analysis.[53] Flow cytometry analysis of fluorescently indexed beads would reduce the number of fluorophores required to track various components, while simultaneously improving data quality.

Cells, and higher organisms have many protection mechanisms, including methods for degrading foreign and unused nucleic acids. As such, when synthetic nucleic acid systems are introduced *in vivo* they will be degraded unless protection

mechanisms are built into the delivery system. Therefore, engineered nucleic acids systems, must be stable in the presence of nucleases.[41,54-58] Encapsulation of circuit components can potentially protect nucleic acids from degradation by nucleases.

1.4 Spatially Organizing DNA-based Molecular Computing Systems to Address These Limitations

Spatial organization contributes significantly to the function of biological and silicon-based systems. From organelles to cells to tissues to tissue systems, the flow of information is intricately controlled by isolating, either on surfaces or within compartments, biomolecular circuits.[59] At all levels, function relies on the spatial organization of biomolecular circuits that would otherwise interact in promiscuous ways.[60] The same spatial organization is found within *in silico* circuit boards, and within almost every dynamical system engineered by man. In all cases, the robustness of the system is directly tied to a structure specifically tailored to achieve an objective.

Previous studies explored reactants that were immobilized onto a solid surface, i.e. directly to microspheres[61] or onto DNA origami scaffolds. [52,65-73] In such systems, reactants can only interact with strands that are directly adjacent to them and do not move beyond their anchor points, which has been utilized as a method for standardizing computing elements. In addition, the thermodynamic and kinetic properties of surface immobilized reactants is significantly altered by the molecular crowding that is a consequence of immobilizing reactions onto surfaces.[62-65] Once the chemistry of these systems is fully understood restricting reactions to surfaces will increase effective concentrations, thereby speeding up

reactions at physiologically relevant concentrations. Surface based reactions will also decrease the need for orthogonality and will prevent spurious interactions that plague solution phase systems.

Lipid bilayers can improve the efficiency of such systems, by providing fluidity. Moreover, with the addition of spectral addresses using fluorescent lipid markers, it also becomes possible to monitor specific reactions in a multi-reaction system individually,[66] while simultaneously reducing the required number of fluorophores. Such multiplexed microsphere populations have simplified many pathogen detection assays by enabling the detection of many pathogenic signatures in a single solution assay that can be quantified by multi-parameter flow cytometry.[67-71]

Naturally occurring biological membranes are primarily composed of phospholipids and proteins. Phospholipids self-assemble into diffusive structures and they are commercially available. There are a wide variety of proteins that naturally insert into biological membranes and are responsible for signaling into cells. However, protein based *in vitro* systems can be unstable and are expensive. A DNA based system that transduces signals across barriers, analogous to protein-based signal transduction, would prove beneficial. The interaction of DNA with lipid bilayers is a growing field of study, as DNA-lipid conjugates allow DNA nanotechnology to be applied in biologically relevant studies that mimic membrane-bound protein interactions.[43,72-76] Additionally, lipid bilayers can be used to compartmentalize DNA-based molecular circuits, if systems are designed to interface with nucleic acid components.[73,77] However, unlike proteins the

interaction between a DNA molecule and a lipid bilayer is not energetically favorable. The negatively charged phosphate backbone of DNA does interact electrostatically with cation lipid headgroups (**Figure 1.6 A-C**), which can be used to drive DNA-lipid interactions. Other approaches include augmenting DNA with a wide range of commercially available modifications, some of which form covalent attachments with lipid head groups (**Figure 1.6 D-G**). Antibodies and aptamer-protein interactions (**Figure 1.6 H and I**) have been demonstrated at a means of restricting DNA-based structures to lipid bilayers surfaces. Finally, portions of the phosphate backbone can be rendered hydrophobic with ethyl-thiophosphate modifications, at which point DNA structures will spontaneously insert into the bilayer (**Figure 1.6 J**). All of these approaches result in relatively stable DNA-lipid interactions, but none of them provide a means of transmembrane communication, nor do they address the issue of non-specific interactions between DNA and lipids.

The phospholipids used in many cases are zwitterionic, with an internal negatively charged phosphate group and an external positively charges amine. In physiological buffer conditions (i.e. phosphate buffered saline, with a Na+ concentration of 138 mM, and no divalent cations) the negative charge of DNA's phosphate backbone is not attracted to the positively charged amine group. However, in the presence of divalent cations, which are required for DNAzyme function and included in many DNA reaction buffers, the phosphates of the lipid head group interact with the divalent cations and the positive charge on the external amine increases in strength.[78,79] When setting up DNA reactions on surfaces, where the strands must be floating beyond the surface at predetermined

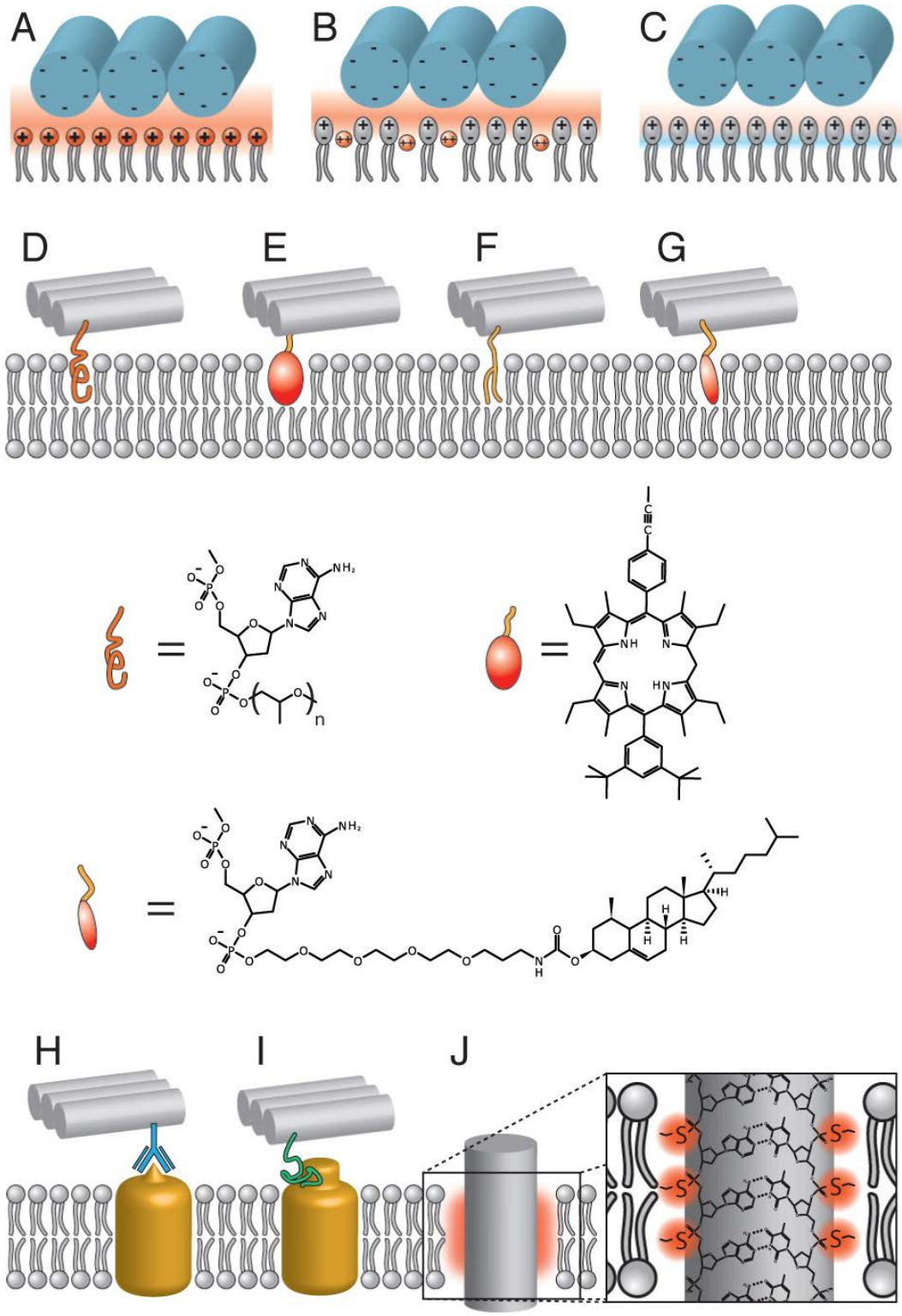

Figure 1.5 - DNA–Lipid Interactions. (**A–C**) Electrostatic binding to (**A**) cationic lipids, (**B**) zwitterionic lipids in the presence and (**C**) in the absence divalent cations. (**D–G**) Amphiphilic DNA conjugates with (**D**) PPO, (**E**) porphyrin, (**F**) lipid, (**G**) cholesterol. (**H, I**) Interactions involving membrane-associated proteins: (**H**) DNA–antibody conjugates and (**I**) aptamer–protein interaction. (**J**) Hydrophobic ethyl-thiophosphate backbone modification. *Reprinted with permission from Langecker et al.*[72] *Copyright 2014 American Chemical Society.*

concentrations, as opposed to non-specifically sticking to the lipid bilayer, this becomes a problem.

These non-specific interactions between DNA and lipids, in the presence of divalent cations, can be overcome by either adjusting the lipid composition or the buffer conditions. Silica microsphere supports greatly increase lipid bilayer stability, which conveniently also allows analysis with flow cytometry, but the positively charged amine at the surface of zwitterionic lipid headgroups is required for stability on the silica surface, a fact that significantly restricts lipid composition adjustments. As such, adjustments to the buffer conditions is the most effective means of reducing these non-specific interactions.

1.5 Present Studies

The most complex molecular systems on earth are the biomolecular circuits found in the human body. The highly complex functions of the human body are directly tied to its spatially organized structure. This dissertation presents a progression towards DNA-based systems that are spatially organized using lipid bilayers. The initial experiments were conducted in solution and demonstrated detection of dsDNA in the form of plasmids. Although the limit of detection for complex dsDNA samples was in the low nanomolar range, while simple ssDNA limits of detections were in the low picomolar range, when multiple regions of a plasmid were detected the response increased to levels comparable with the ssDNA samples. This suggests that the limit of detection for complex dsDNA samples could be reduced if multiple targets were identified and detected in a single tube assay. From here reactions were run on fluid bead surfaces, and a multiplexed Dengue diagnostic was demonstrated along with the development of

biological models. Potential applications for this technology include using multiplexed beads to target multiple genomic signatures for complex dsDNA samples, a full description of which is presented in Chapter 8. Next, with the hopes of achieving DNA-based signal transduction into and back out of synthetic compartments a membrane-spanning molecule was designed. Finally, DNA aptamers were encapsulated within liposomes and small molecule inputs were shown to diffuse across lipid bilayers. Excitingly, these liposomes were also shown to protect DNA components from DNAses and from strands that would cause leakage in a well-mixed solution.

Once again, we live in a rapidly changing world, which is both interesting and threatening. As the planet warms and globalization continues easily adaptable diagnostics will become more and more relevant. Smart diagnostics should be able to correctly identify specific pathogens in a complex sample, and they must do this rapidly. DNA-based molecular computation is an incredibly promising platform to achieve this critical objective, but effective spatial organization coupled with high throughput data analysis must be achieved.

1.6 References

1. Parry, M., Canziani, O., Palutikof, J. & van der Linden, P. J. *Climate change 2007: impacts, adaptation and vulnerability*. (2007).
2. Herlihy, N. *et al.* Climate change and human health: what are the research trends? A scoping review protocol. *BMJ Open* **6,** e012022–6 (2016).
3. World Health Organization…. WHO | What is dengue? *World Health Organization* (2017). Available at: http://www.who.int/denguecontrol/disease/en/. (Accessed: 29 December 2017)
4. Bhatt, S. *et al.* The global distribution and burden of dengue. *Nature Publishing Group* **496,** 504–507 (2013).
5. Kraemer, M. U. G. *et al.* The global distribution of the arbovirus vectors Aedes aegypti and Ae. albopictus. *Elife* **4,** e08347 (2015).
6. Ebi, K. L. & Nealon, J. Dengue in a changing climate. *Environmental Research* **151,** 115–123 (2016).
7. La Cruz Hernández, De, S. I. *et al.* Viral load in patients infected with dengue is modulated by the presence of anti-dengue IgM antibodies. *Journal of Clinical Virology* **58,** 258–261 (2013).
8. Lequime, S., Richard, V., Cao-Lormeau, V.-M. & Lambrechts, L. Full-genome dengue virus sequencing in mosquito saliva shows lack of convergent positive selection during transmission by Aedes aegypti. *Virus Evolution* **3,** 1–8 (2017).
9. Katzelnick, L. C. *et al.* Dengue viruses cluster antigenically but not as descrete serotypes. *Science* **349,** 1338–1343 (2015).
10. Brown, C. W., III *et al.* A Unified Sensor Architecture for Isothermal Detection of Double-Stranded DNA, Oligonucleotides, and Small Molecules. *ChemBioChem* **16,** 725–730 (2015).
11. Fabry-Wood, A. *et al.* A Microsphere-Supported Lipid Bilayer Platform for DNA Reactions on a Fluid Surface. *ACS Appl. Mater. Interfaces* **9,** 30185–30195 (2017).
12. Tezuka, K. *et al.* Development of a novel dengue virus serotype-specific multiplex real-time reverse transcription-polymerase chain reaction assay for blood screening. *Transfusion* **56,** 3094–3100 (2016).
13. Singh, R. *et al.* Biosensors for pathogen detection: A smart approach towards clinical diagnosis. *Sensors & Actuators: B. Chemical* **197,** 385–404 (2014).
14. Sutarlie, L., Ow, S. Y. & Su, X. Nanomaterials-based biosensors for detection of microorganisms and microbial toxins. *Biotechnology Journal* **12,** 567–26 (2016).
15. Simmons, C. P., Farrar, J. J., van Vihn Chau, N. & Wills, B. Dengue. *N Engl J Med* 1423–1432 (2012).
16. Seeman, N. C. Nucleic acid junctions and lattices. *Journal of Theoretical Biology* **99,** 237–247 (1982).
17. Winfree, E., Liu, F., Wenzler, L. A. & Seeman, N. C. Design and self-assembly of two-dimensional DNA crystals. *Nature* **394,** 539–544 (1998).

18. Adleman, L. M. Molecular computation of solutions to combinatorial problems. *Science* **266,** 1021–1024 (1994).
19. Stojanovic, M. N., Mitchell, T. E. & Stefanovic, D. Deoxyribozyme-Based Logic Gates. *J. Am. Chem. Soc.* **124,** 3555–3561 (2002).
20. Liu, J., Karpus, J., Wegner, S. V., Chen, P. R. & He, C. Genetically Encoded Copper(I) Reporters with Improved Response for Use in Imaging. *J. Am. Chem. Soc.* **135,** 3144–3149 (2013).
21. Breaker, R. R. & LI, Y. Deoxyribozymes: new players in the ancient game of biocatalysis. *Current Opinion in Structural Biology* **9,** 315–323 (1999).
22. Li, J., Zheng, W., Kwon, A. H. & Lu, Y. In vitro selection and characterization of a highly efficient Zn(II)-dependent RNA-cleaving deoxyribozyme. *Nucleic Acids Research* **28,** 481–488 (1999).
23. Stojanovic, M. N. & Stefanovic, D. A deoxyribozyme-based molecular automaton. *Nat Biotechnol* **21,** 1069–1074 (2003).
24. Brown, C. W., III *et al.* Signal Propagation in Multi-Layer DNAzyme Cascades Using Structured Chimeric Substrates. *Angew. Chem. Int. Ed.* **53,** 7183–7187 (2014).
25. Schlosser, K. & LI, Y. A Versatile Endoribonuclease Mimic Made of DNA: Characteristics and Applications of the 8-17 RNA-Cleaving DNAzyme. *ChemBioChem* **11,** 866–879 (2010).
26. Pei, R., Matamoros, E., Liu, M., Stefanovic, D. & Stojanovic, M. N. Training a molecular automaton to play a game. *Nat. Nanotechnol.* **5,** 773–777 (2010).
27. Milan N Stojanović, A. & Stefanovic, D. *Deoxyribozyme-Based Half-Adder*. *Journal of the American Chemical Society* **125,** 6673–6676 (American Chemical Society, 2003).
28. Lederman, H., Macdonald, J., Stefanovic, D. & Stojanovic, M. N. Deoxyribozyme-Based Three-Input Logic Gates and Construction of a Molecular Full Adder †. *Biochemistry* **45,** 1194–1199 (2006).
29. Pei, R. *et al.* Behavior of Polycatalytic Assemblies in a Substrate-Displaying Matrix. *J. Am. Chem. Soc.* **128,** 12693–12699 (2006).
30. Yurke, B., Turberfield, A. J., Mills, A. P., Jr, Simmel, F. C. & Neumann, J. L. A DNA-fuelled molecular machine made of DNA. *Nature* **406,** 605–608 (2000).
31. Turberfield, A. J. *et al.* DNA Fuel for Free-Running Nanomachines. *Phys. Rev. Lett.* **90,** 668–4 (2003).
32. Seelig, G., Soloveichik, D., Zhang, D. Y. & Winfree, E. Enzyme-Free Nucleic Acid Logic Circuits. *Science* **314,** 1585–1588 (2006).
33. Zhang, D. Y. & Winfree, E. Control of DNA Strand Displacement Kinetics Using Toehold Exchange. *J. Am. Chem. Soc.* **131,** 17303–17314 (2009).
34. Rothemund, P. W. K. Folding DNA to create nanoscale shapes and patterns. *Nature* **440,** 297–302 (2006).
35. Douglas, S. M. *et al.* Self-assembly of DNA into nanoscale three-dimensional shapes. *Nature Publishing Group* **459,** 414–418 (2009).
36. Funke, J. J. & Dietz, H. Placing molecules with Bohr radius resolution using DNA origami. *Nat. Nanotechnol.* **11,** 47–52 (2016).

37. Castro, C. E. *et al.* A primer to scaffolded DNA origami. *Nat. Methods* **8,** 221–229 (2011).
38. Tikhomirov, G., Petersen, P. & Qian, L. Fractal assembly of micrometre-scale DNA origami arrays with arbitrary patterns. *Nature Publishing Group* **552,** 67–71 (2017).
39. Amir, Y. *et al.* Universal computing by DNA origami robots in a living animal. *Nat. Nanotechnol.* **9,** 353–357 (2014).
40. Douglas, S. M., Bachelet, I. & Church, G. M. A logic-gated nanorobot for targeted transport of molecular payloads. *Science* **335,** 831–834 (2012).
41. Chen, Y.-J., Groves, B., Muscat, R. A. & Seelig, G. DNA nanotechnology from the test tube to the cell. *Nat. Nanotechnol.* **10,** 748–760 (2015).
42. Mohammed, A. M., Šulc, P., Zenk, J. & Schulman, R. Self-assembling DNA nanotubes to connect molecular landmarks. *Nat. Nanotechnol.* **12,** 312–316 (2017).
43. Johnson-Buck, A., Jiang, S., Yan, H. & Walter, N. G. DNA–Cholesterol Barges as Programmable Membrane-Exploring Agents. *ACS Nano* **8,** 5641–5649 (2014).
44. Zadorin, A. S. *et al.* Synthesis and materialization of a reaction-diffusion French flag pattern. *Nature Chemistry* **9,** 990–996 (2017).
45. Qian, L. & Winfree, E. Scaling Up Digital Circuit Computation with DNA Strand Displacement Cascades. *Science* **332,** 1196–1201 (2011).
46. Jiang, Y. S., Bhadra, S., Li, B. & Ellington, A. D. Mismatches Improve the Performance of Strand-Displacement Nucleic Acid Circuits. *Angewandte Chemie* **126,** 1876–1879 (2014).
47. Brown, C. W., III *et al.* Signal Propagation in Multi-Layer DNAzyme Cascades Using Structured Chimeric Substrates. *Angew. Chem. Int. Ed.* **53,** 7183–7187 (2014).
48. Thachuk, C., Winfree, E. & Soloveichik, D. Leakless DNA strand displacement systems. in 133–153 (2015).
49. Dirks, R. M. & Pierce, N. A. Triggered amplification by hybridization chain reaction. *PNAS* **101,** 15275–15278 (2004).
50. Seelig, G., Yurke, B. & Winfree, E. Catalyzed Relaxation of a Metastable DNA Fuel. *J. Am. Chem. Soc.* **128,** 12211–12220 (2006).
51. Qian, L., Winfree, E. & Bruck, J. Neural network computation with DNA strand displacement cascades. *Nature* **475,** 368–372 (2011).
52. Thubagere, A. J. *et al.* A cargo-sorting DNA robot. *Science* **357,** eaan6558–11 (2017).
53. Piyasena, M. E. & Graves, S. W. The intersection of flow cytometry with microfluidics and microfabrication. *Lab Chip* **14,** 1044–1059 (2014).
54. Mei, Q. *et al.* Stability of DNA origami nanoarrays in cell lysate. *Nano Lett.* **11,** 1477–1482 (2011).
55. Jiang, D. *et al.* Multiple-Armed Tetrahedral DNA Nanostructures for Tumor-Targeting, Dual-Modality in Vivo Imaging. *ACS Appl. Mater. Interfaces* **8,** 4378–4384 (2016).
56. Watts, J. K., Glen F, D. & Damha, M. J. Chemically modified siRNA: tools and applications. *Drug Discovery Today* **13,** 842–855 (2008).

57. Amarzguioui, M., Holen, T., Babaie, E. & Prydz, H. Tolerance for mutations and chemical modifications in a siRNA. *Nucleic Acids Research* **31,** 589–595 (2003).
58. Fern, J. & Schulman, R. Design and Characterization of DNA Strand-Displacement Circuits in Serum-Supplemented Cell Medium. *ACS Synth. Biol.* **6,** 1774–1783 (2017).
59. Brent, M. Computational Systems Biology: Reverse engineering advanced, alien technology. (2016).
60. Good, M. C., Zalatan, J. G. & Lim, W. A. Scaffold Proteins: Hubs for Controlling the Flow of Cellular Information. *Science* **332,** 680–686 (2011).
61. Yashin, R., Rudchenko, S. & Stojanovic, M. N. Networking Particles over Distance Using Oligonucleotide-Based Devices. *J. Am. Chem. Soc.* **129,** 15581–15584 (2007).
62. Dunn, K. E., Trefzer, M. A., Johnson, S. & Tyrrell, A. M. Investigating the dynamics of surface-immobilized DNA nanomachines. *Nature* 1–10 (2016). doi:10.1038/srep29581
63. Qian, L. & Winfree, E. in *DNA Computing and Molecular Programming* **8727,** 114–131 (Springer, Cham, 2014).
64. Watkins, H. M., Simon, A. J., Ricci, F. & Plaxco, K. W. Effects of Crowding on the Stability of a Surface-Tethered Biopolymer: An Experimental Study of Folding in a Highly Crowded Regime. *J. Am. Chem. Soc.* **136,** 8923–8927 (2014).
65. Ricci, F., Lai, R. Y., Heeger, A. J., Plaxco, K. W. & Sumner, J. J. Effect of Molecular Crowding on the Response of an Electrochemical DNA Sensor. *Langmuir* **23,** 6827–6834 (2007).
66. Fernandez Oropeza, N. *et al.* Multiplexed Lipid Bilayers on Silica Microspheres for Analytical Screening Applications. *Anal. Chem.* **89,** 6440–6447 (2017).
67. Brown, C. W., III *et al.* Signal Propagation in Multi-Layer DNAzyme Cascades Using Structured Chimeric Substrates. *Angew. Chem. Int. Ed.* **53,** 7183–7187 (2014).
68. Allen, P. B., Arshad, S. A., Li, B., Chen, X. & Ellington, A. D. DNA circuits as amplifiers for the detection of nucleic acids on a paperfluidic platform. *Lab Chip* **12,** 2951–8 (2012).
69. Wang, F., Elbaz, J. & Willner, I. Enzyme-Free Amplified Detection of DNA by an Autonomous Ligation DNAzyme Machinery. *J. Am. Chem. Soc.* **134,** 5504–5507 (2012).
70. Gerasimova, Y. V. *et al.* Deoxyribozyme Cascade for Visual Detection of Bacterial RNA. *ChemBioChem* **14,** 2087–2090 (2013).
71. Lu, C.-H., Wang, F. & Willner, I. Zn 2+-Ligation DNAzyme-Driven Enzymatic and Nonenzymatic Cascades for the Amplified Detection of DNA. *J. Am. Chem. Soc.* **134,** 10651–10658 (2012).
72. Langecker, M., Arnaut, V., List, J. & Simmel, F. C. DNA Nanostructures Interacting with Lipid Bilayer Membranes. *Acc. Chem. Res.* **47,** 1807–1815 (2014).

73. Chan, Y.-H. M., van Lengerich, B. & Boxer, S. G. Lipid-anchored DNA mediates vesicle fusion as observed by lipid and content mixing. *Biointerphases* **3,** FA17–6 (2008).
74. Pfeiffer, I. & Höök, F. Bivalent Cholesterol-Based Coupling of Oligonucletides to Lipid Membrane Assemblies. *J. Am. Chem. Soc.* **126,** 10224–10225 (2004).
75. Burns, J. R., Stulz, E. & Howorka, S. Self-Assembled DNA Nanopores That Span Lipid Bilayers. *Nano Lett.* **13,** 2351–2356 (2013).
76. Conway, J. W. *et al.* Dynamic Behavior of DNA Cages Anchored on Spherically Supported Lipid Bilayers. *J. Am. Chem. Soc.* **136,** 12987–12997 (2014).
77. Hadorn, M., Boenzli, E. & Hanczyc, M. M. Specific and Reversible DNA-Directed Self-Assembly of Modular Vesicle-Droplet Hybrid Materials. *Langmuir* **32,** 3561–3566 (2016).
78. Mengistu, D. H., Bohinc, K. & May, S. Binding of DNA to Zwitterionic Lipid Layers Mediated by Divalent Cations. *J. Phys. Chem. B* **113,** 12277–12282 (2009).
79. Gromelski, S. & Brezesinski, G. DNA Condensation and Interaction with Zwitterionic Phospholipids Mediated by Divalent Cations. *Langmuir* **22,** 6293–6301 (2006).

CHAPTER 2 - GOALS AND OVERVIEW OF WORK

Spatially organized molecular computing circuits, constructed using engineered biomolecules that self-assemble into highly organized structures and interface with biomolecular circuitry have the potential to improve our ability to diagnose and treat disease. This work investigates methods for improving the efficiency of current technologies by restricting components to surfaces and/or encapsulating them, enabling these systems to function at high levels as diagnostics, and as means of developing biological models.

The work presented in **Chapter 3** was published as a research article in the ChemPubSoc Europe journal *ChemBioChem* titled "A Unified Sensor Architecture for Isothermal Detection of Double-Stranded DNA, Oligonucleotides, and Small Molecules" (DOI - 10.1002/cbic.201402615). Here, we developed a unified DNA-based biosensor architecture capable of detecting simple ssDNA inputs, more complex dsDNA targets and small molecules. This work relies on TMSD platforms and aptamers for detection and uses DNAzymes to amplify input signals and a chimeric substrate molecule as a reported. My contribution to this paper included mismatch design and the development of a proof-of-concept for the detection of complex dsDNA systems. To achieve this, I expressed, isolated and denatured plasmid DNA, which was then detected by TMSD-DNAzyme biosensors. I then calculated a limit of detection for both the ssDNA and dsDNA targets. Importantly, when multiple regions of the plasmid were targeted in a single tube assay the response for complex dsDNA increased to levels comparable with the ssDNA, the implications of which will be discussed in Chapter 8. This work was published as

a Communication and therefore the chapter is formatted as it appears in the original publication: abstract, body (including: introduction, results, discussion and conclusions), experimental section, acknowledgements, and references. Supporting Information for the body of work is available in Appendix I.

Chapter 4 presents a versatile microsphere supported lipid bilayer platform for running DNA-based molecular computing reactions on a fluid surface. This work was published as a research article in the American Chemical Society journal of *Applied Materials and Interfaces* titled "A Microsphere-Supported Lipid Bilayer Platform for DNA Reactions on a Fluid Surface" (DOI - 10.1021/acsami.7b11046). Both TMSD and DNAzyme reactions were run on supported lipid bilayer surfaces. A DENV diagnostic was demonstrated with the TMSD reactions, using a multiplexed bead set. For the DNAzyme reactions the buffer conditions had to be considerably optimized, to decrease non-specific interactions between DNA and zwitterionic lipid head groups in the presence of the divalent cations that are required for enzymatic function (discussed in greater detail in Chapter 5). By decreasing the amount of Zn^{2+} and the amount of Na^{+} ions in solution we were able to run loos-of-fluorescence reactions with the DNAzyme in solution and the chimeric substrate on the bead, as well as have both the DNAzyme and the substrate molecule restricted to the bead surface. This work was published as a full article and is presented here as follows: abstract, introduction, experimental, results and discussion, conclusions, acknowledgement and references. Chapters 5-7 will be presented according to this format. Appendix II includes the Supporting Information for this article, along with data on further reducing limits of detections.

Appendix V presents an alternate method for integrating oligonucleotides into lipid bilayers, using a cholesterol tag.

Chapter 5 presents unpublished work pertaining to decreasing non-specific interactions between DNA and lipid bilayers. This chapter will focus on the various attempts to decrease non-specific interactions, including: lipid selection, buffer optimization and estimating the ideal number of oligonucleotides/bead. I was the primary experimentalist for all of this work.

Chapter 6 presents efforts to achieve nucleic acid-based transmembrane signal transduction via a dimerization event. To begin, I designed a molecule with dimensions to match biological membranes. The portion that spans the bilayer consists of an oligophenylenevinylene (OPV), with functional groups that are compatible with standard click chemistry reactions. After successful synthesis, by Dr. Milan Stojanovic and Dr. Stevan Pecic at Columbia University, we ran click chemistry in an attempt to functionalize the OPV with oligonucleotides. Currently, we are trouble shooting the click chemistry reactions. All future work on this project will be completed by Madalyn E. Fetrow in collaboration with Dr. Stojanovic's group at Columbia University and the Molecular Computing group here at University of New Mexico. Appendix III presents Supporting Information for this article.

Chapter 7 presents work that in preparation, as a full journal article titled "Physical Isolation and Protection of Molecular Computing Elements in Giant Vesicles." I will be first author on this publication as I conducted or supervised all experiments. Prof. Nick J. Carroll provided much appreciated expertise on the microfluidic portion of this project and Prof. Matt R. Lakin assisted with sequence

design. Physical isolation of molecular computing elements has the potential to increase complexity, by allowing the reuse of standardized components, and to protect nucleic acid components. We report the encapsulation of steroid-responsive DNA aptamers within giant unilamellar vesicles (GUVs) that are permeable to steroid inputs. Monodisperse GUVs were loaded with aptamers using a high-throughput microfluidic platform. The GUVs also prevent degradation of DNA components by nucleases, providing a mechanism for protecting nucleic acid components *in vivo*. Importantly, our compartments prevent crosstalk between complementary strands in separate GUVs, providing a method for creating a single tube assay with potentially cross-reacting strands. Thus, our system provides a mechanism for spatially organizing computing elements, which increases modularity by allowing standardized components to be reused. Appendix IV presents Supporting Information for this chapter.

Finally, **Chapter 8** will present a number of promising applications that utilize the technologies presented here.

CHAPTER 3 - A UNIFIED SENSOR ARCHITECTURE FOR ISOTHERMAL DETECTION OF DOUBLE-STRANDED DNA, OLIGONUCLEOTIDES, AND SMALL MOLECULES

Carl W. Brown, III[a], Matthew R. Lakin[c], **Aurora Fabry-Wood[a]**, Eli K. Horwitz[a], Nicholas A. Baker[a], Darko Stefanovic*[a,c], and Steven W. Graves*[a,b]

[a] *C. W. Brown, III, A. Fabry-Wood, E. K. Horwitz, N. A. Baker, Dr. D. Stefanovic, Dr. S. W. Graves*
Center for Biomedical Engineering
University of New Mexico, Albuquerque, NM 87131, USA
E-mail: graves@unm.edu, darko@cs.unm.edu

[b] *Dr. S. W. Graves*
Department of Chemical and Biological Engineering
University of New Mexico, Albuquerque, NM 87131, USA

[c] *Dr. M. R. Lakin, Dr. D. Stefanovic*
Department of Computer Science
University of New Mexico, Albuquerque, NM 87131, USA

Supporting information for this article is available on the WWW under http://dx.doi.org/10.1002/cbic.201402615.

QR Code for this publication.

3.1 Abstract

Pathogen detection is an important problem in many areas of medicine and agriculture, which may involve genomic or transcriptomic signatures, or small molecule metabolites. We report a unified, DNA-based sensor architecture capable of isothermal detection of double-stranded DNA targets, single-stranded oligonucleotides, and small molecules. Each sensor contains independent target detection and reporter modules, enabling rapid design. We detected gene variants on plasmids via a straightforward isothermal denaturation protocol. The sensors were highly specific, even with a randomized DNA background. We achieved a limit of detection of ~15 pM for single-stranded targets and ~5 nM for targets on denatured plasmids. By incorporating a blocked aptamer sequence, we also detected small molecules using the same sensor architecture. This work provides a starting point for multiplexed detection of multi-strain pathogens, and disease states caused by genetic variants (e.g., sickle cell anemia).

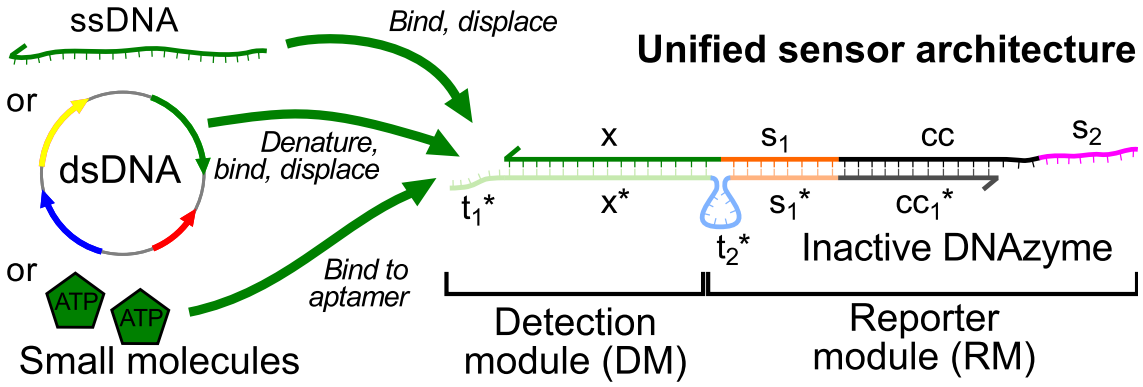

Figure 3.0 – Abstract Figure.

3.2 Introduction, Results, Discussion, Conclusions and Future Directions

Recent advances in DNA nanotechnology have enabled the construction of nucleic acid devices that use the predictable nature of Watson-Crick hybridization to perform computations,[1] and to detect targets with high specificity[2]. These

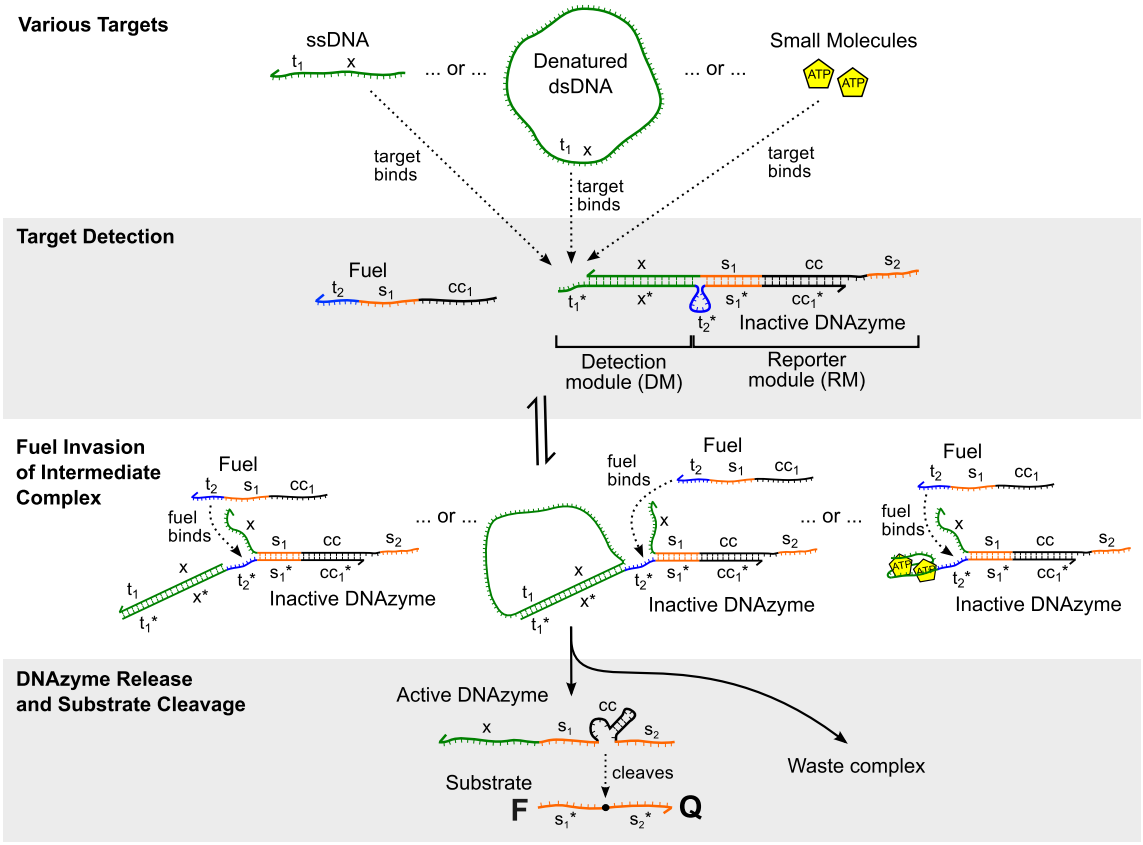

Figure 3.1 - Unified Sensor Architecture and Activation Mechanism in the Presence of Various Target Types. Binding of nucleic acid targets (oligonucleotides or denatured dsDNA) to the detection module by toehold-mediated DNA strand displacement exposed the reporter module toehold. Small molecule targets bound to a structure-switching aptamer in the detection module, similarly exposing the reporter module toehold. In both cases, this allowed the fuel strand to bind and complete displacement of the DNAzyme strand from the complex. The free DNAzyme strand then folded into a catalytically active conformation and generated an amplified fluorescent output by cleaving multiple substrate molecules labeled with a FRET pair.

properties, together with inherent biocompatibility and rapidly decreasing synthesis costs, make DNA an attractive material for the development of low-cost bioassays[3]. These requirements call for a simple, flexible design, for which DNA is ideally suited. However, nearly all bacterial and viral pathogens have double-stranded genomes, and the inaccessibility of gene targets in their natural, double-stranded state makes direct, isothermal detection using hybridization-based biosensors challenging.

Here we present a unified architecture and protocol for modular DNA-based sensors capable of specific detection of single- and double-stranded genetic targets, as well as small molecules. Our sensors combine toehold-mediated strand displacement (TMSD) and DNAzyme-catalyzed substrate cleavage to enable amplified target detection[4]. TMSD[5] is a versatile and powerful DNA computing technique that has been used to implement digital logic circuits[1a, 6], neural networks[7], enzyme-free catalytic networks[8], hairpin assembly systems[9] and molecular walkers[10]. TMSD reactions can be thermodynamically biased towards activation based on the lengths of the toeholds that nucleate the binding reactions[11]; this makes them ideal for detecting targets at low concentrations. By combining TMSD with inherently catalytic DNA strands (known as DNAzymes or deoxyribozymes), we can achieve an amplified signal output via multiple-turnover substrate cleavage. We have previously reported logic gates[12] and multi-layer DNAzyme signaling cascades[13] using these mechanisms.

Inspired by our previous work[12], in this paper we extend the hybrid TMSD-DNAzyme logic gate approach to engineer a unified sensor architecture capable of detecting a range of target types through a multi-step binding pathway. **Figure 3.1** depicts our unified sensor architecture, which consists of a catalytically inactive DNAzyme-inhibitor complex comprising two independent modules, a *detection module* (DM) that is responsible for target detection and a *reporter module* (RM) that produces the output signal, as well as an auxiliary fuel strand. The mechanism of activation for various target types is also shown in **Figure 3.1**. When the correct target is present, it binds to the DM and causes unbinding of the DNAzyme strand

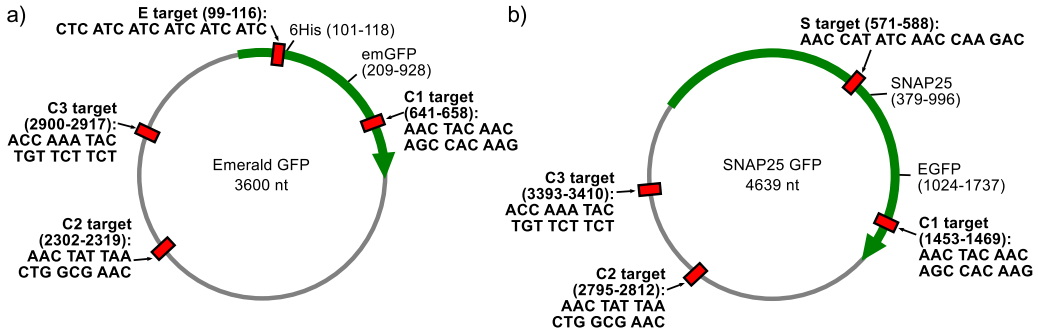

Figure 3.2 - Locations of Genetic Elements and Targets on the Studied Plasmids. Black arrows represent the open reading frame for each GFP protein variant. Locations of target sequences are denoted by white bars. a) Emerald GFP (emGFP) plasmid. b) SNAP25 GFP plasmid.

up to the beginning of the RM. DNA targets bind to the complementary DM toehold t_1* and trigger branch migration across the x domain, whereas small molecule targets displace the x domain via aptamer binding, causing a conformational shift in the DM. Either of these reactions partially displace the DNAzyme strand and open up the RM toehold t_2*, previously sequestered in a small, 5 or 8 nucleotide (nt) bulge between the two modules. The fuel strand then hybridizes to the free RM toehold t_2* and displaces the remainder of the DNAzyme strand via the s_1 and cc_1 domains. The cc_1 domain contains enough of the catalytic core of the DNAzyme to prevent the core from spontaneously attaining a catalytically active conformation when the DNAzyme is bound to the inhibitor. Once displaced, the free DNAzyme is able to fold into a catalytically active conformation as the entire catalytic core (cc) is now single-stranded. This allows it to cleave its complementary FRET-labeled substrate to produce a fluorescent signal. If substrate is present in excess, each DNAzyme is capable of catalyzing the cleavage of many substrate molecules in a multiple-turnover kinetic regime, providing the potential for isothermal signal amplification in the readout module. All

of our designs were based on the 8-17 DNAzyme motif[14] because of its compact size and high catalytic efficiency[15].

The separation of target detection and reporter modules in our unified sensor architecture allowed the sequences of the detection and reporter modules to be varied independently. In particular, we varied the target module while keeping the reporter module fixed, enabling detection of multiple targets with a single fluorescent readout. We used this approach for DNA detection by designing five sensors that target corresponding sequences from two plasmids that encode GFP-fusion protein variants, a commercially available Emerald GFP plasmid (referred to as emGFP) and a Pinpoint Xa plasmid containing a SNAP25-GFP fusion protein (referred to as SNAP25) previously developed in our lab[16]. All five sensors used a common reporter module. The locations of the sensor targets on the plasmids are illustrated in **Figure 3.2**. We chose three targets common to both plasmids, including a conserved region of the GFP sequence (C1), the gene coding for antibiotic resistance (C2), and the origin of replication (C3). We also chose one target specific to the emGFP variant (named E) and one target specific to the SNAP25 GFP variant (named S), enabling discrimination between different GFP-fusion proteins. Data from the initial characterization of the five sensors using synthetic, single-stranded oligonucleotides corresponding to the five detection targets is presented in **Figure 3.3**, including detection of individual targets using single sensors, multiplexed detection of targets using multiple sensors, and the demonstration of a single sensor limit of detection ~15 pM. Error bars indicate one

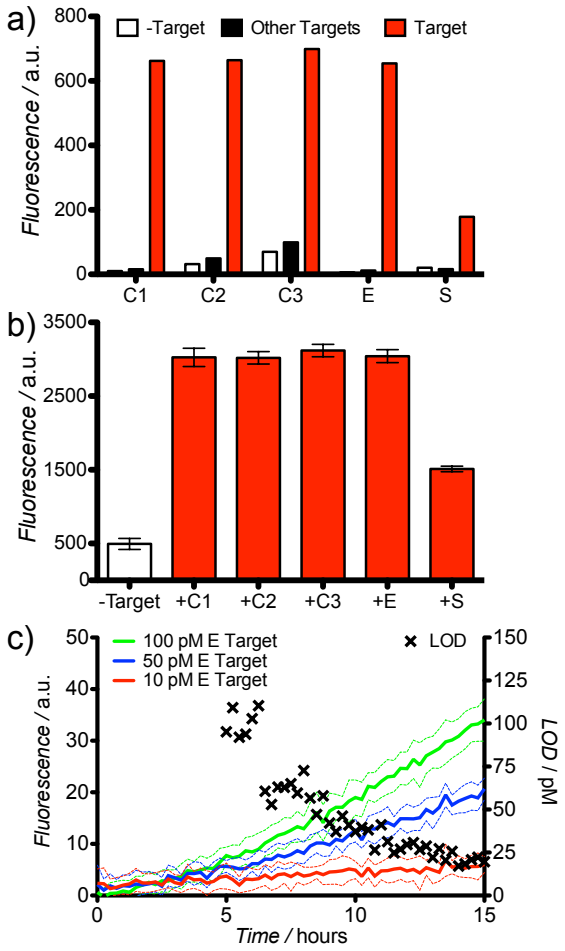

Figure 3.3 - Detection of Single-Stranded DNA Target Oligonucleotides. a) Individual sensor performance in the absence of target (white), other sensor targets (black), and the correct sensor target (gray). b) Multiplex sensor performance with all five sensors present. c) Limit of detection decreased over 15 hours to ~15 pM.

standard deviation from the mean. The performance of the C1-3 and E sensors was comparable, whereas the S sensor was slower to activate. This difference may be due to unwanted secondary structure formation or input sequestration in the S target strand.

Our goal was to use the unified sensor architecture to detect gene targets on the emGFP and SNAP25 plasmids. Detection of double-stranded DNA (dsDNA) is particularly challenging because of its inherent stability. Because toehold-mediated strand displacement relies on the availability of single-stranded toeholds to initiate branch migration, additional treatment steps are necessary to expose the target toeholds. We addressed the challenge of double-stranded DNA detection using an isothermal chemical denaturation protocol based on pH cycling. Briefly, we used a strongly basic solution (1M NaOH) to increase the pH of the plasmid solution, which denatured the duplexes due to the disruption of the

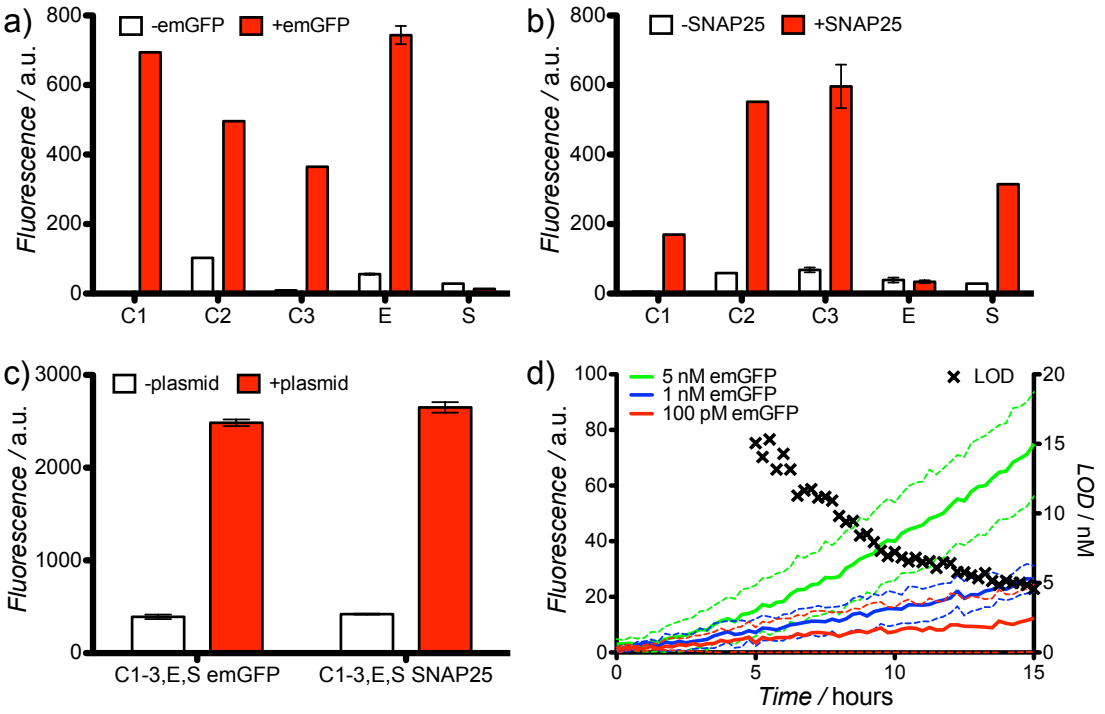

Figure 3.4 - Biosensor Detection of Denatured Plasmid Target Sequences. a) Results from emGFP plasmid detection using the five sensors individually. b) Results from SNAP25 plasmid detection using the five sensors individually. c) Results from emGFP and SNAP25 plasmid detection using all five sensors simultaneously in a combined assay. d) Investigating the limit of detection of the five sensors for emGFP plasmid detection. Lines (left axis) show the response of the five sensors with various concentrations of denatured emGFP plasmid, for an LOD (right axis) of ~5nM after 14-15 hours. Data without error bars indicate representative traces.

hydrogen bonding of DNA base pairs. We then used a strong acid (1M HCl) to bring the solution back down to physiological pH, so that the strand displacement and DNAzyme reactions underlying our sensor architecture could proceed. The denaturation step was essential to expose the single-stranded target domains from double-stranded complexes; in all cases, the control in which the plasmid was not denatured produced no fluorescent response (Figure AI.1). Data illustrating the detection of targets on chemically denatured emGFP and SNAP25 plasmids using the five sensors individually are presented in **Figures 3.4a and 3.4b**, respectively. In each case, we observed a fluorescent response from a given sensor if and only

if the corresponding target was present on the plasmid in question. Additional experiments in the presence of a randomized herring sperm DNA background yielded similarly positive results (Figure AI.2), which showed that the sensors are highly sequence-specific.

To boost the observed signal intensity from positive target detection assays, we used all five sensors in a single assay with the emGFP or SNAP25 plasmids. The effective concentration of accessible binding sites on the plasmids may be a kinetically limiting factor, but additional sensors for different areas of the plasmid can increase the effective concentration of binding sites without increasing the plasmid concentration itself. The multiplexed sensor responses in the presence of emGFP and SNAP25 plasmids are presented in **Figure 3.4c**. Using multiple sensors simultaneously provides a significant kinetic advantage, seen in **Figure 3.5**. The use of all five sensors provides a significant increase in response compared with a single sensor, and it is notable that the use of five sensors to detect plasmid generates a signal comparable to that of a single-stranded target. Thus, the multiplexed sensor approach works well for the detection of low analyte concentrations.

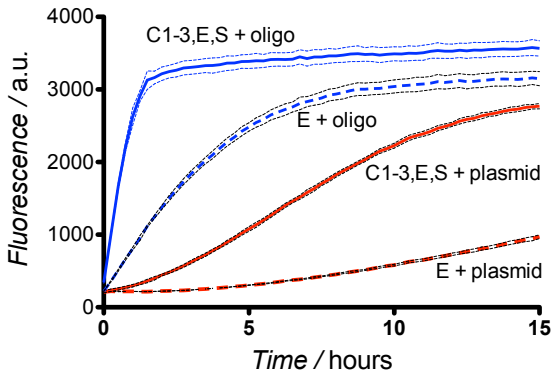

Figure 3.5 - Comparison of Responses. For the E sensor and the combination of all five (C1-3,E,S) sensors, for oligonucleotide targets (solid lines) and emGFP plasmid targets (broken lines). We observed that the plasmid and oligonucleotide targets generated a similar response in the presence of all five sensors after 15 hours.

Detection of low input concentrations is vital in many pathogen detection applications. We investigated the limit of detection (LOD) for the combination of sensors in a plasmid detection assay. The left-hand axis of **Figure 3.4d** shows kinetic traces of all five sensor outputs in the presence of decreasing concentrations of the emGFP plasmid. Lowering the sensor concentrations reduced non-specific signal generation in the absence of input while slowing down the reactions. We determined the optimal LOD to be ~5 nM after 15 hours when all five sensors were used. A single sensor showed no response at these concentrations, demonstrating the benefit of the multiple sensor approach.

While the detection of genetic targets is critical for pathogen identification and typing, small molecule sensors also have important applications, e.g., in drug or metabolite detection[17]. DNA aptamers can bind to small molecules, resulting in a conformational change[18]. We used this capability to replace the detection module of our sensor design with a partially blocked ATP aptamer sequence[19], as shown in **Figure 3.1**, to produce an ATP sensor. As shown in **Figure 3.6**, we observed significant signal over background in the presence of 1 mM ATP but no response in the presence of GTP. These data demonstrate the specificity of our small

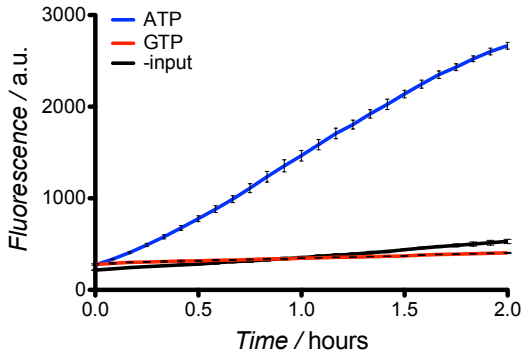

Figure 3.6 - Aptamer Sensing Using Modular DNAzyme Sensors. Replacing the detection module with an ATP aptamer enabled small molecule sensing. The ATP sensor used a 5 nt loop instead of the typical 8 nt loop. Kinetic traces showed a highly specific response to 1 mM ATP concentration, with no activation in the presence of a related small molecule (GTP) at 1mM. Sensor concentrations were 100 nM with 15 nM excess inhibitor.

molecular sensor and show that our unified sensor architecture can detect a range of target types. Constraints imposed by the kinetics of the ATP aptamer (Figures AI.3-AI.5) required us to use a 5 nt loop toehold rather than an 8 nt toehold, and the incorporation of other aptamers may require similar minor sensor modifications. The wide variety of available aptamer sequences, in conjunction with our modular sensor design, provides great flexibility that may be leveraged in future work to detect metabolites in complex biological mixtures. This may serve as an alternative or supplemental means of detecting pathogenic bacteria.

A key aspect of our sensor design is the use of a bulge to sequester the secondary toehold where the fuel strand binds. This is a non-standard approach to the design of multi-step DNA strand displacement processes, which typically rely on spontaneous dissociation of the secondary toehold following incomplete strand displacement. Our approach enabled us to implement a two-step strand displacement reaction using a two-strand complex, as opposed to the three-strand complex that is typically required[1a, 20]. Control experiments (Figure AI.2) showed that the DNAzyme-inhibitor complexes are highly stable in the absence of the fuel strand, even in the presence of the target sequence. However, this was a potential source of leakage (unwanted DNAzyme activation) due to unwanted fuel binding to the single-stranded toehold in the bulge in the absence of target binding. This effect was exacerbated by imperfections in the sensor complex and breathing of the duplexes near to the secondary toehold bulge. We minimized leakage in our designs by introducing a number of mismatched bases into the toehold and branch migration domain on the fuel strand [21]. A comparison of the performance of sensor

variants with different toehold loop lengths and patterns of mismatches is presented in Figures AI.6 and AI.7. Our chosen design employed an 8 nt toehold loop, with two mismatches in the loop adjacent to the beginning of the branch migration domain and a partial (G-T) mismatch in the first base of the migration domain. We used this toehold design in all experiments reported in this paper except for the ATP sensing experiments, as discussed above. Each sensor toehold used a universal sequence chosen from a restricted three-base alphabet (A,C,T) to prevent unwanted binding interactions. Alternative toehold sequences can be used for each of the sensors to obtain similar results (Figures AI.8-AI.11).

Our approach to pathogen detection has the advantage of simplicity compared with approaches based on protein enzymes, such as the polymerase chain reaction (PCR), strand displacement amplification[22], rolling circle amplification[23], or other isothermal nucleic acid amplification approaches[24]. Our rational engineering approach to sensor design is distinct from approaches based on selecting DNAzymes for affinity for the various products excreted by bacteria using directed evolution[25]. However, the methods we used for preparing dsDNA samples prior to detection could also be integrated with other groups' work on DNAzyme-based pathogen sensing[26]. While PCR remains the gold standard for nucleic acid detection in terms of sensitivity, it is protein-based and is not isothermal, which may hinder application in resource-poor areas. Although our sensor architecture addresses such limitations, our aim is not to compete directly with PCR; rather it is to provide an assay format that is more specific, flexible and

cost-effective than alternative approaches, such as the enzyme-linked immunosorbent assay (ELISA).

In summary, this work explores the concepts required to create nucleic acid-only detection systems for the isothermal detection of a range of targets. We have designed a unified sensor architecture and applied it to the detection of oligonucleotides, double-stranded plasmid DNA, and small molecules. The modularity of the unified sensor architecture allowed new sensors to be easily designed to target new genetic variants, enabling swift detection of emerging and evolving pathogen strains. Furthermore, our design requires only simple modification of the reporter module to cleave a different substrate sequence. This enables the use of different readout substrates to multiplex the detection of different targets in a single assay. In the solution phase, each substrate would be monitored in a separate fluorescent channel. In a flow cytometry assay format, substrates labeled with a single fluorophore could be monitored via a multiplex set of fluorescently dyed microspheres.

These sensors achieved direct detection of single-stranded targets at a limit of detection of ~15 pM and ~5 nM for isothermally denatured double-stranded targets. The LOD obtained from the single-stranded targets was nearly 250 times lower than for denatured plasmid targets, which may be due to various factors including diffusion rates, the presence of competing sequences, and steric hindrance and/or secondary structure occluding the target site. However, prediction of the secondary structure of plasmids is particularly challenging due to the lack of computational algorithms for modeling large, circular DNA strands. The

response times and limits of detection for double-stranded DNA targets may be improved by a deeper understanding of the underlying biophysical principles, which would enable the optimization of preparation protocols. The incorporation of additional molecular signal processing motifs, such as signal amplification via input recycling,[6, 8a] may also improve limits of detection by increasing the rate of signal generation.

3.3 Experimental Section

3.3.1 Materials

All oligonucleotides were purchased from Integrated DNA Technologies (Coralville, IA). Substrate molecules (DNA-RNA chimeras) were purified by RNase-free HPLC by the manufacturer. The Emerald GFP (pRSET-emGFP) plasmid was purchased from Life Technologies (Grand Island, NY). The PinPoint Xa plasmid was purchased from Promega (Madison, WI). Sequences for all oligonucleotides used herein are presented in Tables A-I.1 - A-I.6 in the Supporting Information.

3.3.2 Sensor Preparation

DNAzymes and inhibitors were heated together at 95 °C for 3 minutes on a heat block, and subsequently annealed by cooling to room temperature over a minimum of 90 minutes. Typical reaction concentrations were as follows, unless otherwise noted: 5 nM DNAzyme, 5.75 nM inhibitor, 5 nM fuel, 5 nM target DNA oligomer, 25 nM plasmid DNA, and 250 nM substrate, except in experiments to investigate individual sensor performance and LOD, which were run at 50 nM substrate.

3.3.3 Plasmid Preparation

Plasmids were transformed into SCS110 cells (Aligent Technologies, Santa Clara, CA) and grown in LB media (Becton-Dickenson, Franklin Lakes, NJ). Plasmid DNA was extracted with a Qiagen Maxiprep kit (Valencia, CA) into H_2O. The plasmid denaturation used a previously established protocol[27]. Briefly, 2 parts 1M NaOH was added to 9 parts plasmid in H_2O. After 10 min, 2 parts 1M HCl was added.

3.3.4 Limit of Detection Calculation

For these experiments (**Figures 3.3c and 3.4d**), the system contained 1 nM/sensor concentration with 150 pM excess inhibitor and 1 nM fuel for each sensor. The background signal in the absence of input has been subtracted from all traces. Thick lines are mean fluorescence values from 5 replicates, and thin broken lines are one standard deviation above and below the mean in each case. Data points plotted as a cross (right axis) indicates the limit of detection using the IUPAC definition: 3 standard deviations over background[28].

3.3.5 Assay Conditions and Instrumentation

All assays were performed at room temperature (23 °C) in a buffer of 1M NaCl, 50 mM HEPES, 1 mM $ZnCl_2$, pH 7.0. Fluorescence was read on a Spectramax M2e fluorescent plate reader (Molecular Devices, Sunnyvale, CA) in a 200 µL reaction volume (492 nm excitation, 518 nm emission).

3.4 Acknowledgements

This material is based upon work supported by the National Science Foundation under grants 1027877, 1028238 and 1318833. C.W.B. gratefully acknowledges support from INCBN IGERT DGE-0549500. M.R.L. gratefully

acknowledges support from the New Mexico Cancer Nanoscience and Microsystems Training Center (NIH/NCI grant 5R25CA153825).

3.5 Keywords

Pathogen Detection, DNAzymes, Deoxyribozymes, Strand Displacement, Amplification

3.6 References

[1] (a) G. Seelig, D. Soloveichik, D. Y. Zhang, E. Winfree, *Science* **2006**, *314*, 1585; (b) M. N. Stojanovic, D. Stefanovic, *Nat Biotechnol* **2003**, *21*, 1069.
[2] (a) S. X. Chen, D. Y. Zhang, G. Seelig, *Nature Chemistry* **2013**, *5*, 782; (b) D. Y. Zhang, S. X. Chen, P. Yin, *Nat Chem* **2012**, *4*, 208.
[3] R. Carlson, *Nat Biotechnol* **2009**, *27*, 1091.
[4] Y. Li, R. R. Breaker, *Curr Opin Struct Biol* **1999**, *9*, 315.
[5] D. Y. Zhang, G. Seelig, *Nat Chem* **2011**, *3*, 103.
[6] L. Qian, E. Winfree, *Science* **2011**, *332*, 1196.
[7] L. Qian, E. Winfree, J. Bruck, *Nature* **2011**, *475*, 368.
[8] (a) D. Y. Zhang, A. J. Turberfield, B. Yurke, E. Winfree, *Science* **2007**, *318*, 1121; (b) D. Y. Zhang, E. Winfree, *J Am Chem Soc* **2008**, *130*, 13921.
[9] (a) P. Yin, H. M. T. Choi, C. R. Calvert, N. A. Pierce, *Nature* **2008**, *451*, 318; (b) B. Li, A. D. Ellington, X. Chen, *Nucleic Acids Res* **2011**, *39*, e110; (c) X. Chen, N. Briggs, J. R. McLain, A. D. Ellington, *Proc Natl Acad Sci U S A* **2013**, *110*, 5386; (d) B. Li, Y. Jiang, X. Chen, A. D. Ellington, *J Am Chem Soc* **2012**, *134*, 13918.
[10] (a) J. Bath, S. J. Green, K. E. Allen, A. J. Turberfield, *Small* **2009**, *5*, 1513; (b) P. Yin, H. Yan, X. G. Daniell, A. J. Turberfield, J. H. Reif, *Angew Chem Int Ed Engl* **2004**, *43*, 4906.
[11] D. Y. Zhang, E. Winfree, *J Am Chem Soc* **2009**, *131*, 17303.
[12] C. W. Brown, III, M. R. Lakin, D. Stefanovic, S. W. Graves, *ChemBioChem* **2014**, *15*, 950.
[13] C. W. Brown, III, M. R. Lakin, E. K. Horwitz, M. L. Fanning, H. E. West, D. Stefanovic, S. W. Graves, *Angew Chem Int Ed* **2014**, *53*, 7183.
[14] S. W. Santoro, G. F. Joyce, *Proc Natl Acad Sci U S A* **1997**, *94*, 4262.
[15] J. Li, W. Zheng, A. H. Kwon, Y. Lu, *Nucleic Acids Res* **2000**, *28*, 481.
[16] M. J. Saunders, B. S. Edwards, J. Zhu, L. A. Sklar, S. W. Graves, *Curr Protoc Cytom* **2010**, *54*, 13.12.1.
[17] (a) M. N. Stojanovic, P. de Prada, D. W. Landry, *J Am Chem Soc* **2001**, *123*, 4928; (b) M. N. Stojanovic, D. W. Landry, *J Am Chem Soc* **2002**, *124*, 9678.
[18] J. C. Achenbach, R. Nutiu, Y. Li, *Analytica Chimica Acta* **2005**, *534*, 41.

[19] D. E. Huizenga, J. W. Szostak, *Biochemistry* **1995**, *34*, 656.
[20] D. Soloveichik, G. Seelig, E. Winfree, *Proc Natl Acad Sci U S A* **2010**, *107*, 5393.
[21] Y. S. Jiang, S. Bhadra, B. Li, A. D. Ellington, *Angew Chem Int Ed* **2014**, *53*, 1845.
[22] G. T. Walker, M. S. Fraiser, J. L. Schram, M. C. Little, J. G. Nadeau, D. P. Malinowski, *Nucleic Acids Res* **1992**, *20*, 1691.
[23] (a) A. Fire, S. Q. Xu, *Proc Natl Acad Sci U S A* **1995**, *92*, 4641; (b) W. Zhao, M. M. Ali, M. A. Brook, Y. Li, *Angew Chem Int Ed Engl* **2008**, *47*, 6330.
[24] (a) J. Kim, C. J. Easley, *Bioanalysis* **2011**, *3*, 227; (b) M. Vincent, Y. Xu, H. Kong, *EMBO Rep* **2004**, *5*, 795.
[25] (a) S. D. Aguirre, M. Monsur Ali, P. Kanda, Y. Li, *Journal of Visualized Experiments* **2012**, *63*, e3961; (b) S. D. Aguirre, M. Monsur Ali, B. J. Salena, Y. Li, *Biomolecules* **2013**, *3*, 563; (c) P.-J. J. Huang, M. Liu, J. Liu, *Reviews in Analytical Chemistry* **2013**, *32*, 77.
[26] (a) Y. V. Gerasimova, E. M. Cornett, E. Edwards, X. Su, K. H. Rohde, D. M. Kolpashchikov, *ChemBioChem* **2013**, *14*, 2087; (b) Y. V. Gerasimova, D. M. Kolpashchikov, *Angew Chem Int Ed Engl* **2013**, *52*, 10586; (c) Y. V. Gerasimova, D. M. Kolpashchikov, *Biosens Bioelectron* **2013**, *41*, 386; (d) C. H. Lu, F. Wang, I. Willner, *J Am Chem Soc* **2012**, *134*, 10651; (e) F. Wang, J. Elbaz, R. Orbach, N. Magen, I. Willner, *J Am Chem Soc* **2011**, *133*, 17149; (f) F. Wang, J. Elbaz, C. Teller, I. Willner, *Angew Chem Int Ed Engl* **2011**, *50*, 295; (g) F. Wang, J. Elbaz, I. Willner, *J Am Chem Soc* **2012**, *134*, 5504.
[27] S. H. Oh, K. F. Chater, *J Bacteriol* **1997**, *179*, 122.
[28] G. L. Long, J. D. Winefordner, *Analytical Chemistry* **1983**, *55*.

CHAPTER 4 - A MICROSPHERE-SUPPORTED LIPID BILAYER PLATFORM FOR DNA REACTIONS ON A FLUID SURFACE

Aurora Fabry-Wood[1], *Madalyn E. Fetrow*[1], *Carl W. Brown III*[1†], *Nicholas A. Baker*[1, 2], *Nadiezda Fernandez Oropeza*[1], *Andrew P. Shreve*[1, 2], *Gabriel A. Montaño*[4], *Darko Stefanovic*[1, 3*], *Matthew R. Lakin*[1, 2, 3*], *Steven W. Graves*[1, 2*]

1. Center for Biomedical Engineering, University of New Mexico
2. Department of Chemical and Biological Engineering, University of New Mexico
3. Department of Computer Science, University of New Mexico
4. Center for Integrated Nanotechnologies, Los Alamos National Laboratory

QR Code for this publication.

Reprinted (adapted) with permission from Fabry-Wood, A. et al. A Microsphere-Supported Lipid Bilayer Platform for DNA Reactions on a Fluid Surface. ACS Appl. Mater. Interfaces ***9,*** *30185–30195 (2017).*

4.1 Keywords

DNA-lipid conjugates, supported lipid bilayers, multiplexing, toehold-mediated strand displacement, DNAzymes, detection platform, molecular computation

4.2 Abstract

We report a versatile microsphere-supported lipid bilayer system that can serve as a general-purpose platform for implementing DNA nanotechnologies on a fluid surface. To demonstrate our platform, we implemented both toehold-mediated strand displacement (TMSD) and DNAzyme reactions, which are typically performed in solution and which are the cornerstone of DNA-based molecular logic and dynamic DNA nanotechnology, on the surface. We functionalized microspheres bearing supported lipid bilayers (μSLBs) with membrane-bound nucleic acid components. Using functionalized μSLBs, we developed TMSD and DNAzyme reactions by optimizing reaction conditions to reduce non-specific interactions between DNA and phospholipids and to enhance bilayer stability. Additionally, the physical and optical properties of the bilayer were tuned *via* lipid composition and addition of fluorescently tagged lipids to create stable and multiplexable μSLBs that are easily read out by flow cytometry. Multiplexed TMSD reactions on μSLBs enabled the successful operation of a

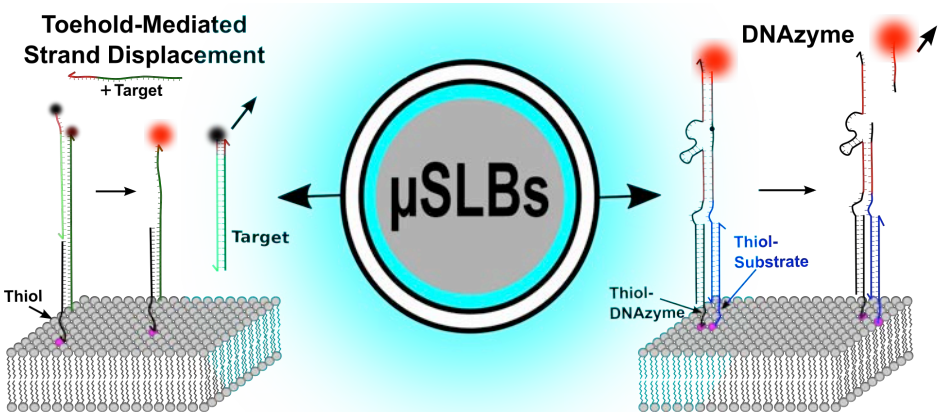

Figure 4.0 – Abstract Figure.

Dengue serotyping assay that correctly identified all sixteen patterns of target sequences to demonstrate detection of DNA strands derived from the sequences of all four Dengue serotypes. The limit of detection for this assay was 3 nM. Furthermore, we demonstrated DNAzyme reactions on a fluid lipid surface, which benefit from free diffusion on the surface. This work provides the basis for expansion of both TMSD and DNAzyme based molecular reactions on supported lipid bilayers for use in molecular logic and DNA nanotechnology. As our system is multiplexable and results in fluid surfaces, it may be of use in compartmentalization and improved kinetics of molecular logic reactions, and as a useful building block in a variety of DNA nanotechnology systems.

4.3 Introduction

The field of DNA nanotechnology uses biomolecules to construct computing components analogous to those in electronic computers,[1-3] and to build synthetic nanostructures to study molecular interactions.[4,5] DNA is attractive for these applications as Watson-Crick base pairing enables straightforward programming of molecular interactions.[1,2] DNA-based biomolecular computation has been used for bioassays targeting pathogen signatures and to integrate detection of multiple pathogen signatures into a single reaction.[6-13] However, non-specific interactions arising from background environmental nucleic acids and from molecular crosstalk due to lack of component separation in solution, can severely limit assay performance.[6]

DNA-based molecular computation is typically performed in solution using toehold-mediated strand displacement (TMSD), DNAzymes, or a combination of the two approaches.[6,10] TMSD molecular computing systems are an enzyme-free

mechanism wherein target strands interact with a gate complex composed of a template strand partially hybridized to an incumbent strand.[2] The gate has a double-stranded DNA (dsDNA) region with a short single-stranded DNA (ssDNA) overhang on the template strand, referred to as a *toehold,* which serves as a nucleation site for target strand binding. The target then displaces the incumbent strand from the template *via* branch migration. Formation of the resulting target/template complex can be programmed to be thermodynamically favored due to a net increase in the number of base pairs. DNAzymes, on the other hand, are single stranded DNA oligonucleotides that catalyze a variety of chemical reactions in the presence of divalent metal ions.[14,15] Of particular interest are DNAzymes that cleave partially complementary chimeric DNA substrate molecules at a single RNA base, such as the 8-17 DNAzyme, chosen for this work due to its small size and high catalytic activity.[1,6,10,16-18] In DNAzyme-driven molecular computation, input signals activate DNAzymes, each of which can cleave multiple substrate molecules, enabling signal amplification *via* catalysis.

Here, we have explored the use of supported lipid bilayers on silica microspheres (μSLBs) as a scaffold for both TMSD networks and DNAzyme reactions. In this system, our nucleic acid components are covalently linked to head groups of the supported lipid bilayer. This approach provides a mechanism to easily segregate or compartmentalize elements of these reactions from each other and from nucleic acids in solution. This offers the potential to reduce nonspecific crosstalk within the system and to improve the scalability of DNA based reactions by permitting the reuse of nucleotide sequences without causing

crosstalk. Alternatively, we sought to improve scalability through the incorporation of fluorescently tagged lipids into the μSLB system, which provides a straightforward method for multiplexed analysis that can be easily monitored *via* flow cytometry.[19] This approach offers benefits for many practical applications, such as bioassay development. Analogous technology (fluorescently multiplexed polystyrene microspheres) has simplified pathogen assays by enabling the detection of multiple signatures in a single solution *via* flow cytometry[20] and provides highly quantitative and rapid analysis.[21] However, lipid bilayers are not readily formed on polystyrene microspheres, making our μSLB system an excellent alternative. While others have used lipid bilayer based systems for nucleic acid based reactions, these systems were not easily analyzable or multiplexable.[22-24] To demonstrate the value of our approach, we developed a bivariate fluorescence tagging approach to increase μSLB multiplexing levels and we demonstrated multiplexed μSLBs for a TMSD assay that accurately types DNA sequences derived from the genomes of the four Dengue virus serotypes.

Although the spatial isolation of molecular computation components *via* immobilization to fixed surfaces (e.g., direct attachment to polymer microspheres[25] and onto DNA origami scaffolds[26-28]) has been explored, reactants in these systems are constrained to their anchor points and cannot interact with molecules outside of the reach of their initial location. This limitation is most relevant to DNAzyme systems, which could otherwise provide signal amplification *via* multiple turnover cleavage of substrates. Therefore, the final goal of this work was to overcome this issue by linking DNAzymes and their substrates to lipid head groups

incorporated into multiplexable microsphere-supported lipid bilayers (μSLBs). The intent of this approach is to enable surface diffusion of DNAzymes so that they can interact with substrate molecules independent of their attachment position. Surface diffusion might also improve reaction kinetics, as diffusion on a two-dimensional surface is more constrained than the three dimensions available to solution phase reactions.[26,29-31]

In summary, we present a μSLB system that enables the compartmentalization of DNA-based molecular computing components. This system is multiplexable, which allows components to be independently monitored in a single tube reaction. Thus, by restricting DNA-based molecular computing components to a μSLB, we are able to design a detection platform that targets specific pathogenic signatures and uses flow cytometry for analysis. This has the potential to greatly reduce non-specific interactions, which would enable the creation of more complex DNA-based molecular reaction networks.

4.4 Experimental Section

4.4.1 Materials

Lipids were purchased from Avanti Polar Lipids (Alabaster, AL). Oligonucleotides were purchased from Integrated DNA Technologies (IDT, Coralville, IA). Ethylenediaminetetraacetic acid (EDTA), disodium phosphate, sodium chloride, and citric acid were purchased from EMD Millipore (Billerica, MA). Nucleosil (50-10) silica microspheres were purchased from GFS Chemicals (Powell, OH). Illustra NAP-5 Columns Sephadex G-25 DNA Grade were purchased from GE Healthcare Life Sciences (Pittsburgh, PA). All other reagents were purchased from Sigma Aldrich (St. Louis, MO).

4.4.2 Silica Microsphere Preparation

To prepare the surface, silica microspheres (SiMS) were treated in a basic solution containing 4% NH_4OH and 4% H_2O_2 at 80 ^oC for 10 minutes. The SiMSs were rinsed three times with distilled water and treated with an acidic solution containing 4% HCl and 4% H_2O_2 at 80^oC for 10 minutes. Finally, SiMSs were rinsed five times with distilled water. After this final wash the SiMSs were suspended in citric acid buffer (CAB6.5) (20mM citric acid, 35 mM disodium phosphate, 108 mM NaCl, 1 mM EDTA at pH 6.5). In addition, the SiMSs were preloaded with an inert oligo (Blocking strand_TSF) to prevent migration of the DNA-lipid conjugates into the porous SiMS by rotating at room temperature for 12 hours with a strand concentration of 10 μM.

4.4.3 Preparation of μSLBs for Multiplex

Four separate lipid mixtures were dried overnight under vacuum, and then hydrated in citric acid buffer (20mM citric acid, 35 mM disodium phosphate, 108 mM NaCl, 1 mM EDTA at pH 6.5 (CAB6.5)). The lipid solution was then extruded to generate monodispersed unilamellar vesicles (100 nm). These unilamellar vesicles were then used to coat $6.7x10^6$ SiMS, by vortexing on high for 10 minutes, followed by low for 30 minutes at 37 ^oC. The lipid-coated SiMSs were washed 3 times in CAB6.5 to remove the 100-fold excess of vesicles. The first vesicle population (P1) was composed of 1-palmitoyl-2-oleoyl-*sn*-glycero-3-phosphocholine (POPC), with 10 mol% 1,2-dioleoyl-*sn*-glycero-3-phosphoethanolamine-N-[4-(p-maleimidophenyl) butyramide] (MPB PE) incorporated into the lipid cake. No fluorescently labeled lipids were included in P1. The second population (P2) contained the same lipid mixture as 1, plus 0.5

mol% 1,2-dioleoyl-*sn*-glycero-3-phosphoethanolamine-N-(carboxyfluorescein) (PECF). The third population (P3) was the same as 1, plus 0.5 mol% 1,2-dioleoyl-*sn*-glycero-3-phosphoethanolamine-N-(lissamine rhodamine B sulfonyl) (PELR). The fourth population (P4) contained the same as P1, plus 0.5 mol% PELR and 0.75 mol% PECF.

4.4.4 Preparation of μSLBs for DNAzyme Reactions

The above procedure was used for the DNAzyme experiments, minus the fluorescently tagged lipids. DOPC was used in place of POPC to increase diffusivity of the bilayer, and the amount of MPB PE was reduced from 10 mol% to 1 mol% (representing 4.5×10^6 DNA-lipid conjugates/μSLB). This change was made to reduce the density of conjugated components on the surface: at 1 mol% MPB PE there is approximately 1 DNA-lipid conjugate per 70 nm^2 of bilayer, as opposed to 1 per 7 nm^2 if 10 mol% MPB PE is used.

4.4.5 Conjugation for the Multiplexing

The 5' Thiol Modifier C6 S-S strand was deoxygenated and reduced in CAB (pH 5.0) (CAB5.0) containing 50 mM dithiothreitol (DTT) for 90 minutes at room temperature. The DTT was removed using a NAP-5 column and the sulfhydryl solution was stored at 4 °C in CAB5.0. The various μSLB populations were then deoxygenated and the reduced thiol oligonucleotide was added into the deoxygenated μSLB solution at a final concentration of 500 nM, in 500 μL CAB6.5. This solution was further deoxygenated for 15 minutes and then sealed with parafilm and rotated at 4 °C for 12 hours. The μSLBs were washed 3 times with 1× phosphate buffer saline (PBS). The μSLBs were coated with bovine serum albumin (BSA) (100 μg/mL, rotated for 30 minutes). BSA is negatively charged at the

physiological pH used in our assays[32] and is used to stabilize the membrane.[33] The μSLB were washed another three times in PBS, resulting in a final concentration of 500 nM thiol strands available for hybridization to the TMSD gates (for 10 mol% MPB PE).

4.4.6 Conjugation for DNAzyme Experiments

The above procedure was modified to include two of three thiol strands, one that hybridizes the DNAzyme (TSD), or one that hybridizes neither the DNAzyme nor the substrate (TSF), and a second strand that hybridizes to the substrate molecule (TSS). In addition, the Na^+ concentration in all buffers was doubled (from the PBS level of 138 mM) to a final concentration of 276 mM (E276-0). The thiol strands were added at different concentrations to achieve a 4-fold excess of TSS. The final concentration of thiol strands available for hybridization is 50 nM, for 1 mol% MPB PE. These μSLBs were also blocked with BSA using the above protocol.

4.4.7 Strand Design for TMSD Reactions

The sequences of the viral genomes for the four dengue serotypes were obtained from the National Center for Biotechnology Information (NCBI) website. Target oligomer subsequences of length 18 nucleotides from each of the four serotypes were then selected using a custom algorithm, as follows. A sliding window of size 18 nucleotides was used to compare each candidate target sequence for a given serotype with all 18-mers from the other three serotypes. A candidate target sequence was rejected if it contained a contiguous subsequence that matched any 18-mer sequence from any other serotype longer than a specified threshold length of 8 nucleotides. This test eliminated potential targets

with long sequences shared with any other serotype genome. For each candidate sequence that passed this initial test, the Hamming distance (defined as the number of positions at which two sequences of same length differ) was computed between the candidate and each of the 18-mer windows from the other three serotype genomes. For each candidate target, the minimum Hamming distance observed was recorded, and the candidate targets were sorted in descending order of the minimum observed Hamming distance. Thus, the targets with larger minimum observed Hamming distances were those which showed the least similarity with subsequences from the genomes of the other dengue serotypes. All sequences are listed in Table AII.1. For each candidate target sequence, the NUPACK secondary structure prediction algorithm[34] was used to compute the individual base-pairing probabilities of each base in the target oligomer at equilibrium, along with the minimum free energy structure and the associated free energy. These were recorded and manually inspected to identify target oligomers that displayed the minimal secondary structure, as oligomers without significant secondary structure can more efficiently initiate and execute TMSD reactions. Template strands are fully complementary to each of the selected targets. The incumbent strands match the corresponding target sequences, minus the toehold region at the 5' end of the target sequences, and including 25 bases, which are complementary to the 3' end of the standardized thiol strand. For each TMSD gate, the NUPACK secondary structure prediction algorithm[34] was used to compute the individual base-pairing probabilities, to ensure minimal secondary structure.

4.4.8 Strand Design for DNAzyme Reactions

Previously reported DNAzyme and substrate sequences were modified to include a subsequence that hybridizes to the TSD and TSS strands, respectively.[6,10,17] All sequences are listed in Table AII.2.

4.4.9 Hybridization of TMSD Gates

For each μSLB population, the corresponding ATTO647-labeled incumbent strand [1 μM] was rotated at room temperature for 15 minutes, to allow complete hybridization to the standardized thiol strand. The μSLBs were washed three times in PBS. Next, the Iowa Black RQ-labeled template strand [1 μM] was rotated with the μSLB population at room temperature for 15 minutes, and the μSLBs were washed a final three times. The μSLB concentration was then cut by ¼ to 1.5×10^6 μSLBs/mL, before addition to the multiplex.

4.4.10 Hybridization of DNAzyme Components

For the solution phase DNAzyme experiments the Blocking strand_TSF at a final concentration of 50 nM was rotated at room temperature for 15 minutes, to create a dsDNA region on TSF. The μSLBs were washed three times and the fluorescently labeled substrate strand [50 nM] was then rotated for 15 minutes at room temperature, to allow hybridization to TSS. Finally, the μSLBs were washed three times in the E276-0 buffer (in the absence of $ZnAc_2$). For the surface bound DNAzyme experiments, the DNAzyme strand at a final concentration of 50 nM was rotated with the μSLB population at room temperature for 15 minutes to allow hybridization to TSD, and the μSLBs were washed three times in E276-0. Next, the fluorescently labeled substrate strand [50 nM] was rotated at room temperature for 15 minutes, to allow hybridization to TSS. Finally, the μSLBs were washed three times in E276-0.

4.4.11 Multiplex Formation

To generate the multiplex 50 µL of each µSLBs population, at 1.5×10^6 µSLBs/mL, was added into 300 µL PBS, for a total volume of 500 µL, bringing the total µSLB concentration to 6×10^5 µSLBs/mL. If target was added, only 250 µL of PBS was added, and 50 µL of target at a final concentration of 50 nM was added to bring the final volume to 500 µL. The multiplexed µSLBs were rotated at room temperature for 1 hour and then tested on a Becton Dickinson (Washington, D.C.) LSR Fortessa flow cytometer. All µSLB populations were initially plotted on a forward scatter (FSC) versus side scatter (SSC) plot (see Supporting Information Figure AII.1a), the µSLBs within this gate were then plotted on a green PECF (488/515-545 nm) versus yellow PELR (561/575-590 nm) plot (Supporting Information Figure AII.1b).

4.4.12 TMSD Reactions

Initial strand tests were run on individual TMSD gates, hybridized to the corresponding µSLB population, using the same parameters as those used for the multiplex experiments. Three separate samples were prepared for each TMSD set. A positive control was established by hybridizing the fluorescently labeled incumbent strand, Supporting Information Figure AII.2, in the absence of template strand. Next the incumbent and template strand, which comprised the complete TMSD gate, were hybridized to the corresponding µSLB, the second bar (black) of Supporting Information Figure AII.2. Finally the corresponding target sequences were added to the µSLB population with the complete TMSD gate hybridized, shown in red with black stripes of Supporting Information Figure AII.2.

4.4.13 DNAzyme Reactions

For the solution phase DNAzyme and surface-bound substrate reactions, the substrate is added in excess to the μSLB solution. After 15 minutes of rotation at room temperature we wash away the excess substrate and add solution phase DNAzyme at a given concentration. Our surface-bound DNAzyme and substrate setup begins by adding DNAzyme in excess to the μSLBs with TSD covalently linked to the MPB PE, which creates a surface that has DNAzyme bound to all available TSD strands. These μSLBs are washed and resuspended to remove free DNAzyme in solution. The substrate molecule is added in excess, and washed. This process creates a surface that has all TSS sites taken up by substrate and the DNAzyme molecules either bound to the surface-bound substrate or an excess substrate. After hybridization of the substrate and DNAzyme, the μSLBs were rotated at room temperature in 25 μM Zn^{2+} (E276-25) buffer.

4.4.14 Confocal Microscopy

To verify that DNA-lipid conjugates were freely diffusing on the surface of μSLBs, a multi-photon laser scanning confocal microscope (Olympus FV1000, Tokyo, Japan) with a fluorescence lifetime imaging attachment (Becker & Hickl, Berlin, Germany) was used for fluorescence recovery after photo bleaching (FRAP) experiments. The DNA tag (Cy5, 647/670 nm) laser was run at 15% transmissivity. Run mode was 40 μs/pixel, and stimulus mode was one pre-

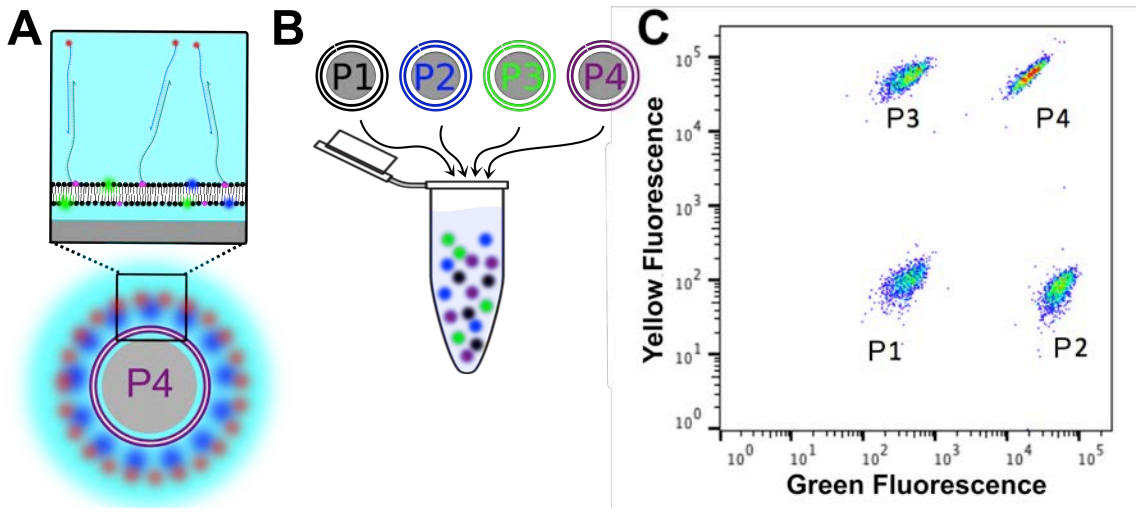

Figure 4.1 - Silica Microsphere Supported Lipid Bilayers (μSLB) A) The supported lipid bilayer (SLB), with a POPC (black circles) base coating a 10 μm SiMS. To generate distinct spectral addresses 0.5 mol% of a lipid tagged with a green fluorophore (PECF) (green circles) and 0.5 mol% of a lipid tagged with a yellow fluorophore (PELR) (blue circles) are added. The maleimide lipid (MPB PE) (magenta circles) is incorporated to enable conjugation of thiolated oligonucleotides. There is a ~2 nm aqueous layer between the microsphere and the bilayer (~5 nm), shown in cyan. The DNA at the surface of the SiMP is shown in blue, and its tag in red. **B)** Four microparticle populations are then combined in a single tube. P1 – 90% POPC, 10% MPB PE. P2 – 89.5% POPC, 10% MPB PE, 0.5% PECF. P3 – 89.5% POPC, 10% MPB PE, 0.5% PELR. P4 – 88.75% POPC, 10% MPB PE, 0.5% PELR, 0.75% PECF. **C)** Bivariate flow cytometry data, showing the 4 microsphere populations in a single tube. The green PECF channel (488/515-545 nm) is plotted on the x-axis, against the yellow PELR channel on the y-axis.

activation frame, and 5 activation frames. The FRAP interval was 3.264 seconds/frame (see Movie AII.1). For the FRAP experiments the Cy5-tagged oligo was hybridized to a thiol strand, which was conjugated to MPB PE (incorporated at 0.5 mol%). The FRAP experiments were run with one batch of MPB PE lipid, the cost of which prohibited replicates across batches, a second data set, from this batch, is included (Supporting Information Figure AII.3).

4.5 Results and Discussion

4.5.1 Preparation of μSLBs

The μSLBs consist of a 10 μm mesoporous silica microsphere bearing a supported POPC or DOPC phospholipid bilayer that contains up to two fluorescently tagged phospholipids for multiplexing and maleimide phospholipids for covalent coupling of DNA molecules that serve as linker strands (**Figure 4.1A**).

Above the transition temperature of the base lipid (-2 ºC for POPC, and <-2 ºC for DOPC), bilayers formed on mesoporous silica microspheres maintain the ability to diffuse laterally.[35,36] Multiplexed μSLB populations are created by incorporation of lipids with fluorescently-labeled headgroups (one with a yellow rhodamine dye (PELR) and one with a green fluorescein dye (PECF)) at varying percentages (**Figure 4.1B**). μSLB populations were analyzed *via* multi-parameter flow cytometry and demonstrated a well resolved 4-plex (**Figure 4.1C**). We have created up to 9-plex μSLB populations (Supporting Information, Figure AII.1b). The approach here represents an advance over our recently reported single fluorophore indexing approach,[19] as it allows facile creation of bivariate populations and higher multiplexing levels. Standard flow cytometry gating (**Figure**

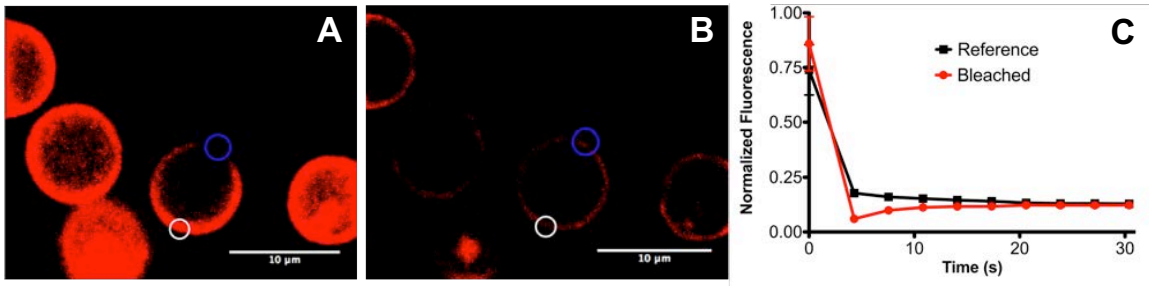

Figure 4.2 - Fluorescence Recovery After Photobleaching (FRAP). A) Frame directly after photobleaching. The blue circle shows the ROI that was bleached, and the white shows the reference. This image was processed in ImageJ (NIH) and a screenshot was taken to show the ROIs. Brightness and contrast were adjusted to overcome the dimness resulting from low concentrations. **B)** Six frames after photobleaching showing full recovery. The entire video is available for viewing (Movie AII.1). **C)** With 0.5 mol% MPB PE, which represents ~×10^6 DNA-lipid conjugates/μSLB. Using simFRAP the diffusion coefficient was calculated to be 0.25 μm^2/sec. The decrease in overall fluorescence, seen in the Reference line as well, is due to photobleaching caused by scanning laser confocal microscopy. The error bars represent standard error of mean for 5 replicates.

4.1C) let us use a single reporter fluorophore to monitor reactions taking place on individual microsphere populations, thereby enabling multiplexed reporting with a limited number of fluorophores. Within the time frame of our experiments the

microsphere populations remain discretely separated (Supporting Information, Figure AII.4).

4.5.2 Demonstration of Lipid Bilayer Fluidity *via* FRAP

Figure 4.2 shows DNA-lipid conjugate diffusion on a μSLB with 0.5 mol% MPB PE. While this concentration is predicted to provide ~10^6 conjugation sites per μSLB, typical conjugation efficiencies to the surface are expected to result in a small fraction of available sites to be covalently linked to the available thiolated lipids within the μSLB. Less than optimal conjugation efficiencies, along with potentially uneven partitioning of the MPB PE between the two leaflets of the bilayer[33], make it difficult to provide a precise calculation of the number of Cy5 molecules on the surface. Regardless, **Figure 4.2** shows photobleaching (panel A) and then recovery (panel B), respectively, on the surface of a μSLB. For the FRAP experiments the Cy5 bearing DNA oligo was used because ATTO647 does

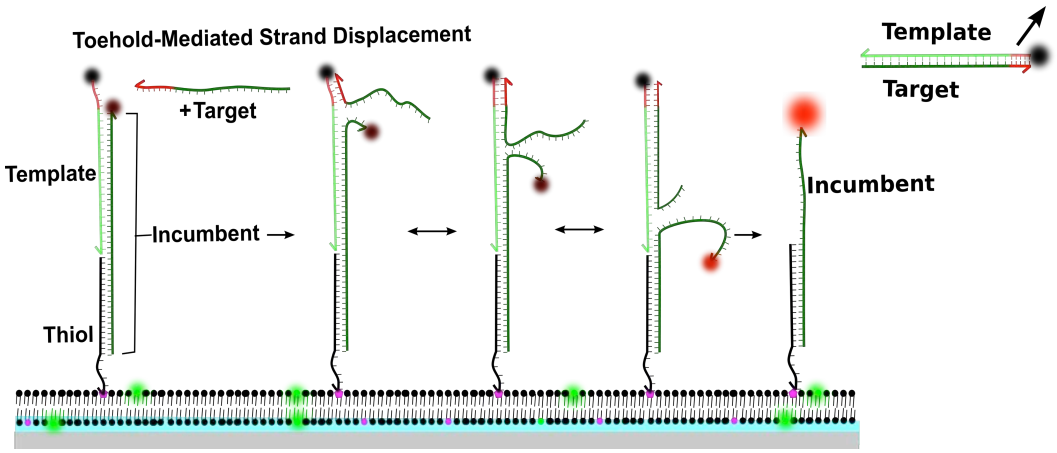

Figure 4.3 - TMSD Reaction on μSLB Surface - The gate comprises an ATTO647-labeled incumbent strand hybridized to the thiol linker that attaches it to the μSLB. The μSLB is composed of POPC (black circles), a lipid with a headgroup labeled with a green fluorophore (green circles), and for the TMSD reactions MPB PE (magenta circles) is incorporated at 10 mol%. The part of the incumbent that is not hybridized to the linker is fully complementary to a longer Iowa Black RQ-labeled template strand. Thus the gate complex has a double-stranded DNA (dsDNA) region with a short ssDNA overhang on the template strand. In the template/incumbent duplex fluorescence is blocked *via* fluorescence resonance energy transfer (FRET). Upon binding of the target strand branch migration begins. Eventually the template strand is displaced and fluorescence increases for the microparticle population.

not readily photobleach. The fluorescence data were plotted as a function of time (**Figure 4.2C**), and using the ImageJ plug-in simFRAP[37], the diffusion coefficient was calculated as 0.25 μm^2/second, which falls just below the expected range of 0.5 – 5 μm^2/second for fluid phospholipid bilayers at room temperature.[33,38] While multiple factors, such as variance between lipid preparations or differing conjugation efficiencies might result in variations in this calculated value, the value is comparable to diffusion coefficients reported for DNA oligos tethered to vesicles.[39] While further studies are underway to confirm the effect of DNA conjugation on lipid diffusion, it is evident from this data that DNA-lipid conjugates do diffuse and will allow DNA molecules to move from their original attachment point.

4.5.3 Multiplexed TMSD Reactions

To demonstrate the utility of multiplexed μSLBs, we constructed a Dengue serotype specific TMSD gate on each of four microsphere populations. The four gates were designed to target one of four single-stranded DNA (ssDNA) target sequences chosen from the genomes of the four dengue virus serotypes (Dengue 1 – 4, from GenBank sequence accession numbers NC_001477.1, NC_001474.2, NC_001475.2, and NC_002640.1 respectively). **Figure 4.3** presents the mechanism of a basic TMSD reaction in the context of the μSLB system. For the TMSD reactions, the linker strand sequence is complementary to a binding region on the TMSD gate structures. For each microsphere population, the corresponding TMSD gate was annealed and hybridized to the linker strand and washed (see

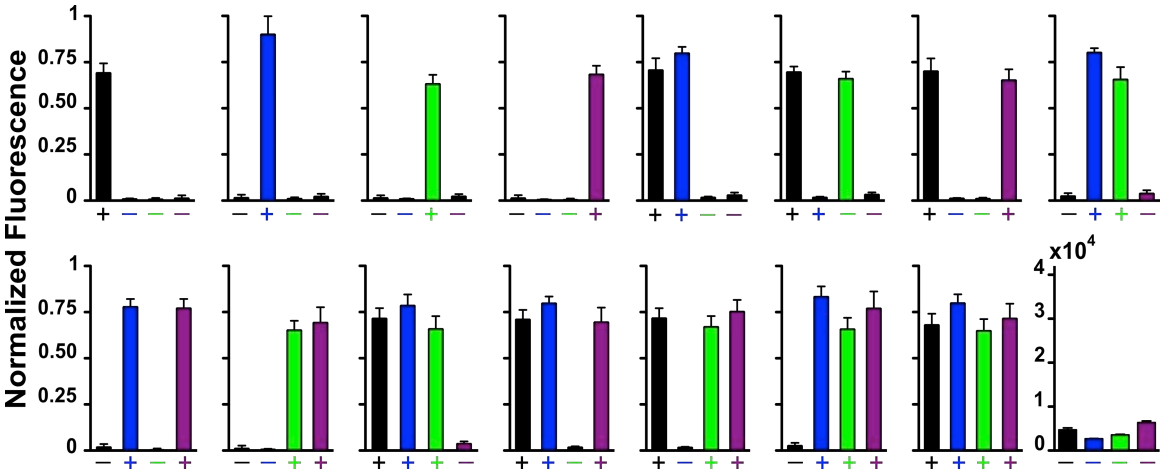

Figure 4.4 - Dengue Serotyping Assay. Response for all multiplexed microsphere populations, in the presence of 16 possible combinations of four ssDNA targets relevant to Dengue serotyping. For each chart the addition of target is indicated by +, lack of target is indicated by –. The lower right (- - - -) was used as a baseline, and was subtracted from the remaining 15 charts. This chart is not normalized, but plotted as median fluorescence. The other 15 charts were normalized to an arbitrary number (1 = 3.6×10^4 fluorescent units on the ATTO647 channel (640/663-677 nm)), which ensures that all values are plotted on the same scale. The limit of detection is 3 nM. Error bars represent standard error of mean for 3 replicates.

Supporting Information, Figure AII.5 for depiction of individual TMSD gates, and Figure AII.2 for functionality of individual TMSD gates). The four μSLB populations were combined in a single tube and various combinations of target strands were added at 50 nM, and the solution was rotated at room temperature for 1 hour. In the presence of the correct target sequence, the corresponding template strands, bearing quenchers, were displaced and fluorescence of the ATTO647 tagged incumbent strand increased due to dequenching. To demonstrate specificity, we used the four multiplexed receptor populations to detect all 16 possible combinations of the four target strands in 16 single tube assays with high signal-to-background ratios (**Figure 4.4**). Using established methods,[40] we calculated the limit of detection as 3 nM (see Supporting Information/Appendix II page 3). We include this value, not in direct competition with current DNA or RNA techniques that use target amplification (e.g., PCR), [41,42] but to establish the limits of the

system, which compare favorably with the nanomolar dissociation constants typically encountered in many bioassays. This system demonstrates the feasibility of using multiplexed μSLBs to monitor specific reactions in a multi-reaction system individually.

4.5.4 Optimization of Conditions for DNAzyme Reactions

To demonstrate the modularity of the μSLB platform, we also used it to perform DNAzyme reactions. To optimize experimental conditions for DNAzyme reactions, we began by studying the interactions of a fluorescent substrate analog with the μSLB surface in conditions typical of solution phase DNAzyme reactions (1 M NaCl, 1 mM $ZnAc_2$, and 50 mM HEPES).[6,10] The inclusion of $ZnAc_2$ in this buffer was crucial because the 8-17 DNAzyme requires Zn^{2+} ions as cofactors for its catalytic activity.[16] We show schematic scenarios in **Figure 4.5** and report results in **Figure 4.6**. The blank μSLB (**Figure 4.5A**) had a non-complementary strand (TSF) conjugated to the bilayer, but was not exposed to the fluorescent substrate analog. The negative control μSLB (**Figure 4.5B**) contained the fluorescent substrate analog in solution with TSF. The experimental μSLB (**Figure 4.5C**) contained the fluorescent substrate analog in solution with the correct linker strand (TSS) conjugated to the bilayer. Thus, nonspecific binding is likely occurring in both systems, and the equivalent binding levels suggest that at higher Zn^{2+} concentrations nonspecific binding is dominant. The purpose of including TSF in the negative control was to ensure that the total amount of DNA conjugated to the μSLB surface (and thus the electrostatic environment) was constant. **Figures 4.5D and 4.5E** depict the system in the absence of Zn^{2+} and **Figure 4.5F** depicts the system with Zn^{2+} at 0.1 mM. With 1 mM Zn^{2+}, we saw the same amount of DNA

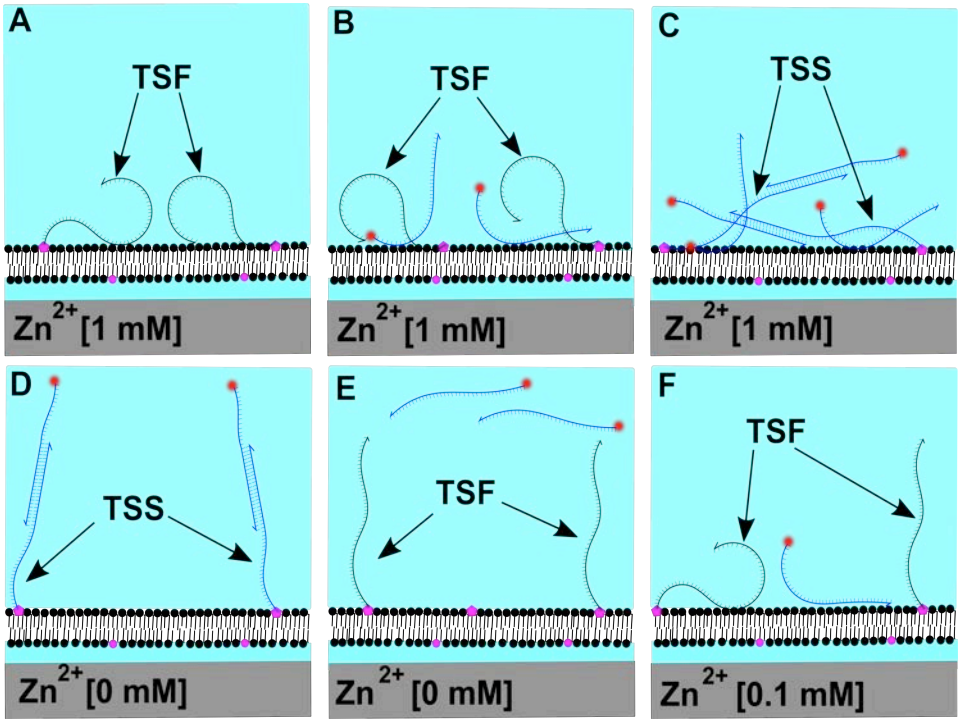

Figure 4.5 - Non-Specific Interactions. A) Blank control, which has not been exposed to the fluorescently labeled (Cy5) strand. **B)** Bead population with non-complementary TSF conjugated to the bilayer in the presence of 1 mM Zn^{2+}. **C)** Bead population with TSS conjugated to the bilayer in the presence of 1 mM Zn^{2+}. TSS is complementary and hybridizes the Cy5 labeled strand. **D)** Bead population with TSS conjugated to the bilayer in the absence of Zn^{2+}. **E)** Bead population with TSF conjugated to the bilayer in the absence of Zn^{2+}. **F)** Bead population with TSF conjugated to the bilayer in the presence of 0.1 mM Zn^{2+}.

binding to the negative control μSLB as the experimental μSLB (**Figure 4.6A**). The lack of specific binding is consistent with the literature, which shows that divalent cations, such as Zn^{2+}, form "salt bridges" between DNA and zwitterionic lipid headgroups (here, DOPC), leading to non-specific binding of DNA to the bilayer.[43,44] Our results show that as Zn^{2+} is increased from 0 to 100 μM nonspecific binding increases. In the absence of Zn^{2+} and at Zn^{2+} concentrations of 100 mM and below we see that non-specific binding is greatly reduced (**Figure 4.6B**), presumably due to reduced salt bridge formation. This data suggested that 25 μM was the optimal Zn^{2+} concentrations for specific TSS hybridization.

As solution phase experiments have routinely used 1 mM Zn^{2+} for optimal DNAzyme activity,[6,10] we compared the activity of the DNAzyme at 25 μM and 1 mM Zn^{2+} using a FRET substrate in solution. While the DNAzyme had reduced activity at 25 μM Zn^{2+} vs. 1 mM Zn^{2+}, the reaction ran to completion in ~2 hours (**Figure 4.6C**). Finally, as lipids aggregate during extrusion in the presence of 1 M NaCl, which complicates the process of vesicle formation by extrusion, we tested the effects of reduced sodium chloride concentration on DNAzyme reactions run at 25 μM Zn^{2+}(**Figure 4.6D**, for the kinetic traces see Figure AII.6). The experiment indicated that 276 mM NaCl performed similarly to the typical solution phase concentration of 1 M NaCl. Therefore, 276 mM was used in our DNAzyme experiments on μSLBs, as this concentration did not cause lipid aggregation.

4.5.5 DNAzyme Reactions

We configured μSLB-based DNAzyme reactions in one of two ways: in the first there is a solution phase DNAzyme and the substrate molecule is surface-bound *via* hybridization to a partially complementary bilayer-conjugated oligomer (TSS), as shown in **Figure 4.7A**, and in the second both the DNAzyme and the substrate are surface-bound *via* conjugated linker strands, the substrate to TSS as before and the DNAzyme to an orthogonal linker strand (TSD), as shown in **Figure 4.7B**. Both of these approaches are easily monitored through loss-of-fluorescence assays with flow cytometry,[45,46] which provides excellent discrimination between free vs. bound signals at the surface of microspheres.[46]

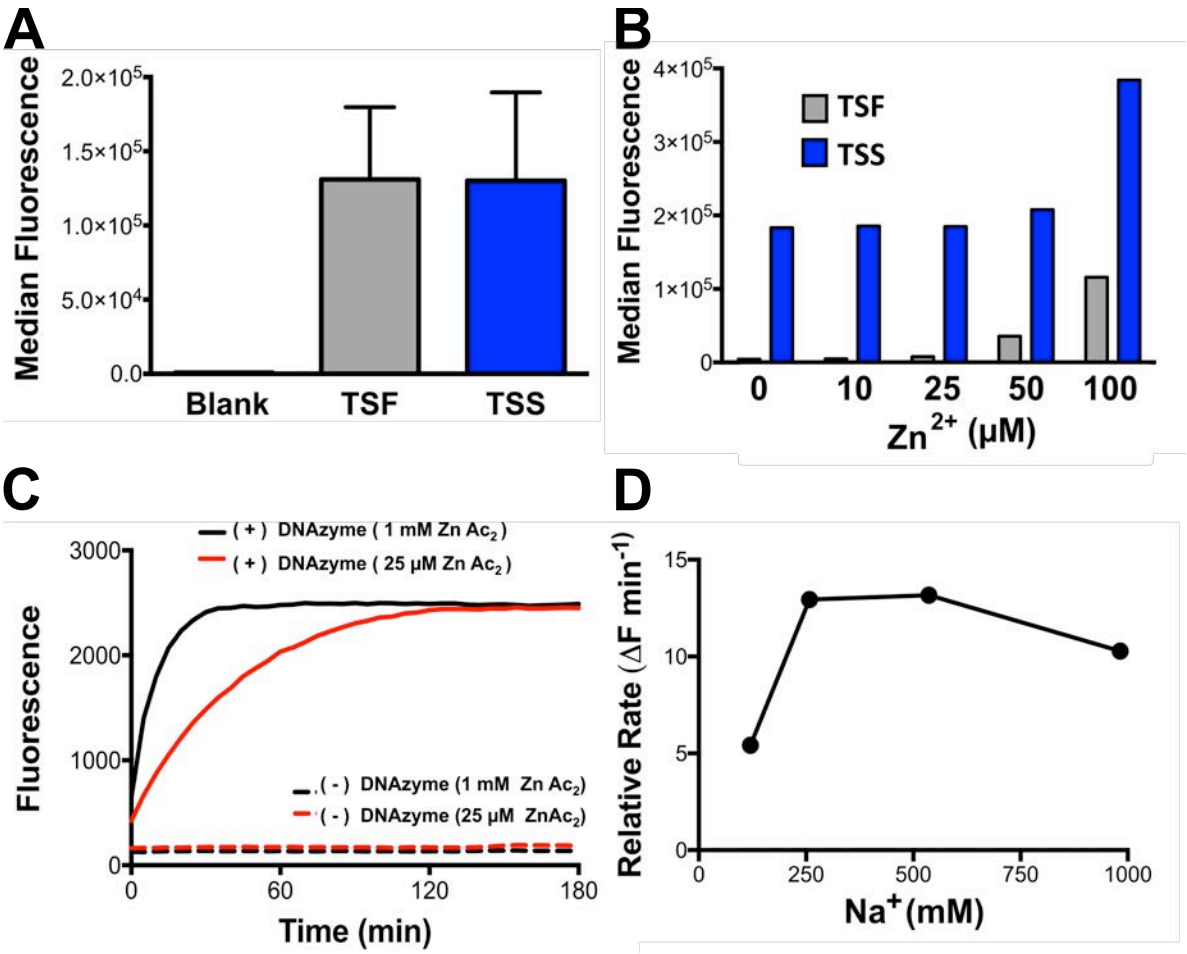

Figure 4.6 - Optimization of Buffer Conditions A) Three bead populations in the presence of 1 mM $ZnAc_2$. The blank bead population has TSF conjugated to the bilayer and has not been exposed to the fluorescently labeled (Cy5) strand, the second has TSF conjugated to the bilayer, and the third has TSS conjugated to the bilayer. Error bars represent standard error of the mean for 3 replicates. **B)** TSF and TSS bead populations in the presence of increasing $ZnAc_2$ concentrations. Again, TSF will not hybridize the Cy5-labeled strand and so any fluorescence is a result of non-specific binding to the μSLB, and TSS does hybridize the Cy5-labeled strand and fluorescence above the TSF level is specific and due to hybridization to TSS. **C)** Solution phase DNAzyme and solution phase substrate reaction with 1 mM $ZnAc_2$, which is the standard concentration for DNAzyme reactions, and 25 μM $ZnAc_2$. The 25μM reaction is slower compared to the standard but is completed at 2 hours. **D)** Relative rates of solution phase DNAzyme and solution phase substrate reactions in the presence of increasing Na^+ concentrations. The standard DNAzyme concentration is 1 M; however, optimal rates were achieved at 276 mM Na^+.

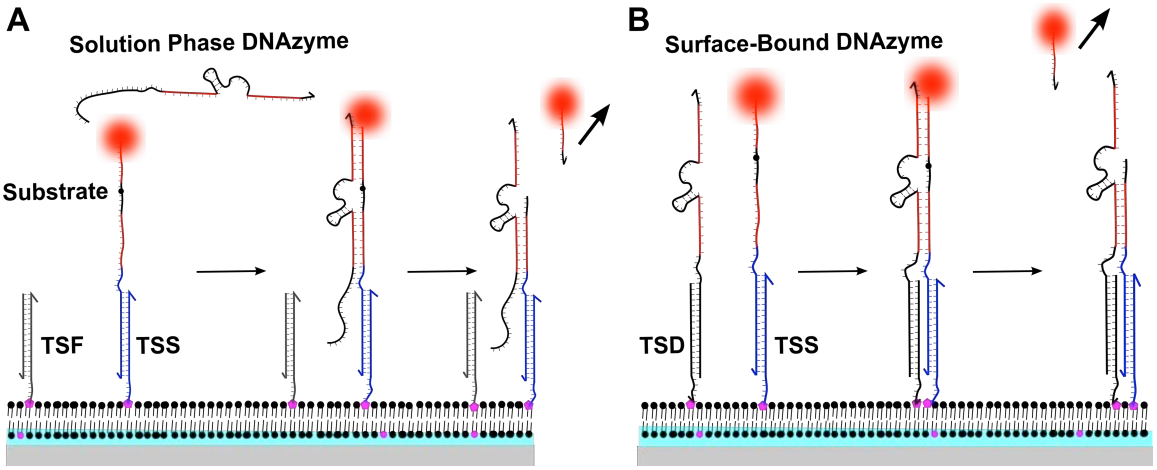

Figure 4.7 - DNAzyme Reaction Schemes. A) Solution Phase DNAzyme - For all DNAzyme experiments, the lipid bilayer is composed of DOPC (black dots), which increases the diffusivity of the bilayer as compared to POPC, and MPB PE is incorporated at 1 mol%. For this first set of DNAzyme reactions there are 2 thiol strands conjugated: the thiol strand that hybridizes the substrate (TSS) and a space filler thiol strand (TSF). The DNAzyme hybridizes the surface-bound substrate, and cleavage occurs in the presence of metal ion cofactors, 25 μM Zn^{2+}. After cleavage of the substrate the DNAzyme dissociates from the substrate-binding arms and returns into solution along with the fluorescently labeled upper portion of the substrate, and fluorescence decreases for the microsphere population. **B) Surface-Bound DNAzyme** - TSS and a thiol strand that hybridized the DNAzyme (TSD) present on the bilayer. The surface-bound DNAzyme and substrate diffuse and hybridize and cleavage occurs in the presence of metal ion cofactors, 25 μM Zn^{2+}. After cleavage of the substrate the fluorescently labeled upper portion of the substrate moves into solution, and fluorescence decreases for the microsphere.

Using optimized assay conditions, we performed reactions where solution phase DNAzyme cleaved surface-bound substrates (**Figure 4.7A**) at varying concentrations of Zn^{2+}. While we observed signal (i.e., loss of fluorescence) at concentrations greater than 10 μM Zn^{2+}, the best signal-to-noise ratio was observed at 25 μM Zn^{2+} (**Figure 4.8A**). The signal becomes unobservable at higher Zn^{2+} as a result of non-specific binding, which overwhelms any loss of fluorescence due to DNAzyme activity. The data presented in **Figure 4.8A**, along with the non- specific interaction experiments (**Figure 4.6B**), indicate that the optimal Zn^{2+} concentration is 25 μM. Having optimized the buffer conditions for the μSLBs system, we tested the effect of having higher concentrations of solution phase DNAzyme cleaving surface-bound substrate. Using the same setup as above, we added DNAzyme to the solution at final concentrations of 50 nM, 150

nM, 500 nM, and 1.5 μM. The microspheres were then incubated for 1 hour in the absence of Zn^{2+} prior to initiating the reactions with the addition of 25 μM Zn^{2+}. The results (**Figure 4.8B**) show an increased loss of fluorescence at higher concentrations. The rapid initial loss of fluorescence at higher concentrations is likely due to an increased on-rate for the solution phase DNAzyme to the surface-bound substrate. It is also notable that even at high concentrations of DNAzyme the cleavage does not remove all fluorescence from the μSLBs. This is most likely due to either non-specific interaction between the fluorescent substrate and the μSLB or some level of substrate inaccessibility during the cleavage reaction.

Finally, we aimed to demonstrate that surface-bound DNAzymes could cleave surface-bound substrates, as shown schematically in **Figure 4.7B**. Here, the ratio of substrate to DNAzyme on the surface is set by the initial conjugation reactions, so we added a 4-fold higher concentration of TSS (which hybridizes to the substrate) than TSD (which hybridizes to the DNAzyme). This estimate of a 4:1 ratio of substrate to DNAzyme concentration on the surface assumes that there is no bias between the efficiency of conjugation for TSS and TSD. We believe that this assumption is valid because the only difference between the TSD and the TSS strands is in nucleotide sequence. However, the potential partitioning of the maleimide lipids[33,38] and inability to guarantee highly efficient conjugation efficiency, due to low percentages of maleimide on the μSLB surface and/or charge effects of the phospholipid headgroups, precludes the precise calculation of surface-attached molecules. Regardless of the exact concentration of surface molecules, addition of Zn^{2+} at 25 μM results in rapid loss of fluorescence from

μSLBs compared with the negative control, a μSLB with TSF conjugated in place of TSD and no DNAzyme present, indicating successful cleavage of surface-bound substrate by surface-bound DNAzyme (**Figure 4.8C**). However, the loss of fluorescence is not complete, which is consistent with observations for solution phase DNAzyme cleaving substrate from μSLB

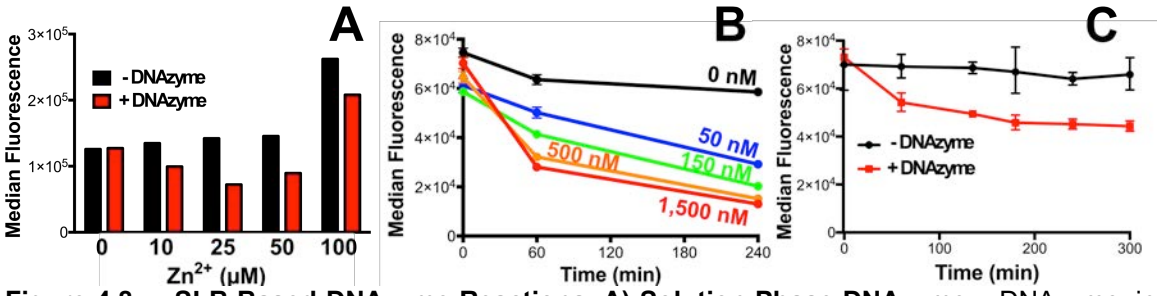

Figure 4.8 - μSLB-Based DNAzyme Reactions. A) Solution Phase DNAzyme – DNAzyme, in solution at a final concentration of 50 nM, and surface-bound substrate reactions in the presence of increasing Zn^{2+} concentration. Optimal cleavage was seen at 25 μM Zn^{2+}. **B) Solution Phase DNAzyme** - Surface-bound substrate, with increasing solution phase DNAzyme concentrations. No DNAzyme was added for the black trace; this is our negative control. The blue trace is 50 nM DNAzyme, the green 150 nM, the orange 500 nM, and the red 1.5 μM. Error bars are standard error of the mean for 3 replicates. **C) Surface-Bound DNAzyme** – Reaction with both DNAzyme and substrate surface-bound, showing ~30% decrease in fluorescence. For this reaction there was a fourfold excess of TSS, compared with TSD. The reaction was run with 276 mM Na^{+} and 25 μM Zn^{2+}. Error bars are standard error of the mean for 3 replicates.

surfaces. Again, this lack of completion may be due to non-specific binding of cleaved substrate to the μSLB surface or substrate inaccessibility, but it also might be due to more complex effects such as reduced dissociation of DNAzyme from cleaved substrates that are bound to a surface (see Appendix V for a description of efforts to destabilize the post cleavage products). Our graphical representations of the model show cleavage of the substrate molecule, but they do not show disassociation of the DNAzyme and lower portion of the substrate because we do not have evidence that disassociation is occurring. While it remains possible that reduced or limited diffusion of DNAzyme and substrates on the surface could also result in the observed incomplete cleavage, we do not believe such effects occur

since a diffusion coefficient of 0.25 μm^2/sec is measured for the conjugated DNA molecules on μSLB surfaces (**Figure 4.3** and Movie AII.1).

Future work will investigate the detailed mechanisms of DNAzyme reactions on μSLB surfaces, which are expected to be affected by surface transport principles that have been explored in detail for receptor protein interactions on surfaces. [47] Such work will benefit from more robust methods of DNA integration into the bilayer, which include oligomer modifications such as cholesterol tags (preliminary efforts are presented in Appendix V), or copper(1)-catalyzed conjugation of an azide and an alkyne.[48] Improving DNA integration into the bilayer will enable precise control over membrane bound DNA concentrations, which is critical to detailed mechanistic studies of such systems. Another fruitful direction may be to investigate programmable control of the diffusion rates of DNA components integrated with the bilayer, which might be achieved by modulating the physical properties of the bilayer or of the components themselves (e.g., to incorporate a second bilayer linker to provide additional drag on the diffusion process). Such a system could then potentially be used to implement two-dimensional spatial patterning on the microparticle surface, such as that achieved *via* reaction-diffusion systems in protein systems on membranes[49].

4.6 Conclusions

In summary, we implemented DNA-based molecular computing systems, using fluid, microsphere-supported lipid bilayers. These systems provide a multiplexable platform for bioassay development, and as a proof of concept here we designed DNA strand displacement gates for the detection of the four Dengue serotypes and demonstrated that every combination of the four targets was

correctly identified. We then optimized the system to allow DNAzyme reactions to be carried out on a zwitterionic lipid bilayer, in the presence of divalent cations. The use of a fluid bilayer as the supporting surface allows multi-component reactions to be engineered, which may eventually be used for signal amplification if multiple turnover reactions can be demonstrated. Thus, this work offers a route toward the implementation of sophisticated, multi-reaction cascades on single particle surfaces and/or compartmentalization of particular reactions on individual particles. Such DNA-lipid conjugate systems, with stable and tunable bilayers that are easily monitored using flow cytometery, could lead to new smart materials with potential applications in targeted drug delivery, advanced molecular computation, and self-assembling nanomaterials.

4.7 Associated Content

4.7.1 Supporting Information

The Supporting Information is available free of charge on the ACS Publications website at DOI: 10.1021/acsami.7b11046.

The Supporting Information document includes all supplementary figures as described in the main text, details on strand design, the non-specific interaction controls, the limit of detection calculations, details on the confocal microscopy experiments, and merging data for multiplex microspheres.

Three movies are included as well.

Movie AII.1 (AVI): A video of Fluorescence Recovery After Photobleaching (FRAP) data for our microsphere systems.

Movie AII.2 (AVI): A video of a confocal stack of images of showing the fluorescence from the DNA lipid-conjugate as described in the text of the Supporting Information File.

Movie AII.3 (AVI): A video of a confocal stack of images of showing the fluorescence from the lipid (PECF) channel as described in the text of the Supporting Information File.

4.8 Author Information

4.8.1 Corresponding Authors

*graves@unm.edu, *darko@cs.unm.edu, *mlakin@cs.unm.edu

4.8.2 Present Address

† Center for Bio/Molecular Science and Engineering, Code 6900, U.S. Naval Research Laboratory, Washington, DC 20375, USA and College of Science, George Mason University, Fairfax, Virginia 22030, USA

4.8.3 Author Contributions

All authors contributed to writing the paper. AFW, NAB and MEF conducted experiments. MRL designed sequences. CWB ran initial multiplexing experiments. APS, NFO and GAM assisted with FRAP analysis, membrane characterization, and lipid design. DS, MRL and SWG supervised the project.

4.8.4 Funding Sources

This material is based upon work supported by the National Science Foundation under grants 1525553, 1518861, and 1318833. Assay development for Dengue was in part supported by NIH NIAID 5 R21 AI115105-02. The LRS Fortessa data was collected at the UNM Shared Flow Cytometry and High Throughput Screening Resource Center supported by the University of New Mexico Health Sciences Center and the University of New Mexico Cancer Center

with current funding from NCI 2P30 CA118100-11 "UNM Cancer Center Support Grant". This work was performed, in part, at the Center for Integrated Nanotechnologies, an Office of Science User Facility operated for the U.S. Department of Energy (DOE) Office of Science. Los Alamos National Laboratory, an affirmative action equal opportunity employer, is operated by Los Alamos National Security, LLC, for the National Nuclear Security Administration of the U.S. Department of Energy under contract DE-AC52-06NA25396.

4.8.5 Notes

SWG, MRL, and DS have financial interest in a company, Helion Scientific, Inc., which is exploring the use of molecular logic technologies for biological assays.

4.9 Acknowledgements

The authors would like to thank Loreen Stromberg, for training and assistance with the confocal imaging and FRAP experiments at the Center for Integrated Nanotechnologies (CINT, and Milan Stojanovic, for suggestions regarding the diffusion experiments.

4.10 Abbreviations

μSLB(s), silica microsphere supported lipid bilayer(s); **TMSD**, toehold-mediated strand displacement; **POPC**, 1-palmitoyl-2-oleoyl-*sn*-glycero-3-phosphocholin; **DOPC**, 1,2-dioleoyl-*sn*-glycero-3-phosphocholine; **MPB PE**, 1,2-dioleoyl-*sn*-glycero-3-phosphoethanolamine-N-[4-(p-maleimidophenyl) butyramide]; **PECF**, 1,2-dioleoyl-*sn*-glycero-3-phosphoethanolamine-N-(carboxyfluorescein); **PELR**, 1,2-dioleoyl-*sn*-glycero-3-phosphoethanolamine-N-(lissamine rhodamine B sulfonyl); **BSA**, bovine serum albumin; **PBS**, phosphate buffered saline

4.11 References

(1) Stojanovic, M. N.; Stefanovic, D. A Deoxyribozyme-Based Molecular Automaton. *Nat Biotechnol* **2003**, *21* (9), 1069–1074.

(2) Seelig, G.; Soloveichik, D.; Zhang, D. Y.; Winfree, E. Enzyme-Free Nucleic Acid Logic Circuits. *Science* **2006**, *314* (5805), 1585–1588.

(3) Katz, E.; Privman, V. Enzyme-Based Logic Systems for Information Processing. *Chem. Soc. Rev.* **2010**, *39* (5), 1835–1857.

(4) Funke, J. J.; Dietz, H. Placing Molecules with Bohr Radius Resolution Using DNA Origami. *Nat. Nanotechnol.* **2016**, *11* (1), 47–52.

(5) Mohammed, A. M.; Šulc, P.; Zenk, J.; Schulman, R. Self-Assembling DNA Nanotubes to Connect Molecular Landmarks. *Nat. Nanotechnol.* **2017**, *12* (4), 312–316.
(6) Brown, C. W., III; Lakin, M. R.; Fabry-Wood, A.; Horwitz, E. K.; Baker, N. A.; Stefanovic, D.; Graves, S. W. A Unified Sensor Architecture for Isothermal Detection of Double-Stranded DNA, Oligonucleotides, and Small Molecules. *ChemBioChem* **2015**, *16* (5), 725–730.
(7) Wang, F.; Elbaz, J.; Willner, I. Enzyme-Free Amplified Detection of DNA by an Autonomous Ligation DNAzyme Machinery. *J. Am. Chem. Soc.* **2012**, *134* (12), 5504–5507.
(8) Gerasimova, Y. V.; Cornett, E. M.; Edwards, E.; Su, X.; Rohde, K. H.; Kolpashchikov, D. M. Deoxyribozyme Cascade for Visual Detection of Bacterial RNA. *ChemBioChem* **2013**, *14* (16), 2087–2090.
(9) Allen, P. B.; Arshad, S. A.; Li, B.; Chen, X.; Ellington, A. D. DNA Circuits as Amplifiers for the Detection of Nucleic Acids on a Paperfluidic Platform. *Lab Chip* **2012**, *12* (16), 2951–2958.
(10) Brown, C. W., III; Lakin, M. R.; Horwitz, E. K.; Fanning, M. L.; West, H. E.; Stefanovic, D.; Graves, S. W. Signal Propagation in Multi-Layer DNAzyme Cascades Using Structured Chimeric Substrates. *Angew. Chem. Int. Ed.* **2014**, *53* (28), 7183–7187.
(11) Lu, C.-H.; Wang, F.; Willner, I. Zn 2+-Ligation DNAzyme-Driven Enzymatic and Nonenzymatic Cascades for the Amplified Detection of DNA. *J. Am. Chem. Soc.* **2012**, *134* (25), 10651–10658.
(12) You, M.; Zhu, G.; Chen, T.; Donovan, M. J.; Tan, W. Programmable and Multiparameter DNA-Based Logic Platform for Cancer Recognition and Targeted Therapy. *J. Am. Chem. Soc.* **2015**, *137* (2), 667–674.
(13) Pei, H.; Liang, L.; Yao, G.; Li, J.; Huang, Q.; Fan, C. Reconfigurable Three-Dimensional DNA Nanostructures for the Construction of Intracellular Logic Sensors. *Angew. Chem. Int. Ed. Engl.* **2012**, *51* (36), 9020–9024.
(14) Liu, J.; Karpus, J.; Wegner, S. V.; Chen, P. R.; He, C. Genetically Encoded Copper(I) Reporters with Improved Response for Use in Imaging. *J. Am. Chem. Soc.* **2013**, *135* (8), 3144–3149.
(15) Breaker, R. R.; LI, Y. Deoxyribozymes: New Players in the Ancient Game of Biocatalysis. *Current Opinion in Structural Biology* **1999**, *9*, 315–323.
(16) Li, J.; Zheng, W.; Kwon, A. H.; Lu, Y. In Vitro Selection and Characterization of a Highly Efficient Zn(II)-Dependent RNA-Cleaving Deoxyribozyme. *Nucleic Acids Research* **1999**, *28* (2), 481–488.
(17) Schlosser, K.; LI, Y. A Versatile Endoribonuclease Mimic Made of DNA: Characteristics and Applications of the 8-17 RNA-Cleaving DNAzyme. *ChemBioChem* **2010**, *11* (7), 866–879.
(18) Pei, R.; Matamoros, E.; Liu, M.; Stefanovic, D.; Stojanovic, M. N. Training a Molecular Automaton to Play a Game. *Nat. Nanotechnol.* **2010**, *5* (11), 773–777.
(19) Fernandez Oropeza, N.; Zurek, N. A.; Galvan-De La Cruz, M.; Fabry-Wood, A.; Fetzer, J. M.; Graves, S. W.; Shreve, A. P. Multiplexed Lipid Bilayers on Silica Microspheres for Analytical Screening Applications. *Anal.*

Chem. **2017**, *89* (12), 6440–6447.
(20) Nolan, J. P.; Mandy, F. Multiplexed and Microparticle-Based Analyses: Quantitative Tools for the Large-Scale Analysis of Biological Systems. *Cytometry* **2006**, *69A* (5), 318–325.
(21) Piyasena, M. E.; Graves, S. W. The Intersection of Flow Cytometry with Microfluidics and Microfabrication. *Lab Chip* **2014**, *14* (6), 1044–1059.
(22) Langecker, M.; Arnaut, V.; List, J.; Simmel, F. C. DNA Nanostructures Interacting with Lipid Bilayer Membranes. *Acc. Chem. Res.* **2014**, *47* (6), 1807–1815.
(23) Yasuga, H.; Kawano, R.; Takinoue, M.; Tsuji, Y.; Osaki, T.; Kamiya, K.; Miki, N.; Takeuchi, S. Logic Gate Operation by DNA Translocation Through Biological Nanopores. *PLoS ONE* **2016**, *11* (2), e0149667.
(24) Yasuga, H.; Kawano, R.; Takinoue, M.; Tsuji, Y.; Osaki, T.; Kamiya, K.; Miki, N.; Takeuchi, S. Droplet Network Connected by Biological Nanopores for DNA Computing; 2013; pp 1221–1222.
(25) Yashin, R.; Rudchenko, S.; Stojanovic, M. N. Networking Particles Over Distance Using Oligonucleotide-Based Devices. *J. Am. Chem. Soc.* **2007**, *129* (50), 15581–15584.
(26) Teichmann, M.; Kopperger, E.; Simmel, F. C. Robustness of Localized DNA Strand Displacement Cascades. *ACS Nano* **2014**, *8* (8), 8487–8496.
(27) Chatterjee, G.; Dalchau, N.; Muscat, R. A.; Phillips, A.; Seelig, G. A Spatially Localized Architecture for Fast and Modular Computation at the Molecular Scale. *bioRxiv* **2017**, 110965.
(28) Gerasimova, Y. V.; Kolpashchikov, D. M. Towards a DNA Nanoprocessor: Reusable Tile-Integrated DNA Circuits. *Angew. Chem. Int. Ed. Engl.* **2016**, *55* (35), 10244–10247.
(29) Chandran, H.; Gopalkrishnan, N.; Phillips, A.; Reif, J. Localized Hybridization Circuits. In *DNA Computing and Molecular Programming*; Springer, Berlin, Heidelberg, 2011; pp 64–83.
(30) Muscat, R. A.; Strauss, K.; Ceze, L.; Seelig, G.; Muscat, R. A.; Strauss, K.; Ceze, L. *DNA-Based Molecular Architecture with Spatially Localized Components*; ACM, 2013; Vol. 41, pp 177–188.
(31) Ädelroth, P.; Brzezinski, P. Surface-Mediated Proton-Transfer Reactions in Membrane-Bound Proteins. *Biochimica et Biophysica Acta (BBA) - Bioenergetics* **2004**, *1655*, 102–115.
(32) Rezwan, K.; Meier, L. P.; Gauckler, L. J. Lysozyme and Bovine Serum Albumin Adsorption on Uncoated Silica and AlOOH-Coated Silica Particles: the Influence of Positively and Negatively Charged Oxide Surface Coatings. *Biomaterials* **2005**, *26* (21), 4351–4357.
(33) Howland, M. C.; Sapuri-Butti, A. R.; Dixit, S. S.; Dattelbaum, A. M.; Shreve, A. P.; Parikh, A. N. Phospholipid Morphologies on Photochemically Patterned Silane Monolayers. *J. Am. Chem. Soc.* **2005**, *127* (18), 6752–6765.
(34) Dirks, R. M.; Bois, J. S.; Schaeffer, J. M.; Winfree, E.; Pierce, N. A. Thermodynamic Analysis of Interacting Nucleic Acid Strands. *SIAM Rev.* **2007**, *49* (1), 65–88.

(35) Piyasena, M. E.; Zeineldin, R.; Fenton, K.; Buranda, T.; Lopez, G. P. Biosensors Based on Release of Compounds Upon Disruption of Lipid Bilayers Supported on Porous Microspheres. *Biointerphases* **2008**, *3* (2), 38–49.
(36) Conway, J. W.; Madwar, C.; Edwardson, T. G.; McLaughlin, C. K.; Fahkoury, J.; Lennox, R. B.; Sleiman, H. F. Dynamic Behavior of DNA Cages Anchored on Spherically Supported Lipid Bilayers. *J. Am. Chem. Soc.* **2014**, *136* (37), 12987–12997.
(37) Blumenthal, D.; Goldstien, L.; Edidin, M.; Gheber, L. A. Universal Approach to FRAP Analysis of Arbitrary Bleaching Patterns. *Nature* **2015**, *5*, 11655.
(38) Shreve, A. P.; Howland, M. C.; Sapuri-Butti, A. R.; Allen, T. W.; Parikh, A. N. Evidence for Leaflet-Dependent Redistribution of Charged Molecules in Fluid Supported Phospholipid Bilayers. *Langmuir* **2008**, *24* (23), 13250–13253.
(39) Yoshina-Ishii, C.; Chan, Y.-H. M.; Johnson, J. M.; Kung, L. A.; Lenz, P.; Boxer, S. G. Diffusive Dynamics of Vesicles Tethered to a Fluid Supported Bilayer by Single-Particle Tracking. *Langmuir* **2006**, *22* (13), 5682–5689.
(40) Long, G. L.; Winefordner, J. D. Limit of Detection. *Anal. Chem.* **1983**, *55* (7), 712–724.
(41) Mokany, E.; Bone, S. M.; Young, P. E.; Doan, T. B.; Todd, A. V. MNAzymes, a Versatile New Class of Nucleic Acid Enzymes That Can Function as Biosensors and Molecular Switches. *J. Am. Chem. Soc.* **2010**, *132* (3), 1051–1059.
(42) Gerasimova, Y. V.; Kolpashchikov, D. M. Folding of 16S rRNA in a Signal-Producing Structure for the Detection of Bacteria. *Angew. Chem. Int. Ed. Engl.* **2013**, *52* (40), 10586–10588.
(43) Mengistu, D. H.; Bohinc, K.; May, S. Binding of DNA to Zwitterionic Lipid Layers Mediated by Divalent Cations. *J. Phys. Chem. B* **2009**, *113* (36), 12277–12282.
(44) Gromelski, S.; Brezesinski, G. DNA Condensation and Interaction with Zwitterionic Phospholipids Mediated by Divalent Cations. *Langmuir* **2006**, *22* (14), 6293–6301.
(45) Saunders, M. J.; Graves, S. W.; Sklar, L. A.; Oprea, T. I.; Edwards, B. S. High-Throughput Multiplex Flow Cytometry Screening for Botulinum Neurotoxin Type a Light Chain Protease Inhibitors. *ASSAY and Drug Development Technologies* **2010**, *8* (1), 37–46.
(46) Saunders, M. J.; Kim, H.; Woods, T. A.; Nolan, J. P.; Sklar, L. A.; Edwards, B. S.; Graves, S. W. Microsphere-Based Protease Assays and Screening Application for Lethal Factor and Factor Xa. *Cytometry* **2006**, *69A* (5), 342–352.
(47) Goldstein, B.; Coombs, D.; He, X.; Pineda, A. R.; Wofsy, C. The Influence of Transport on the Kinetics of Binding to Surface Receptors: Application to Cells and BIAcore. *J. Mol. Recognit.* **1999**, 1–9.
(48) Presolski, S. I.; Hong, V. P.; Finn, M. G. Copper-Catalyzed Azide-Alkyne Click Chemistry for Bioconjugation. *Current Protocols in Chemical Biology* **2011**, *3* (4), 153–162.

(49) Loose, M.; Fischer-Friedrich, E.; Ries, J.; Kruse, K.; Schwille, P. Spatial Regulators for Bacterial Cell Division Self-Organize Into Surface Waves in Vitro. *Science* **2008**, *320* (5877), 789–792.

CHAPTER 5 - RUNNING DNAZYME REACTIONS ON A SURFACE THAT BECOMES OVERWHELMINGLY ATTRACTIVE IN THE PRESENCE OF REQUISITE DIVALENT CATIONS

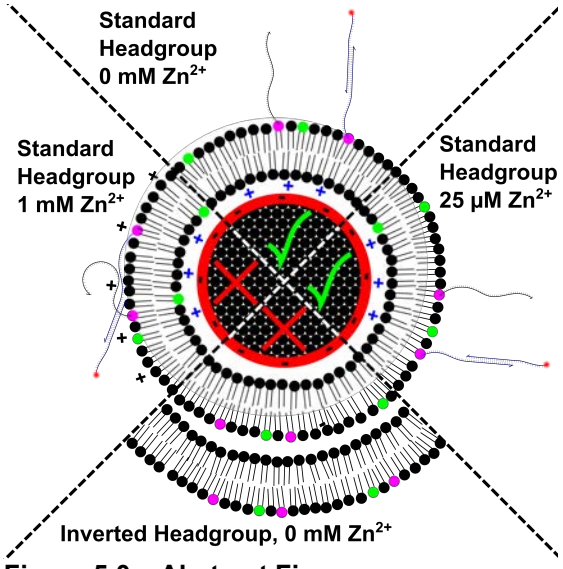

Figure 5.0 – Abstract Figure

5.1 Abstract

Zwitterionic phospholipids are commonly used for *in vitro* studies. In the absence of divalent cations, there is no non-specific interactions between DNA and the zwitterionic lipid headgroup. However, most DNAzyme require divalent cations and previous reactions buffers contained cations at 1 mM. Here, we develop a system that allows DNAzyme reactions to be run on lipid surfaces, while ensuring little to no non-specific interactions.

5.2 Introduction

Although ubiquitous in biological systems lipid bilayers are very delicate, especially in the absence of supportive proteins and linkages to surrounding structures (i.e. extra cellular matrix proteins, cytoskeleton filaments, or biopolymers such as peptidoglycan that encapsulate and support membranes). Thus, in biological settings this two-dimensional fluid is stabilized by a three-dimensional supportive matrix. However, when simplifying these structures *in vitro* the vast majority of this support is lost. In addition, the hydrophobic interactions, which drive lipid bilayer assembly in aqueous environments, can easily be overwhelmed by electrostatic repulsion of the charged headgroups,[1] or by *in vitro* experimental set-

ups that introduce charged surfaces. Further complicating lipid systems is their inherent instability in buffer systems which do not resemble biological systems, and their propensity towards degradation. Lipid degradation is a result of either lipid oxidation or the hydrolysis of ester bonds present in the lipid.[2] Finally, when designing lipid systems that interface with nucleic acid systems the presence of ionic species can greatly alter behaviors of both the lipids and the nucleic acids.

The delicate nature of lipid bilayers requires they be treated with great care. Thus, many *in vitro* lipid bilayers systems are stabilized, and this is often achieved using a silica support. Supported lipid bilayers have been formed on planar silica surfaces[3,4] and on spherical silica particles.[5-7] The stability of these supported bilayers results primarily from an electrostatic interaction between the negatively charged silica surface and the positively charged amine group at the terminus of zwitterionically charged phospholipid headgroups, such as 1,2-dioleoyl-*sn*-glycero-3-phosphocholine (DOPC). Meaning, silica supported lipid bilayer systems require an external positive charge at the surface of the lipid bilayer, although in typical buffer solutions this positive charge is considered neutral due to the proximity of the negatively charged phosphate group. However, in the presence of divalent cations, which are attracted to the phosphate group, the positive charge becomes organized and increases in strength as the negative charge of the phosphate group is shielded by the divalent cation.

A) DOPC

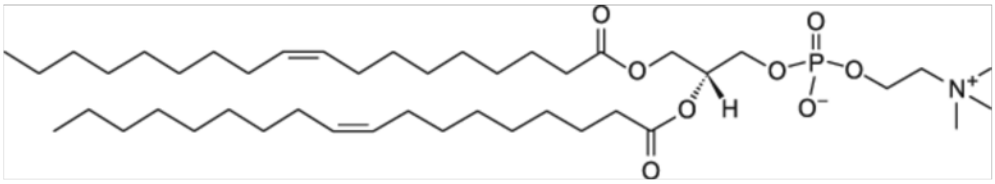

B) DOCP

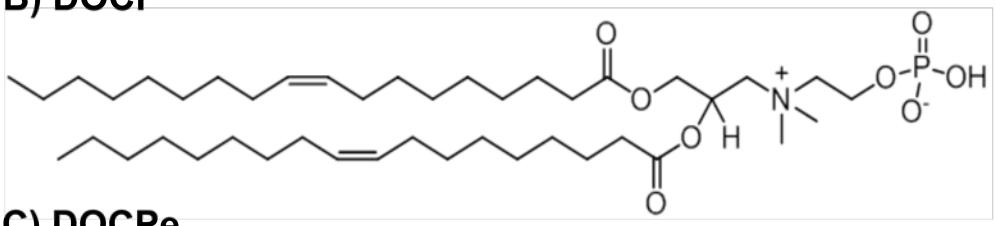

C) DOCPe

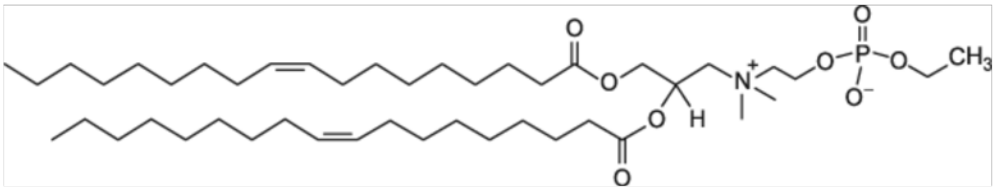

Figure 5.1 - Lipid Structures. All structures taken from Avanti Polar Lipids website. **A)** 1,2-dioleoyl-*sn*-glycero-3-phosphocholine (DOPC), with a naturally occurring lipid with a zwitterionic headgroup. **B)** 2-((2,3-bis(oleoyloxy)propyl)dimethylammonio)ethyl hydrogen phosphate (DOCP), a zwitterionic inverted headgroup lipid that is not stable on silica surfaces. **C)** 2-((2,3-bis(oleoyloxy)propyl)dimethylammonio)ethyl ethyl phosphate (DOCPe), a zwitterionic inverted headgroup lipid, which is stable on silica surfaces.

Solution phase DNAzyme reactions are typically run with 1 M Na^+ and 1 mM Zn^{2+}.[8,9] In PBS (136 mM Na^+), DNA's negatively charged phosphate backbone is not attracted to the external positive charge of a zwitterionic phospholipid. However, in the presence of 1 mM Zn^{2+}, that external positive charge is no longer shielded by the neighboring phosphate and DNA's phosphates want to party.[10,11] In addition, the high Na^+ concentrations can cause the lipids to aggregate, as evidenced by increased pressure during the extrusion process. As such, the buffer conditions used for solution phase DNA reactions will not work when running these reactions on supported lipid bilayer surfaces. There are two ways to approach this problem - the lipid composition can be adjusted, or the buffer conditions can be altered. This works presents an investigation into the most

effective methods for running DNA reactions on fluid silica microsphere supported lipid bilayers (μSLBs).

5.3 Results and Discussion

5.3.1 DOPC, DOCP, and DOCPe Structures

Small amounts of charged, anionic or cationic, lipids can be incorporated into neutral zwitterionic phospholipids without disrupting stability. However, at higher concentration electrostatic repulsion of the headgroups will destabilize the bilayer. As such, neutral lipid headgroups must comprise the majority of a lipid bilayer. In biological systems the most abundant lipids are zwitterionic such as DOPC (**Figure 5.1A**), although there are completely uncharged lipid head groups such as monogalactosyldiacylglycerol.[12] Recently, inverted headgroup lipids have become commercially available. The simplest of these inverted headgroup lipid 2-((2,3-bis(oleoyloxy)propyl)dimethylammonio)ethyl hydrogen phosphate (DOCP, **Figure 5.1B**) simply flips the location of the negatively charged phosphate group and the positively charged amine group. However, this inversion renders DOCP unstable on silica surfaces.[13] A second version of the inverted headgroup lipids 2-((2,3-bis(oleoyloxy)propyl)dimethylammonio)ethyl ethyl phosphate (DOCPe, **Figure 5.1C**) adds an ethyl to the shield the negative charge at the surface, which allows bilayers to be formed on silica surfaces.[13]

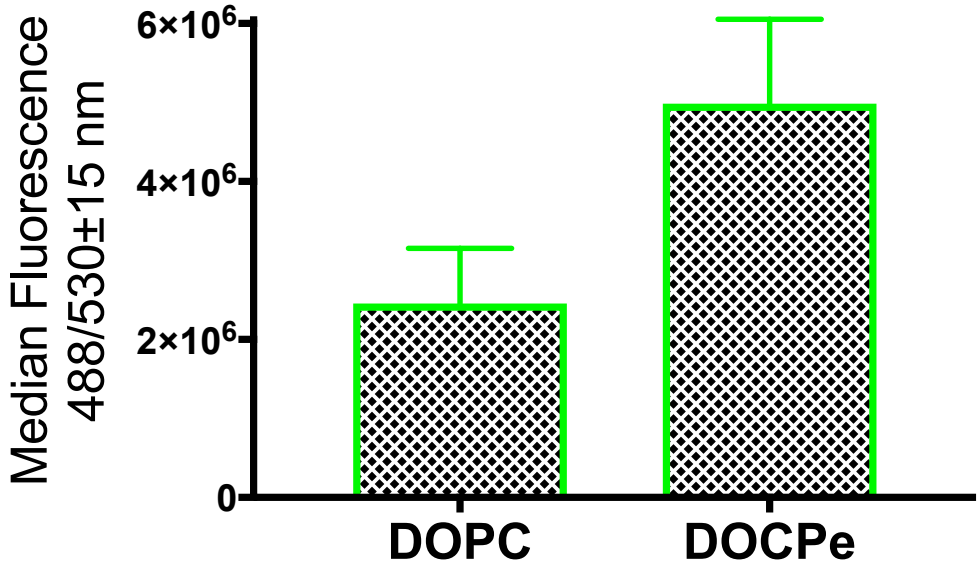

Figure 5.2 – DOCPe Forms Multilamellar Structures. Silica microsphere supported lipid bilayer, in PBS, with 0.5 mol% PECF in DOPC or DOCPe. Error bars represent SEM of 3 replicates.

To begin, we formed μSLBs with DOCPe as the base lipid with 0.5 mol% of the fluorescently tagged lipid 1,2-dioleoyl-sn-glycero-3-phosphoethanolamine-N-(carboxyfluorescein) (ammonium salt) (PECF) so we could monitor bilayer stability with a flow cytometry. We compared this to μSLBs formed using DOPC as the base lipid, because unilamellar bilayer formation with DOPC was well established.[5] When the DOCPe coated μSLBs were tested alongside the DOPC μSLBs we noted a doubling in fluorescent intensity (**Figure 5.2**). Indicating that multilamellar structures, which would increase the amount of PECF present at the surface of the μSLB, were most likely being formed.

Nonetheless we decided to investigate whether or not DOCPe would decrease the non-specific interaction between oligonucleotides and the bilayer surface in the presence of 1 mM Zn^{2+}. To test this, we incorporated a maleimide lipid, 1,2-dioleoyl-*sn*-glycero-3-phosphoethanolamine-N-[4-(p-maleimidophenyl) butyramide] (MPB PE), into both the DOPC and DOCPe lipid bilayer. We could

then conjugate thiolated oligonucleotides to MPB PE, using the protocol outlined in Chapter 4. The first thiolated oligonucleotide (TSD) served as our negative control, as is was not complementary to a Cy5 tagged oligonucleotide (Cy5_Substrate_no_r_TSS, see Table A-II.2 for sequences). The second oligonucleotide (TSS) served as our experimental as it was complementary to Cy5_Substrate_no_r_TSS, meaning we should only see high fluorescence for this bead population. In PBS both lipids systems show low fluorescence when TSD (-) is conjugated to the bilayer and high fluorescence when TSS is conjugated (**Figure 5.3A**). In the E6 buffer (50 mM HEPES, 1 M NaCl, 1 mM $ZnCl_2$), which has been used for DNAzyme reactions by our group in the past, we saw a decrease in non-specific binding of the fluorescently tagged strand for DOCPe compared to DOPC (**Figure 5.3B**). However, the decrease in non-specific binding was not significant enough to justify working with the multilamellar structures formed by DOCPe, so we decided to investigate a DNAzyme that does not require divalent cations.

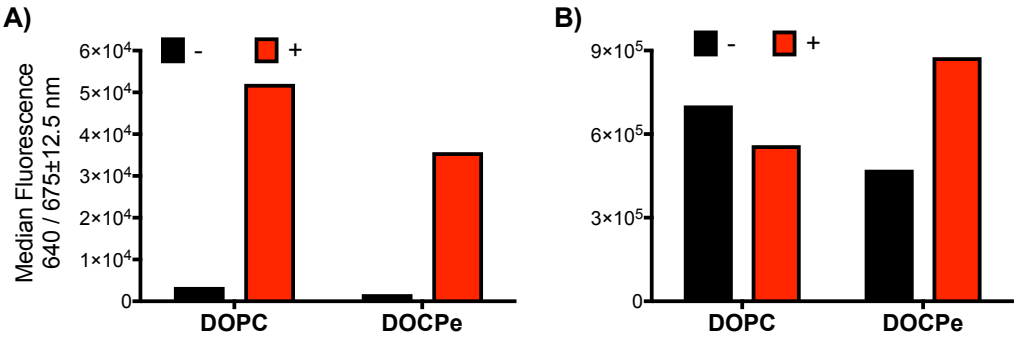

Figure 5.3 – Non-Specific Interaction with DOPC vs DOCPe. A) Both lipids, with 1 mol% MPB PE, 0.5 mol% PECF, in PBS (138 mM Na^+, no Zn^{2+}). The negative controls has TSD conjugated to MPB PE, while the experimental has TSS conjugated. TSS is complementary to the Cy5 labeled Cy5_Substrate_no_r_TSS, while TSD is not. **B)** The same lipids in E6 buffer (1 M Na^+, 1 mM Zn^{2+}). Raw numbers are plotted to show the true negative values.

5.3.2 A Sodium Dependent DNAzyme

In 2015, a sodium dependent DNAzyme (NaA43) was published,[14] which presented an alternative to previously reported divalent cation-dependent DNAzymes. We initially tested the DNAzyme function in solution, using a chimeric substrate molecule (NaA43_SolPh_Substrate) similar to the one presented in Chapter 3. **Figure 5.4A** shows the results of a reaction run in PBS, made with RNAse free water. The NaA43_Enzyme strand [50 nM] rapidly cleaved its NaA43_SolPh_Substrate [250 nM] in this solution phase experiment (strand sequences are presented in **Table 5.1**). For the μSLB experiments we were expecting a decrease in fluorescence as the cleaved substrate would move into solution, and the bead's fluorescence would decrease (as described in Chapter 4). Here we incorporated MPB PE at 1 mol%, and conjugated both TSD and TSS, with a 4-fold excess of TSS. The reaction (**Figure 5.4B**) was run in PBS, and the beads were rotated at room temperature. Even at three

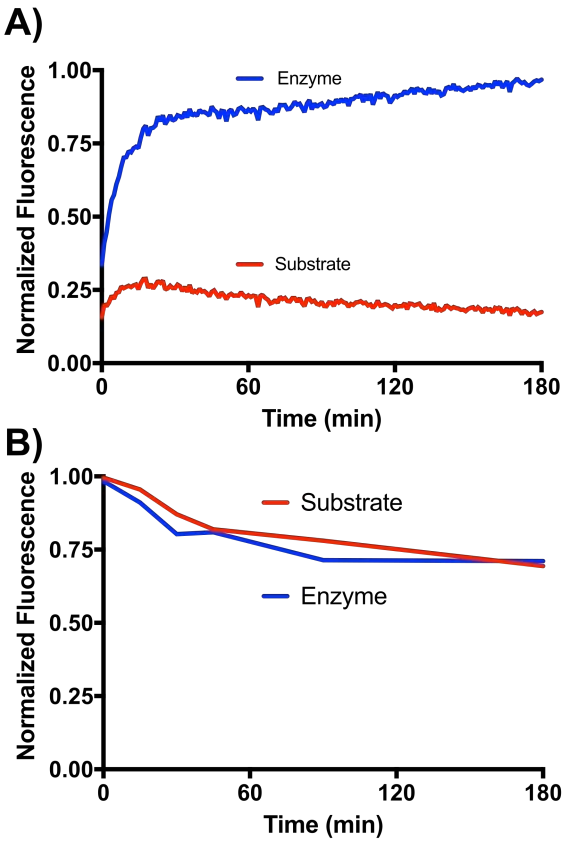

Figure 5.4 – Na^+ Dependent DNAzyme Function. A) The sodium dependent DNAzyme worked well in PBS. The substrate [250 nM] alone showed slight non-specific activation. However, in the presence of the DNAzyme [50 nM] we saw the expected increase in fluorescence within 30 minutes. **B)** For the μSLB experiments we were expecting a decrease in fluorescence as the cleaved substrate would move into solution, Here, we incorporated MPB PE at 1 mol% and conjugated both TSD and TSS to the bilayer, with a four-fold excess of TSS.

hours, we did not see a decrease compared to our negative control (the substrate alone on the bead).

5.3.3 Zinc Salts

So, we returned to the divalent cation dependent 8-17 DNAzyme and began adjusting our buffer conditions. The results presented in Chapter 4 demonstrated full DNAzyme function at Zn^{2+} concentrations as low as 25 μM. However, to achieve this level of function we needed to switch from the commonly used $ZnCl_2$

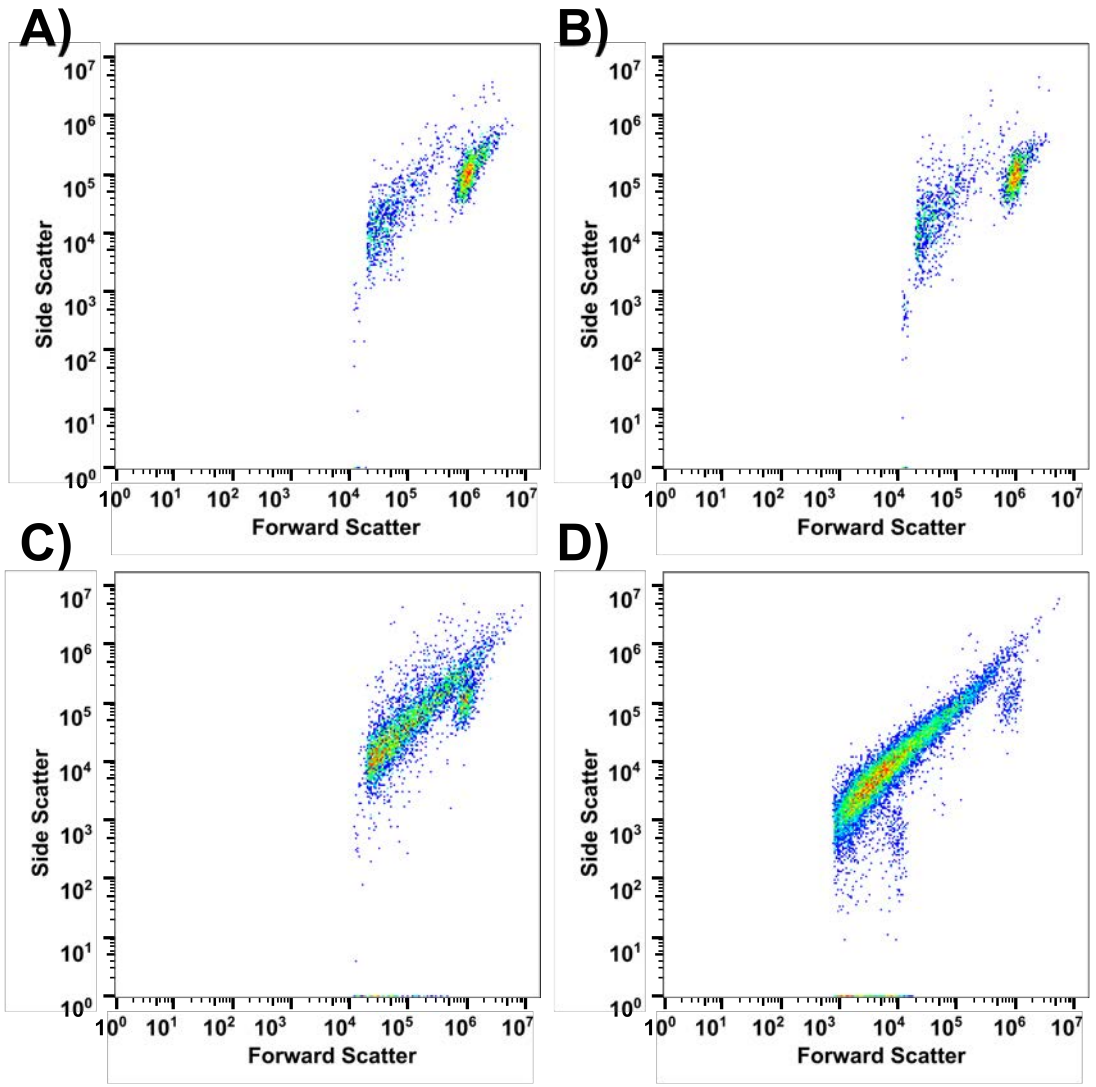

Figure 5.5 – Oxychloride Precipitates. A) Flow cytometry dot plot of forward scatter (FSC) versus side scatter (SSC) in the absence of $ZnCl_2$, showing the SiMS population and debris. **B)** Same as A with 0.1 mM $ZnCl_2$. **C)** Same was A with 1 mM $ZnCl_2$. **D)** Same sample as C with the threshold decreased from 80,000 FSC units to 800 FSC units.

to $ZnAc_2$ which does not form the oxychloride precipitate.[15] We first noticed the oxychloride precipitates with flow cytometry, as with increasing $ZnCl_2$ we saw in increase in debris on a forward scatter (FSC) versus side scatter (SSC) plot (**Figure 5.5**). In **Figure 5.5A**, there is no $ZnCl_2$ present in solution, we then increase to 0.1 mM $ZnCl_2$ (**Figure 5.5B**) and 1 mM $ZnCl_2$ (**Figure 5.5C**). For **Figure 5.5D**, we ran the same sample as Figure 5.5C but decreased the threshold from $8x10^4$ FSC units to 800 FSC units to show a much larger population of what we believe to be oxychloride precipitates. We also began making fresh zinc buffers for every reaction, because we noticed decreased function when older zinc solutions were used (**Figure 5.6**).

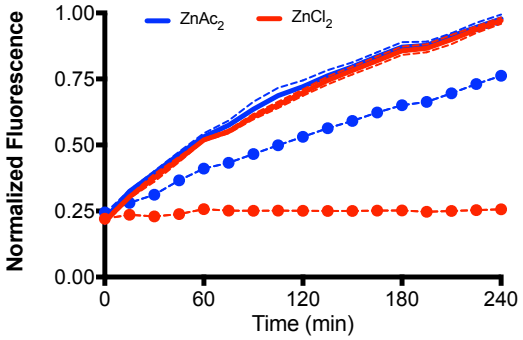

Figure 5.6 – $ZnCl_2$ and $ZnAc_2$, Fresh and Old. We tested DNAzyme function in the presence of both $ZnCl_2$ and $ZnAc_2$ both at 10 µM. With the DNAzyme [50 nM] and Substrate [250 nM], in a buffer that contained 276 mM NaCl, and 50 mM HEPES. The solid lines represent freshly made Zn^{2+} solutions, and the dashed lines represent a Zn^{2+} which sat on the bench for >1 month.

5.4 Conclusions and Future Directions

Working with lipids in the laboratory leaves little room for deviation from established parameters. Changing even a single parameter often results in system failure. Here, we present a description of our efforts to run DNAzyme reactions on stable silica supported lipid bilayers, with minimal non-specific interactions. An inverted head group lipid (DOCPe) was shown to slightly decrease non-specific interactions, but multilamellar structures, instead of unilamellar structures, were formed. We then tested the function of a sodium dependend DNAzyme, which worked in a solution phase reaction with PBS. However, when run on a lipid bilayer

the reaction did not proceed. Finally, we optimized our buffer conditions, by using a zinc salt that did form precipitates which allowed us to decrease the Zn^{2+} concentration.

5.5 Materials and Methods

5.5.1 Materials

All oligonucleotides were purchased from Integrated DNA Technologies (IDT, Coralville, IA). IDT purified unmodified strands by standard desalting, and the fluorescently tagged and thiolated strands were purified by high performance liquid chromatography. Lipids were purchased from Avanti Polar Lipids (Alabaster, AL).

5.5.2 Bilayer Formation and Flow Cytometry

Silica supported lipid bilayers were formed and analyzed as decribed in Chapter 4.

5.5.3 Strand Sequences

Table 5.1 – Strand Sequences

Name	Sequence
NaA3_Enzyme	5'-GCGGCGGTACCAGGTCAAAGGTGGGTGAGGGGACGCCAA GAGTCCCCGCGGTTAGATAGAG -3'
NaA43_SolPh_Substrate	5'-/56-FAM/CTCTATCTATrAGGAAGTACCGCCGCT/36-TAMSp/ -3'
NaA43_Enzyme_TSD	5'- GAGTGTAGATGTGAAGTTTGAAAAAGCGGCGGTACCAGGTCA AAGGTGGGTGAGGGGACGCCAAGAGTCCCCGCGGTTAGATAG AGGCC -3'
NaA43_Substrate_TSS	5'-/5ATTO647NN/CTCTATCTATrAGGAAGTACCGCCGCAAAAAGTT TCTGTCTTGTTCTATTC -3'

5.6 References

(1) Zhao, W.; Róg, T.; Gurtovenko, A. A.; Vattulainen, I.; Karttunen, M. Atomic-Scale Structure and Electrostatics of Anionic Palmitoyloleoylphosphatidylglycerol Lipid Bilayers with Na+ Counterions. *Biophysical Journal* **2007**, *92* (4), 1114–1124.

(2) Anderson, M.; Omri, A. The Effect of Different Lipid Components on the in Vitro Stability and Release Kinetics of Liposome Formulations. *Drug Delivery* **2003**, *11* (1), 33–39.

(3) Shreve, A. P.; Howland, M. C.; Sapuri-Butti, A. R.; Allen, T. W.; Parikh, A. N. Evidence for Leaflet-Dependent Redistribution of Charged Molecules in Fluid Supported Phospholipid Bilayers. *Langmuir* **2008**, *24* (23), 13250–13253.

(4) Howland, M. C.; Sapuri-Butti, A. R.; Dixit, S. S.; Dattelbaum, A. M.; Shreve, A. P.; Parikh, A. N. Phospholipid Morphologies on Photochemically Patterned Silane Monolayers. *J. Am. Chem. Soc.* **2005**, *127* (18), 6752–6765.
(5) Piyasena, M. E.; Zeineldin, R.; Fenton, K.; Buranda, T.; Lopez, G. P. Biosensors Based on Release of Compounds Upon Disruption of Lipid Bilayers Supported on Porous Microspheres. *Biointerphases* **2008**, *3* (2), 38–49.
(6) Fernandez Oropeza, N.; Zurek, N. A.; Galvan-De La Cruz, M.; Fabry-Wood, A.; Fetzer, J. M.; Graves, S. W.; Shreve, A. P. Multiplexed Lipid Bilayers on Silica Microspheres for Analytical Screening Applications. *Anal. Chem.* **2017**, *89* (12), 6440–6447.
(7) Fabry-Wood, A.; Fetrow, M. E.; Brown, C. W., III; Baker, N. A.; Fernandez Oropeza, N.; Shreve, A. P.; Montano, G. A.; Stefanovic, D.; Lakin, M. R.; Graves, S. W. A Microsphere-Supported Lipid Bilayer Platform for DNA Reactions on a Fluid Surface. *ACS Appl. Mater. Interfaces* **2017**, *9* (35), 30185–30195.
(8) Stojanovic, M. N.; Stefanovic, D. A Deoxyribozyme-Based Molecular Automaton. *Nat Biotechnol* **2003**, *21* (9), 1069–1074.
(9) Brown, C. W., III; Lakin, M. R.; Horwitz, E. K.; Fanning, M. L.; West, H. E.; Stefanovic, D.; Graves, S. W. Signal Propagation in Multi-Layer DNAzyme Cascades Using Structured Chimeric Substrates. *Angew. Chem. Int. Ed.* **2014**, *53* (28), 7183–7187.
(10) Mengistu, D. H.; Bohinc, K.; May, S. Binding of DNA to Zwitterionic Lipid Layers Mediated by Divalent Cations. *J. Phys. Chem. B* **2009**, *113* (36), 12277–12282.
(11) Gromelski, S.; Brezesinski, G. DNA Condensation and Interaction with Zwitterionic Phospholipids Mediated by Divalent Cations. *Langmuir* **2006**, *22* (14), 6293–6301.
(12) van den Brink-van der Laan, E.; Antoinette Killian, J.; de Kruijff, B. Nonbilayer Lipids Affect Peripheral and Integral Membrane Proteins via Changes in the Lateral Pressure Profile. *Biochimica et Biophysica Acta (BBA) - Biomembranes* **2004**, *1666* (1-2), 275–288.
(13) Wang, F.; Liu, J. A Stable Lipid/TiO 2Interface with Headgroup-Inversed Phosphocholine and a Comparison with SiO 2. *J. Am. Chem. Soc.* **2015**, *137* (36), 11736–11742.
(14) Torabi, S.-F.; Wu, P.; McGhee, C. E.; Chen, L.; Hwang, K.; Zheng, N.; Cheng, J.; Lu, Y. In Vitro Selection of a Sodium-Specific DNAzyme and Its Application in Intracellular Sensing. *Proceedings of the National Academy of Sciences* **2015**, *112* (19), 5903–5908.
(15) Peacock, J. C.; Peacock, B. L. D. Some Observations the Dissolving of Zinc Chloride and Several Suggested Solvents*. *The Journal of the American Pharmaceutical Association (1912)* **1918**, *7* (8), 689–697.

CHAPTER 6 - DNA FUNCTIONALIZED OLIGOPHENYLENEVINYLENES FOR TRANSMEMBRANE SIGNAL TRANSDUCTION

6.1 Abstract

Our aim in this work is to achieve nucleic acid-based transmembrane signal transduction via a dimerization event. To begin, we designed a molecule with dimensions to match biological membranes. The portion that spans the bilayer consists of an oligophenylenevinylene (OPV), with functional groups that are compatible with standard click chemistry reactions. After successful synthesis, the OPV was functionalized with oligonucleotides. Ultimately, two versions of this molecule, each representing one half of a split DNAzyme, will be inserted into a PEG cushioned, silica microsphere supported phospholipid bilayer and a nucleic acid input will tether the two DNAzyme halves. At this point, a chimeric substrate molecule, encapsulated within the vesicle, will be cleaved and fluorescence will increase within the vesicle.

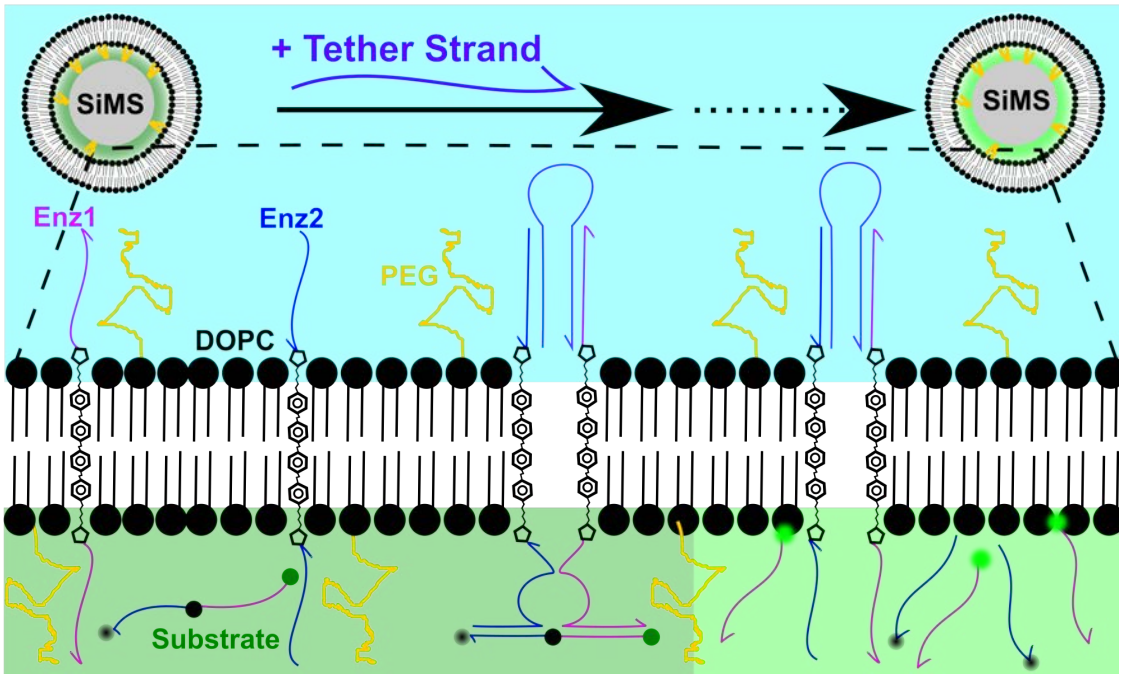

Figure 6.0 – Abstract Figure.

6.2 Introduction

The incredible complexity of silicon-based computation is achieved using a small set of spatially isolated, standardized components (i.e. logic gates). Biology also reuses standard components to process information[1,2] and the flow of this information is precisely controlled to prevent promiscuous interactions. [3,4] DNA-based molecular computation has great potential in theranostic and diagnostic applications[5,6] and in the development of biological models.[5,6] However, to date most DNA-based systems have been run in well-mixed solutions, which lack spatial organization.[7-10] In such systems the reuse of standardized components is not possible, as all components are free to interact and to prevent spurious interactions the nucleotide sequence of functionally similar components must be orthogonal, which significantly limits scalability.[11]

Compartmentalization of computing elements using lipid bilayers, analogous to cell membranes, will potentially allow standardized components to be used. Lipid bilayers form the vast majority of compartments in cellular systems, including the cell membrane, the nuclear envelope and the mitochondrial membranes. For each biological compartment there exists a method for signal transduction and in most cases, this is achieved using integral membrane proteins (IMPs). For instance, receptor tyrosine kinases transduce signals via a dimerization event, while ligand binding in G-protein coupled receptors initiates a conformational change within the cell and pores selectively allow the passage of ions, nucleic acids and proteins. For synthetic systems, signal transduction that are activated by nucleic acid inputs will allow a much broader range of activity *in vitro* and eventually *in vivo*. DNA-based synthetic pores have been designed,[12-16]

but there are no current methods to transduce signals via dimerization or conformational changes. Aptamers that allow dimerization to be monitored without genetically altering the IMP were recently introduced,[17] however this system does not transduce a signal across the bilayer. To achieve this, a molecule which fully spans the lipid bilayer is required and oligonucleotides must be covalently linked to either end of this molecule.

Oligophenylenevinylenes (OPV) are flexible hydrophobic conjugated oligomers that have been shown to span phospholipid bilayers.[18] OPV chemistry allows functional groups to be placed at either end, to which nucleic acids can be conjugated using click chemistry.[19] The resulting amphiphilic molecule can then be inserted into a phospholipid bilayer, as the length of the hydrophobic region of this compound matches the width of common lipid bilayers, making this molecule an excellent candidate for nucleic acid based transmembrane communication.

A simple way to initiate signal transduction into the membrane compartment will be through the dimerization of two halves of a split DNAzyme. Split DNAzymes are pairs of molecules that have enzymatic activity once the pair is brought into close proximity, this is often achieved using a nucleic acid tether strand.[20] The tether strand would be added into a solution containing lipid vesicles with two OPV-DNA conjugates incorporated into the bilayer. Binding of the tether strand would bring both halves of the DNAzyme into proximity, and cleavage of a chimeric substrate molecule within the vesicle would result in an increase in fluorescence.

6.3 Results and Discussion

6.3.1 Synthesis of the OPV

We based the molecular design on an OPV that was previously demonstrated to insert into phospholipid bilayers (**Figure 6.1A**).[18] However, the optimal structure for our purposes would contain a single alkyl group at either end, as opposed to the pair of alkyl groups attached to a nitrogen in the published molecule. So, we decided to replace the nitrogen with an oxygen, the chemistry of which would ensure a single alkyl (**Figure 6.1B**). As it turned out this molecule

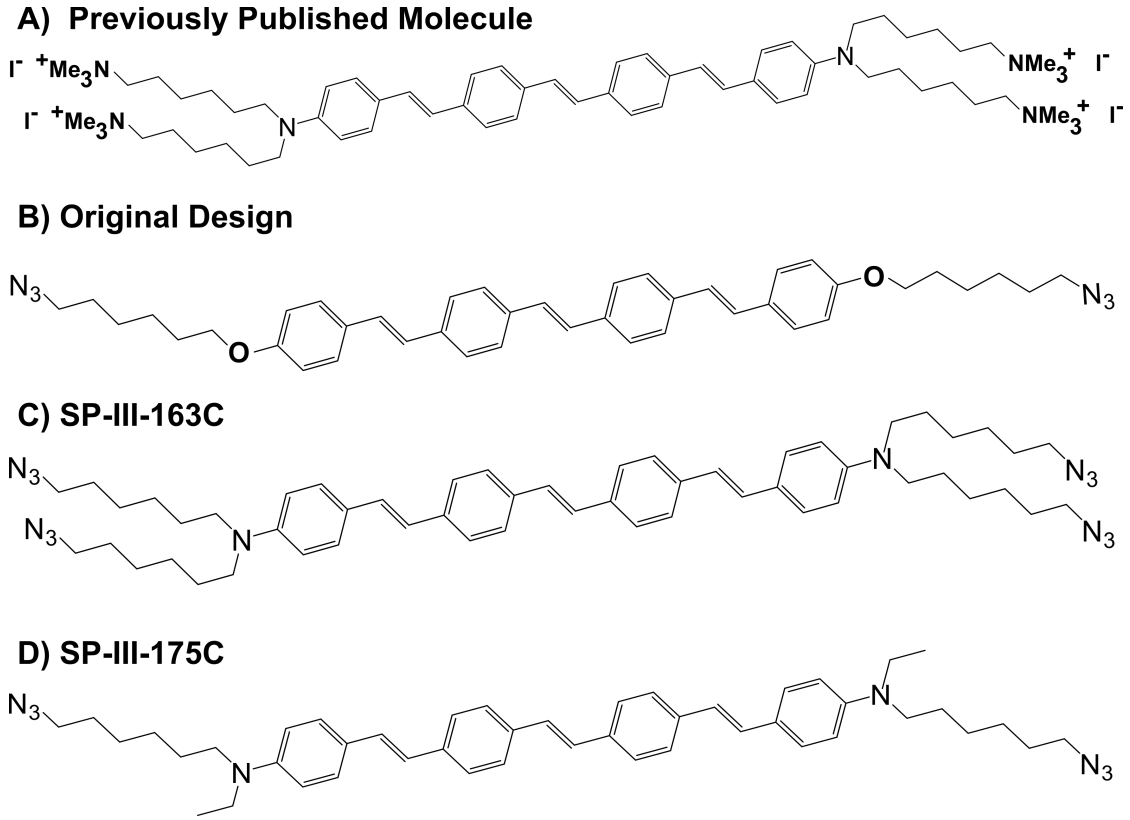

Figure 6.1 – Molecular Design. A) The previously published molecule[19] had two alkyl chains at each terminus with a positively charged trimethylamine at each terminus (the counter ion of which was a negatively charged iodide). **B)** The initial OPV design replaced the nitrogen molecules adjacent to the phenyl rings with an oxygen, to create a single alkyl branch. However, this molecule would not have been soluble in the aqueous click chemistry buffer. **C)** To overcome this the nitrogens were brought back in, which created four conjugation sites for click chemistry. However, the conjugation of oligonucleotides to this molecule did not produce the desired product. **D)** As such, a final molecule was designed, which has two alkyl branches off the nitrogen. Conveniently, one of the alkyl groups was an ethyl and the other an six-carbon alkyl halide (explained in the next figure). Thus, we achieved the desired single azide at each terminus of the final compound.

would not have been soluble in the aqueous click buffers. So, we returned to the original design, with a nitrogen at either end of the phenyl rings and modified the terminal trimethylamines with azides (**Figure 6.1C**). Synthesis of this molecule and the high-performance liquid chromatography spectrum are shown in Appendix III. To summarize, we were unable to conjugate an oligonucleotide to each of the azides and the molecule did not behave in a predictable fashion. Thus, we adapted to molecular design a final time, to achieve a single terminal azide (**Figure 6.1D**). This molecule will be referred to as OPV, or SP-III-175C in the description of the synthesis (**Figure 6.2**). Details of the reaction and the analysis for each compound are provided in the text.

6.3.1.1 Synthesis of Intermediate SP-III-131C

This procedure was adopted from Garner et al.,[18] and began with the preparation of (*E*)-1,2-bis(4-(chloromethyl)phenyl)ethene (SP-III-130C). A 250 mL round-bottom flask was placed under an Argon atmosphere and flame dried, to which 40 mg of 2nd generation Grubbs catalyst (0.047 mmol, 1 eq.) dissolved in anhydrous CH_2Cl_2 was added and this solution was degassed. Then 1.34 mL (202 eq., 9.5 mmol) dry 4-vinylbenzyl chloride was added to the reaction flask.

Figure 6.2 – Synthesis of the Membrane Spanning Azide Functionalized OPV (SP-III-175C). Shown on the next page. The synthesis begins with the metathesis condensation of 4-vinylbenzyl chloride to yield SP-III-130C. This is followed by an Arbuzov reaction to yield **SP-III-131C**. Synthesis of the intermediate **SP-III-169C** begins with replacing N-ethyl aniline's proton with a hexanol moiety. At which point, the electron rich aromatic **SP-III-167C** is converted to **SP-III-169C** via a Vilsmeier-Haack formulation. A Horner-Wadsworth-Emmons reaction yields **SP-III-172C**, by dropwise addition of **SP-III-169C** to a solution containing **SP-III-131C**. From here the terminal chlorine groups are replaced by iodine with a Finkelstein reaction, which is an equilibrium reaction that is pushed to completion because one of the side products, NaCl, is not soluble in acetone. Finally, a nucleophilic substitution (S_N2) replaces the alkyl iodide with an azide, to yield the final compound, **SP-III-175C**.

Figure 6.2

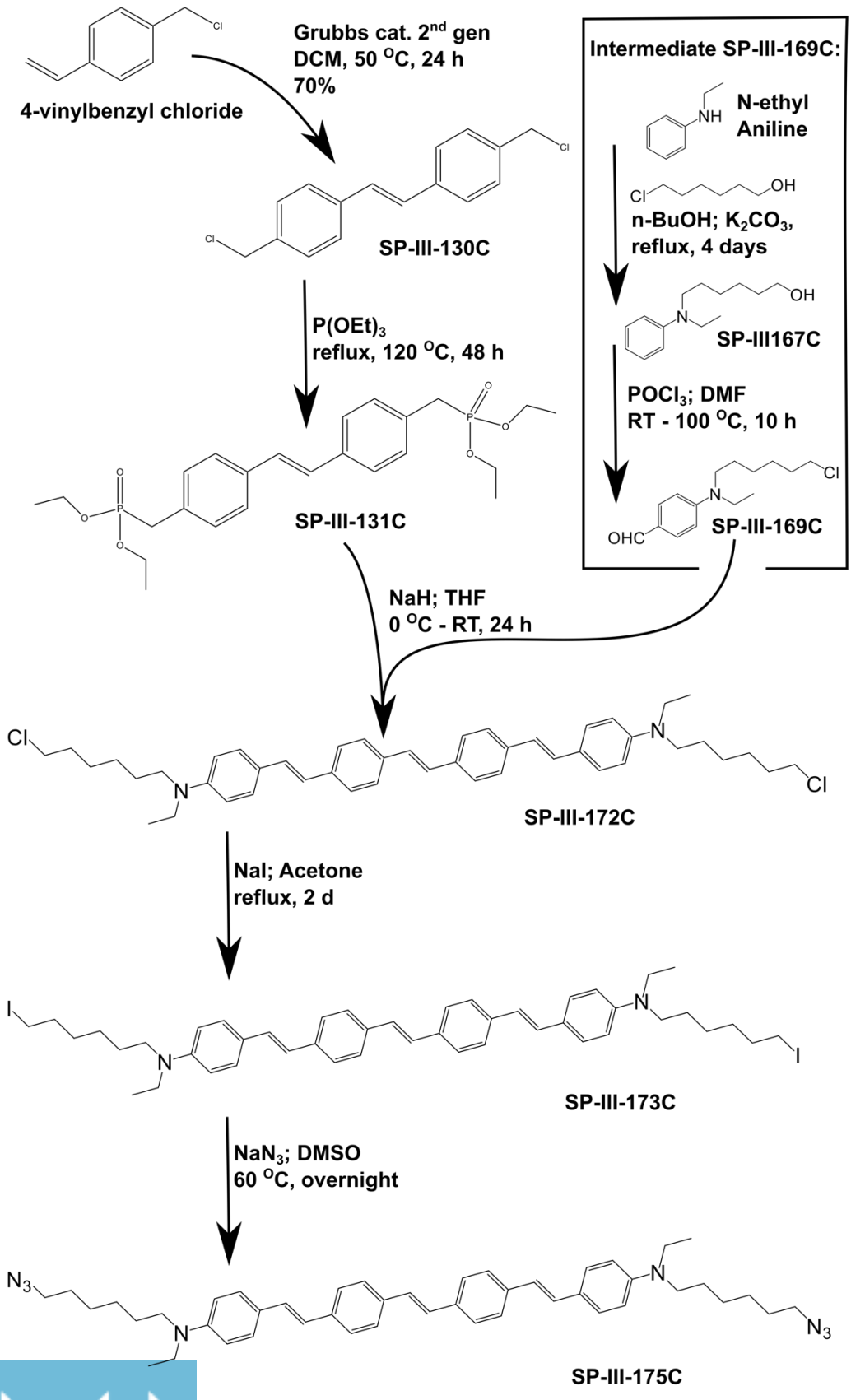

The solution was slowly refluxed under Argon at 50 °C for 24 hours. The reaction solution was then allowed to cool slowly and concentrated up to ~10 mL. The product crystallized out of the reaction solution and the crude (off-white needle crystals) was collected via filtration and washed with cold hexanes. Following silica gel chromatography using 1:1 dichloromethane:hexane solvent system, the pure product was afforded as a white solid 920 mg (35% yield). MP: 160-163 °C. ^{1}H NMR (400 MHz, $CDCl_3$): δ 7.51 (d, *J*= 8.4 Hz, 4H), 7.38 (d, *J*= 7.6 Hz, 4H), 7.11 (s, 2H), 4.60 (s, 4H). ^{13}C (100 MHz, $CDCl_3$): δ 137.47, 137.03, 129.16, 128.77, 127.00, 46.20.

To prepare (*E)*-4,4'-bis(diethylphosphonatemethyl)stilbene (SP-III-131C), 500 mg of SP-III-130C (1 eq., 1.8 mmol) and 10 mL of neat triethylphosphite was combined in a 100 mL round bottom flask equipped with a reflux condenser. This solution was allowed to reflux at 120 °C for 48 hours. Upon completion of the reaction, this solution was allowed to cool, and the off-white solid crude product was isolated via removal of excess $P(OEt)_3$ by vacuum distillation. Pure SP-III-131C was obtained as white crystals in 35 % yield by recrystallization from diethyl ether. ^{1}H NMR (400 MHz, $CDCl_3$): δ 7.42 (d, *J*= 7.6 Hz, 4H), 7.25 (d, *J*= 14 Hz, 4H), 7.03 (s, 2H), 3.99 (t, (d, *J*= 7.6 Hz, 8H), 3.13 (d, (d, *J*= 22 Hz, 4H), 1.22 (t, (d, *J*= 6.8 Hz, 12H). ^{13}C (100 MHz, $CDCl_3$): δ 136.14, 136.10, 131.14, 131.05, 130.27, 130.20, 128.28, 126.78, 126.75, 62.37, 62.31, 34.41, 33.04, 16.55, 16.49.

6.3.1.2 Synthesis of Intermediate SP-III-169C

To synthesize 6-(ethyl(phenyl)amino)hexan-1-ol (SP-III-167C), a procedure adopted from Woo et al. was used.[21] A mixture of 1.04 mL (8.25 mmol, 1 eq) of *N*-ethyl aniline, 1.65 mL (12.4 mmol, 1.5 eq) of 6-chloro-1-hexanol, and 1.7 g (12.4

mmol, 1.5 eq) potassium carbonate was heated in 20 mL of *n*-butanol under reflux for 4 days. After cooling, the remaining solids were filtered off, and the solvent was removed under reduced pressure to afford the crude product. Purification by silica gel chromatography (2:1 ethyl acetate/hexane) yielded 1.25 g (70% yield) of SP-III-167C as a red-orange thick oil. Keep in refrigerator overnight, use immediately.

To synthesize 4-((6-chlorohexyl)(ethyl)amino)benzaldehyde (SP-III-169C) phosphorus oxychloride (1.5 mL, 16.5 mmol, 2 eq) was added dropwise to 5 mL of dry DMF at 0 °C. After 30 min, 1 mL (8.25 mmol, 1 eq) of SP-III-167C in 3 mL of DMF was added to the above solution. The resulting mixture was heated to 100 °C for 3 h. After cooling to room temperature, 50 mL of ice water was poured into reaction mixture. The pH of the mixture was adjusted to 7 by addition of saturated potassium acetate aqueous solution. The mixture was extracted with dichloromethane, and the combined organic phase was washed with water and dried over Na_2SO_4. The solvent was evaporated and the crude product was purified by silica gel chromatography (starting with 10% hexane:ethyl acetate and increased to 1:1 hexane:ethyl acetate) to afford SP-III-169C (0.35 mg, 33%) as a dark yellow oil. ^{1}H NMR (400 MHz, $CDCl_3$): δ 9.67 (s, 1H), 7.69 (d, *J*= 8 Hz, 2H), 6.64 (d, *J*= 8.4 Hz, 2H), 3.54-3.51 (m, 2H), 3.53 (d, *J*= 7.2 Hz, 2H), 3.35-3.31 (m, 2H), 1.79-1.76 (m, 2H), 1.64-1.61 (m, 2H), 1.50-1.47 (m, 2H), 1.38-1.36 (m, 2H), 1.20-1.17 (m, 3H). ^{13}C (100 MHz, $CDCl_3$): δ 190.14, 152.48, 132.41, 124.65, 110.75, 50.40, 45.29, 44.99, 32.55, 27.35, 26.76, 26.40, 12.32.

6.3.1.3 Synthesis of the Final Compound (SP-III-175C)

Synthesis of the final compound required the intermediate 4,4'-((1E,1'E)-(((E)-ethene-1,2-diyl)bis(4,1-phenylene))bis(ethene-2,1-diyl))bis(N-(6-chlorohexyl)-N-ethylaniline) (SP-III-172C), and began by suspending NaH (60 mg, 1.45 mmol, 60% in oil, 5 eq) in 5 mL anhydrous THF at 0 °C under argon atmosphere with stirring. SP-III-131C (140 mg, 0.29 mmol, 1 eq) dissolved in THF was added dropwise, followed by addition of SP-III-169C (195 mg, 0.73 mmol, 2.5 eq) dissolved in THF. The stirring was continued at room temperature overnight. The reaction mixture was cooled to 0 °C then water (2 mL) was added dropwise under argon with stirring. 2N Hydrochloric acid (5 mL) was added dropwise to the reaction mixture then it was extracted with diethyl ether. The organic layers were collected, dried ($MgSO_4$), filtered and the solvent removed under reduced pressure to give the crude product, which was applied to a silica gel column chromatography using 1:1 dichloromethane:hexane solvent system. Fractions containing the required product were collected and the solvent removed under reduced pressure. Yellowish crystals (50 mg, 25%). ^{1}H NMR (400 MHz, $CDCl_3$): δ 7.54 (s, 8H), 7.47 (d, *J*= 4 Hz, 4H), 7.43-7.31 (m, 2H), 7.17-7.10 (m, 4H), 6.98-6.94 (m, 2H), 6.73-6.69 (m, 4H), 3.64-3.59 (m, 4H), 3.46 (s, 4H), 3.36 (s, 4H), 1.88-1.84 (m, 4H), 1.70-1.68 (m, 4H), 1.62-1.53 (m, 4H), 1.45 (s, 4H), 1.31-1.23 (m, 6H). ^{13}C (100 MHz, $CDCl_3$): δ 149.9, 146.0, 134.7, 128.9, 128.0, 127.8, 126.8, 126.3, 123.6, 111.9, 53.9, 47.5, 45.2, 32.7, 27.6, 26.9, 26.6, 12.5.

To synthesize a final intermediate, 4,4'-((1E,1'E)-(((E)-ethene-1,2-diyl)bis(4,1-phenylene))bis(ethene-2,1-diyl))bis(N-ethyl-N-(6-iodohexyl)aniline) (SP-III-173C), under argon atmosphere SP-III-172C (20 mg, 0.03 mmol, 1 eq)

dissolved in 5 mL anhydrous acetone was added to a flame dried round bottom flask containing sodium iodide (130 mg, 0.85 mmol, 30 eq). The reaction mixture was refluxed for 48 hours under argon atmosphere. Upon cooling down to room temperature, acetone was evaporated, and the reaction mixture dissolved in 50 mL CH_2Cl_2, washed twice with water (to remove excess NaI) and dried over $MgSO_4$. A yellow solid was obtained after recrystallization in diethyl ether and used immediately for next step without further purification.

The final compound, 4,4'-((1E,1'E)-(((E)-ethene-1,2-diyl)bis(4,1-phenylene))bis(ethene-2,1-diyl))bis(N-(6-azidohexyl)-N-ethylaniline) (SP-III-175C), was synthesized by dissolving SP-III-173C (10 mg, 0.01 mmol, 1 eq) in 2 mL DMF and then adding sodium azide (22 mg, 0.33, 30 eq). The reaction mixture was heated for 2 hours at 60 °C and stirred overnight at room temperature. Water was added (50 mL) to extract the product with 35 mL ethyl acetate. The organic layer was washed twice with water (25 mL each), dried over $MgSO_4$ and concentrated under vacuum. Recrystallization in diethyl ether yielded red solid compound, which fluoresced (λ_{Ex}: 425 nm, λ_{Em}: 525 nm) in chloroform (**Figure 6.3**). ^{1}H NMR (400 MHz, $CDCl_3$): δ 7.46 (t, *J*= 9.6 Hz, 8H), 7.39 (d, *J*= 8.4 Hz, 4H), 7.09-7.03 (m, 4H), 6.88 (d, *J*= 16.4 Hz, 2H), 6.64 (d, *J*= 8.8 Hz, 4H), 3.39 (d, *J*= 6.8 Hz, 4H)),

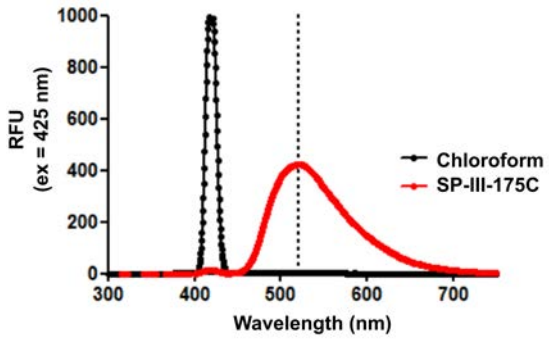

Figure 6.3 - Emission Spectrum of SP-III-175C in Chloroform. The emission spectrum of SP-III-175C, with excitation at 425 nm, shows maximal emission at 525 nm.

3.28 (t, *J*= 6.4 Hz, 4H), 1.64-1.59 (m, 8H), 1.43-1.37 (m, 8H), 1.25 (s, 4H), 1.17 (t, *J*= 6.4 Hz, 6H).

6.3.2 Click Chemistry

To functionalize the synthesized OPV, SP-III-175C, with oligonucleotides click chemistry was used. To begin, SP-III-175C was resuspended in tetrahydrofuran (THF) at 10 µM. The click chemistry reaction was set up by adding the following reagents in a stepwise fashion: Enzyme strand 1 (Enz1) [10 µM], 142.5 µL potassium phosphate buffer (200 mM potassium phosphate, pH of 7) to bring the final volume to 500 µL, 200 µL of tetrahydrofuran (THF), 50 µL of SP-III-175C [1 µM], 7.5 µL $CuSO_4$ [200 µM] premixed with ligand (THPTA) [1 mM], 25 µL of aminoguanidine hydrochloride [10 mM], 25 µL of freshly made sodium ascorbate [10 mM]. This reaction mixture was deoxygenated for 10 minutes and then stirred for 1 hour in a sealed vial at room temperature. The reaction vial was then placed under vacuum to remove THF and water. The product, excess DNA, and reaction

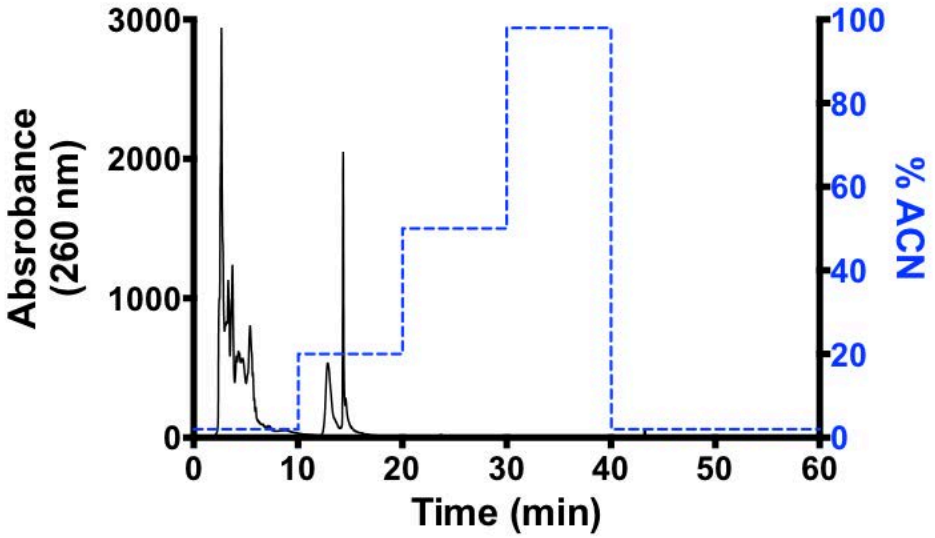

Figure 6.4 – HPLC Spectrum of OPV-Enz1 Products. The initial 10 minutes were run with 2% ACN/98% Milli-Q water, to remove excess Enz1 and the click chemistry salts. At 10 minutes we immediately increased to 20 % ACN, at which point two distinct peaks were eluted. We believed the first peak to be OPV-$(Enz1)_2$, and the second to be OPV-(Enz1). The spectrum represents the mean of 7 replicates, error bars were not included as they obstructed the view of the peaks.

salts were resuspended in EDTA [2 mM], to sequester the Copper, and this solution was purified by High-Performance Liquid Chromatography (HPLC).

It was noted that although THF is considered to be biologically inert and does not appear to have an effect on the oligonucleotides, it does degrade the ATTO647 fluorophore. When a test reaction, lacking both the OPV and THF, was run alongside the typical click reaction, lacking only the OPV, we saw a complete loss of fluorescence after one week (see **Figure A-III.4**).

6.3.3 HPLC for Purification of the Click Chemistry Product (OPV-Enz1)

To begin HPLC purification we ran 2% acetonitrile (ACN)/98% Milli-Q water to remove excess DNA and the click chemistry salts. After ten minutes we immediately increased to 20 % ACN/80% water, at which point two distinct peaks were eluted (**Figure 6.4**). We believed the initial peak, being more polar, to be the OPV with both azide group functionalized with Enz1 (OPV-$(Enz1)_2$), while second peak was the OPV with only one Enz1 conjugated (OPV-(Enz1)). However, this hypothesis was disproved when mass spectrometry analysis (**Figure 6.5**) showed the major component to have a molecular weight of 6,801.4 and 6.801.5 D

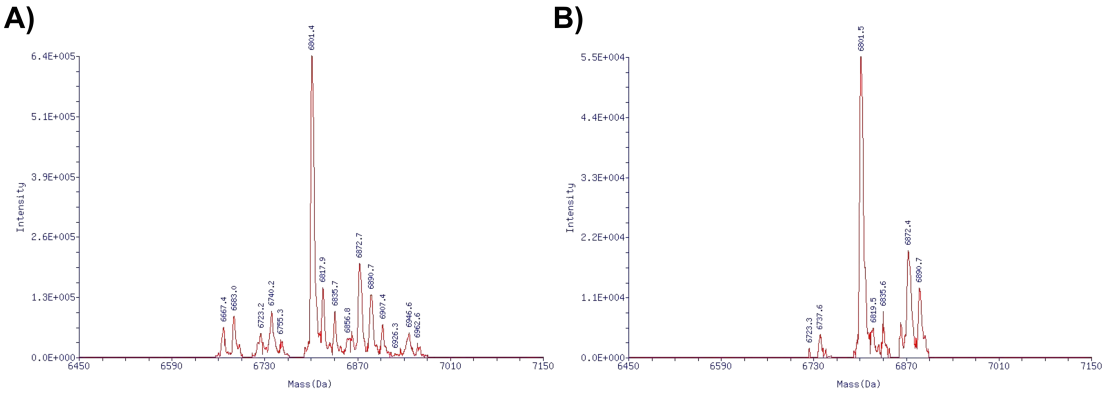

Figure 6.5 – Mass Spectrometry Analysis of HPLC Fractions. A) First HPLC fraction (12.5 minutes). **B)** Second HPLC fraction (15 minutes). The molecular weight of Enz1, without a fluorescent tag, is 6,801.6 D, which is the major component for both the first and second HPLC fractions according to mass spectrometry analysis.

respectively, which almost exactly matches the molecular weight of Enz1 (6,801.6 D), without a fluorescent tag, which was used in the conjugation. The other peaks were analyzed to determine if dividing by the molecular weight of SP-III-175C resulted in an integer, which could indicate formation of an OPV multimer, however, none of the peaks indicated such a formation. The peaks were also analyzed to determine if various reaction components were associating with the oligonucleotides or SP-III-175C, again no peak indicated such an association.

6.3.4 Incorporation of the OPV-Enz1 into Lipid Bilayers

The next steps will be to functionalize the same OPV with the second half of the split DNAzyme. At which point, we will have two separate molecules, both of which will be incorporated at 0.5 mol%, for a total of 1 mol%, into a DOPC lipid bilayer (**Figure 6.0**). This bilayer will also contain a PEGylated lipid, which will provide a cushion between the bilayer and a silica microsphere (SiMS).[22,23] After extruding the DOPC-PEG-(OPV-$(Enz1)_2$)-(OPV-$(Enz2)_2$) vesicles, cushioned supported lipid bilayers will be formed on 10 μm mesoporous SiMSs. This will allow analysis with flow cytometry.[24,25]

6.3.5 Split Enzyme Reactions in Lipid Bilayers

To design the split enzyme strands we used variant 1, from Table S2 of the Mokany et al. paper,[20] for the conserved catalytic core (see Appendix IV-T1 for strand sequences). We then used binding arms complementary to the U2 Substrate, which was previously used in our lab. To initiate signal transduction across the lipid bilayer a nucleic acid-based input strand will be added to the solution containing SiMS cushioned supported lipid bilayers. This tether strand will be designed to fully hybridize Enz1 and Enz2, thereby bringing the two OPV molecules into close proximity at the outer leaflet of the lipid bilayer. Consequently, the two halved of the split DNAzyme will be in close proximity within the bilayer as well, at which point the DNAzyme will be fully activated and will begin to cleave the chimeric U2 Substrate molecule (**Figure 6.6**). This substrate molecule will have both a fluorophore and a corresponding quencher molecule and will not emit photons before cleavage. After cleavage the fluorophore and quencher will move apart, and fluorescence will increase within the bilayer.

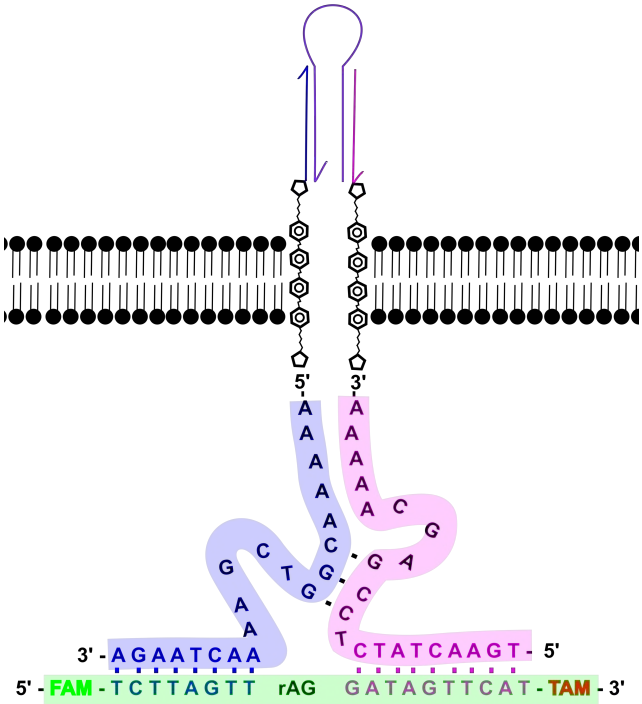

Figure 6.6 – Activated Split Enzyme Structure. Once the tether strand has activated the split DNAzyme, the two halves will be brought into close proximity within the bilayer and the DNAzyme will be fully activated.

6.3.6 Conclusion and Future Directions

Chapter 7 will present a body of work exploring the use of steroids, which passively

diffuse across lipid bilayers, as another means of transmembrane signal transduction. The use of polymersomes[14] should also be considered, as lipid stability (discussed in Chapter 5) continues to prove problematic. Additionally, polymersomes could allow for the use of a polymer with functional groups to which DNA can be conjugated, should the conjugation of oligonucleotides to the SP-III-175C prove unsuccessful using click chemistry.

6.4 Materials and Methods

6.4.1 Materials

For the synthesis of SP-III-163C and SP-III-175C, all solvents and reagents were obtained from Sigma–Aldrich (St. Louis, MO) and used without further purification. For the click chemistry reaction, all reagents were purchased from Sigma-Aldrich. All oligonucleotides were purchased from Integrated DNA Technologies (IDT, Coralville, IA). IDT purified unmodified strands by standard desalting, and the fluorophore/quencher tagged strands were purified by high performance liquid chromatography. Lipids were purchased from Avanti Polar Lipids (Alabaster, AL).

6.4.2 Synthesis

Analytical thin-layer chromatography (TLC) was performed on aluminum plates pre-coated with silica gel, also obtained from Sigma–Aldrich. Column chromatography was carried out on Merck 938S silica gel. Proton NMR spectra were recorded with a Varian 400 MHz NMR spectrometer. Spectra were referenced to the residual solvent peak, and chemical shifts are expressed in parts per million (ppm) from the internal reference peak. All compounds described were of >95% purity. Purity was confirmed by analytical LC/MS recorded with a Shimadzu system. Elution started with water (95 %, +0.1% formic acid)/ACN (5 %,

+0.1% formic acid) and ended with ACN (95 %, 0.1% formic acid)/water (5 %, 0.1% formic acid) and used a linear gradient at a flow rate of 0.2 mL per minute. The molecular ions [M]+, with intensities in parentheses, are given, followed by peaks corresponding to major fragment losses. Melting points were measured with a MEL-TEMP II melting point apparatus and are reported uncorrected.

6.4.3 High-Performance Liquid Chromatography

Reverse phase HPLC was performed on an Agilent 1100 Series, with a Zorbax ODS, 4.6 x 250 mm, 5 µm liquid chromatography column. HPLC analysis was run at room temperature, at 1 mL per minute, with elution being monitored by UV-Vis absorbance at 260 nm. The following gradient was used: 0-10 minutes 2% ACN/98% Milli-Q purified water; 10-20 minutes 20% ACN/80% water; 20-30 minutes 50% ACN/50% water; 30-40 minutes 98 %/2% water; 40-60 minutes 2% ACN/98% water.

6.4.4 Uv-Vis

UV/Vis measurements were taken on a PerkinElmer Lambda 35 UV/Vis Spectrometer in quartz cuvettes.

6.4.5 Mass Spectroscopy

Mass spectrometry was completed by Novatia, LLC.

6.5 References

(1) Milo, R.; Shen-Orr, S.; Itzkovitz, S.; Kashtan, N.; Chklovskii, D.; Alon, U. *Science* **2002**, 1.
(2) Chou, C. T. *Synthetic Biology* **2017**, *2* (1), 893.
(3) Brent, M. University of New Mexico November 2, 2016.
(4) Good, M. C.; Zalatan, J. G.; Lim, W. A. *Science* **2011**, *332*, 680.
(5) Johnson-Buck, A.; Jiang, S.; Yan, H.; Walter, N. G. *ACS Nano* **2014**, *8* (6), 5641.
(6) Zadorin, A. S.; Rondelez, Y.; Gines, G.; Dilhas, V.; Urtel, G.; Zambrano, A.; Galas, J.-C.; Estevez-Torres, A. *Nature Chemistry* **2017**, *9* (10), 990.
(7) Stojanovic, M. N.; Stefanovic, D. *Nat Biotechnol* **2003**, *21* (9), 1069.
(8) Zhang, D. Y.; Winfree, E. *J. Am. Chem. Soc.* **2009**, *131* (47), 17303.

(9) Brown, C. W., III; Lakin, M. R.; Fabry-Wood, A.; Horwitz, E. K.; Baker, N. A.; Stefanovic, D.; Graves, S. W. *ChemBioChem* **2015**, *16* (5), 725.
(10) Brown, C. W., III; Lakin, M. R.; Horwitz, E. K.; Fanning, M. L.; West, H. E.; Stefanovic, D.; Graves, S. W. *Angew. Chem. Int. Ed.* **2014**, *53* (28), 7183.
(11) Qian, L.; Winfree, E. *Science* **2011**, *332* (6034), 1196.
(12) Yasuga, H.; Kawano, R.; Takinoue, M.; Tsuji, Y.; Osaki, T.; Kamiya, K.; Miki, N.; Takeuchi, S. 2013; pp 1221–1222.
(13) Burns, J. R.; Stulz, E.; Howorka, S. *Nano Lett.* **2013**, *13* (6), 2351.
(14) Messager, L.; Burns, J. R.; Kim, J.; Cecchin, D.; Hindley, J.; Pyne, A. L. B.; Gaitzsch, J.; Battaglia, G.; Howorka, S. *Angewandte Chemie* **2016**, *128* (37), 11272.
(15) Howorka, S. *Nat. Nanotechnol.* **2017**, *12* (7), 619.
(16) Yasuga, H.; Kawano, R.; Takinoue, M.; Tsuji, Y.; Osaki, T.; Kamiya, K.; Miki, N.; Takeuchi, S. *PLoS ONE* **2016**, *11* (2), e0149667.
(17) Liang, H.; Chen, S.; Li, P.; Wang, L.; Li, J.; Li, J.; Yang, H.-H.; Tan, W. *J. Am. Chem. Soc.* **2018**, jacs.7b11311.
(18) Garner, L. E.; Park, J.; Dyar, S. M.; Chworos, A.; Sumner, J. J.; Bazan, G. C. *J. Am. Chem. Soc.* **2010**, *132* (29), 10042.
(19) Presolski, S. I.; Hong, V. P.; Finn, M. G. *Current Protocols in Chemical Biology* **2011**, *3* (4), 153.
(20) Mokany, E.; Bone, S. M.; Young, P. E.; Doan, T. B.; Todd, A. V. *J. Am. Chem. Soc.* **2010**, *132* (3), 1051.
(21) Han Young Woo; Bin Liu; Bernhard Kohler; Dmitry Korystov; Alexander Mikhailovsky, A.; Bazan, G. C. *Solvent Effects on the Two-Photon Absorption of Distyrylbenzene Chromophores*; American Chemical Society, 2005; Vol. 127, pp 14721–14729.
(22) Richter, R. P.; Bérat, R.; Brisson, A. R. *Langmuir* **2006**, *22* (8), 3497.
(23) Diaz, A. J.; Albertorio, F.; Daniel, S.; Cremer, P. S. *Langmuir* **2008**, *24* (13), 6820.
(24) Fabry-Wood, A.; Fetrow, M. E.; Brown, C. W., III; Baker, N. A.; Fernandez Oropeza, N.; Shreve, A. P.; Montano, G. A.; Stefanovic, D.; Lakin, M. R.; Graves, S. W. *ACS Appl. Mater. Interfaces* **2017**, *9* (35), 30185.
(25) Oropeza, N. F.; Zurek, N. A.; La Cruz, M. G.-D.; Fabry-Wood, A.; Fetzer, J. M.; Graves, S. W.; Shreve, A. P. *Anal. Chem.* **2017**, *89* (12), 6440.

CHAPTER 7 - PHYSICAL ISOLATION AND PROTECTION OF MOLECULAR COMPUTING ELEMENTS IN GIANT UNILAMELLAR VESICLES

Aurora Fabry-Wood,[†] Madalyn Elise Fetrow,[†] Ayomide Oloyede,[†] Kyung-Ae Yang,[#] Milan Stojanovic,[#,⊥] Darko Stefanovic,[†,§] Steven W. Graves,[†,‡,*] Nick J. Carroll,[†,‡,*] Matthew R. Lakin[§,†,*]

[†]Center for Biomedical Engineering, [‡]Department of Chemical and Biological Engineering, and [§]Department of Computer Science, University of New Mexico, Albuquerque, New Mexico 87131, United States

[#]Division of Experimental Therapeutics, Department of Medicine, [⊥]Departments of Biomedical Engineering and Systems Biology, Columbia University Medical Center, New York, New York 10032, United States

7.1 Abstract

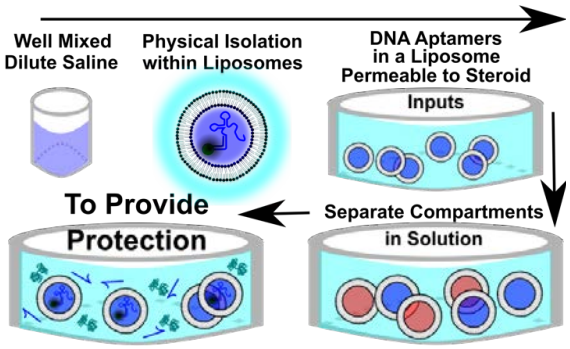

Figure 7.0 – Abstract Figure

The physical isolation of molecular computing elements has the potential to increase complexity, by allowing the reuse of standardized components, and to protect nucleic acid components from environmental degradation. However, once elements have been compartmentalized, methods for communicating into these compartments are needed. We report the encapsulation of steroid-responsive DNA aptamers within giant unilamellar vesicles (GUVs) that are permeable to steroid inputs. Monodisperse GUVs were loaded with aptamers using a high-throughput microfluidic platform. We demonstrate the target-specific activation of individual aptamers within the GUVs and then load two non-interfering aptamers into the same GUV and demonstrate specific responses to all possible combinations of the two input steroids. Crucially, the GUVs prevent degradation of

DNA components by nucleases, providing a mechanism for deploying nucleic acid components *in vivo*. Importantly, our compartments also prevent crosstalk between complementary strands in separate GUVs, providing a method for multiplexing potentially cross-reacting components. Thus, we provide a mechanism for spatially organizing computing elements, which increases modularity by allowing standardized components to be reused.

7.2 Introduction

Living systems comprise highly organized sets of compartments and this structure is directly tied to survival and reproduction. Each compartment contains highly specialized molecular circuitry, and communication between compartments is essential. From organelles to cells to tissues to organisms, the flow of information is precisely controlled and correct function relies on the spatial organization of biomolecular circuits that would otherwise interact in promiscuous ways.[1]

The field of molecular computation uses logic gates, built using biological polymers, to make decisions at the nanoscale. DNA, thanks to its highly predictable thermodynamic and mechanical properties, is an ideal building material for designing dynamic molecular systems, and Watson-Crick base pairing enables rapid design of molecular interactions. However, most DNA-based systems built up to now have been run in well-mixed dilute saline solutions, which lack spatial organization.[2-5] Spurious interactions, known as leakage, occur when output signals are generated in the absence of activating input signals, and lead to reduced signal to noise ratios. In solution phase DNA systems, efforts to decrease leakage include careful sequence design, thresholding,[6] the

incorporation of mismatches to prevent the formation of undesirable complexes,[7,8] structural designs that protect sequences vulnerable to leakage,[4,5] and domain-level motifs that prevent leakage by increasing the number of spurious events required for leakage to occur.[9] Efforts to decrease leakage by restricting computing elements to DNA origami scaffolds[10-14] have also been made. However, without full physical encapsulation, some leakage is still observed. Total encapsulation of computing elements using lipid bilayers, analogous to cell membranes, decreases spurious interactions even further, and allows the use of standardized components in distinct physical compartments. Lipid bilayers form the majority of compartments in cellular systems, including the cell membrane, the nuclear envelope and the mitochondrial membranes. Naturally occurring biological membranes are primarily composed of phospholipids, which self-assemble into fluid structures. In order to use lipid bilayers to physically isolate DNA-based molecular circuits, systems must be designed to allow signal transduction into the compartments and this requires an input layer that senses signals capable of crossing lipid bilayers.

In biological systems, signal transduction is achieved via integral membrane proteins or via passive diffusion (i.e., permeation of small moderately polar or non-polar molecules directly across the cell membrane). Steroids are hydrophobic small molecules, that passively diffuse across lipid bilayers,[15] making them good candidates for signal transduction into giant unilamellar vesicles (GUVs). We recently reported a set of ssDNA aptamers that specifically bind steroid inputs, and can be monitored with fluorescent microscopy.[16] Thus, aptamers that specifically bind steroid targets are ideal for use in the input layer of DNA-based biosensors

encapsulated within lipid bilayers. Crucially, they provide a method for signaling across the bilayer without physically disrupting it, which would directly expose the components within to the external chemical environment.

The cellular environment is tightly controlled and has many protection mechanisms, such as nucleases that degrade foreign and unused nucleic acids. A key goal of nucleic acid nanotechnology is to deploy engineered systems *in vivo* for autonomous diagnostic, and potentially therapeutic, applications.[17] However, for engineered nucleic acid systems to function reliably *in vivo* they must be stable in the presence of nucleases.[18-20] This requires total physical isolation of the computing elements within a compartment that is impermeable to the nucleases that would otherwise degrade the nucleic acids. Thus, our GUV system offers a route to implement nucleic acid-based biosensors that are robust to degradation and can thus operate in the intracellular environment for extended periods of time.

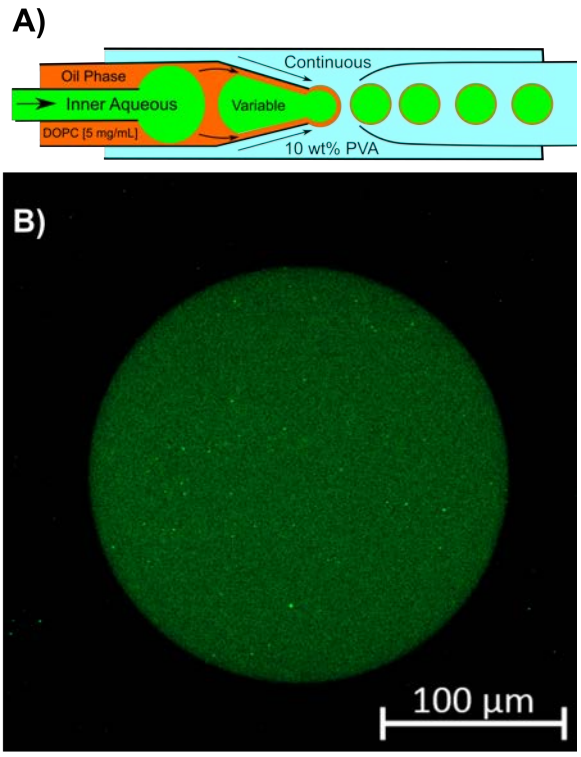

Figure 7.1 - The Microfluidic System. A) For the initial experiments GUVs were loaded with 10 wt% PVA in PBS, pH of 7.4, and a fluorescently tagged oligonucleotide [500 nM], to confirm microfluidic chip function and membrane stability in the presence of these compounds. The continuous phase consisted of 10 wt% PVA in PBS, pH 7.4, and the oil phase consisted of DOPC [5 mg/mL] in 36 vol% chloroform and 64 vol% hexane. See Movie S1 for video of device operation. **B)** The GUVs were then images on a Zeiss LSM 800 Airyscan confocal microscope (488/520 nm).

7.3 Results and Discussion

7.3.1 Microfluidics to Generate Monodispersed GUVs

We used a previously reported glass capillary microfluidic platform[21] to generate monodispersed GUVs, loaded with a range of aptamer cargos. Various aptamer cargos could easily be loaded, because this system allows all phases (inner aqueous, continuous and oil) to be modulated independently (**Figure 7.1A**). In addition, this system requires the use of a polymer, poly(vinyl alcohol) (PVA) in this case, to increase the viscosity and stabilize the lipid headgroups. Injection pumps are used for each of the phases, allowing the rates to be modulated independently. Generally speaking, the continuous phase is run at the highest flow rate. This introduces shear forces that pinch the lipid stream, thereby forming vesicles. The rates of the inner aqueous and oil phases effect the shell thickness, which must be <500 nm to achieve stable GUVs.[22] Directly after fabrication, the GUVs are incubated in a collection solution, at which point a good solvent (chloroform in this case) moves into solution, leaving behind a bad solvent (hexanes in this case) which gradually dewets allowing the lipids to assemble into a bilayer with an expected thickness of 5 nm. If this dewetting process happens too quickly, the lipids will not organize into bilayers and the GUVs will burst. Saturating the collection solution with the good solvent helps to slow the dewetting process. The collection container is also essential for stability, as any hydrophobic surface will disrupt the GUVs, and we exclusively used glass containers for collection.

To begin, we introduced salts and a buffer to the aqueous components, as the previous system consisted of PVA (M_W 13,000-23,000) in water. Nucleic acids

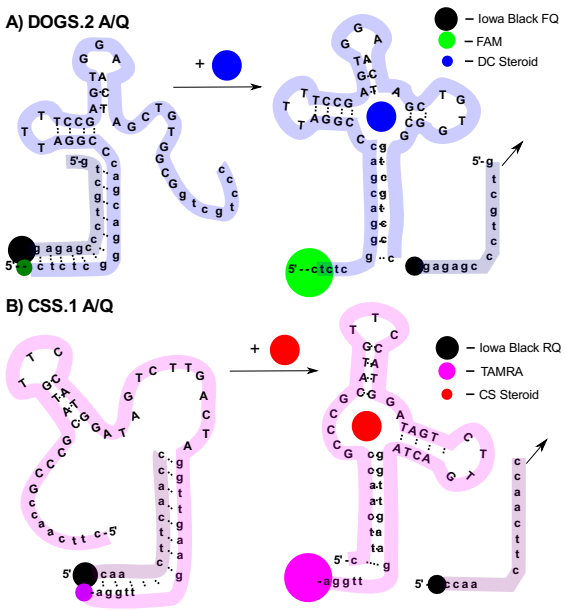

Figure 7.2 - Aptamer Structure and Response to Steroid Inputs. A) The DOGS.2 aptamer is labeled with fluorescein (FAM) and has a complementary quencher strand labeled with an Iowa Black FQ quencher. This aptamer/quencher (A/Q) pair is activated by the DC steroid, which causes a conformational change, ultimately displacing the quencher strand, resulting in an increase in FAM fluorescence. The capitalized bases represent the conserved target binding region of the aptamer, while the lower-case bases represent the stem region of the aptamer sequence and the complementary quencher strand. **B)** The CSS.1 aptamer is labeled with ATTO647 and has a complementary strand labeled with the Iowa Black RQ quencher. This A/Q pair is activated by the CS steroid.

require salt for hybridization, and we wanted to maintain a physiologically relevant pH, thus phosphate buffered saline (PBS) was selected and PVA was dissolved into the PBS buffer at 10 wt%. This solution was used for both the inner aqueous phase and the continuous phase (**Figure 7.1A**, Movie S1 shows the device in operation). We also introduced a fluorescein (FAM) labeled oligonucleotide [500 nM] into the inner aqueous phase and generated GUVs that were imaged on a Zeiss LSM 800 confocal microscope (**Figure 7.1B**). From here various components could be loaded into the GUVs that were collected in a solution containing 5 wt% PVA in PBS, the higher PVA percentage within the GUVs caused them to settle in this solution. As previously described, this collection solution was saturated with chloroform to slow the dewetting process.

7.3.2 The DOGS.2 and CSS.1 Aptamer/Quenchers

Two previously reported, aptamer-ligand sets were selected: the DOGS.2 aptamer that binds deoxycorticosterone (DC) with high selectivity and the CSS.1 that aptamer binds cortisol (CS).[16] The published solubility for the DC steroid is

100 µg/mL (302.6 µM) in ethanol, however, solubility at 500 µM in ethanol was achieved. Neither aptamer-ligand set is activated by the other, ensuring little to no non-specific activation between sets. The two aptamers were labeled with spectrally distinct fluorophores: DOGS.2 with FAM and CSS.1 with ATTO647. Each aptamer was hybridized to a partially complementary quencher strand labeled with an Iowa Black quencher specific to the fluorophore, forming an aptamer/quencher (A/Q) pair (**Figure 7.2**). Fluorescence resonance energy transfer (FRET) between the fluorophore and the Iowa Black quencher results in low fluorescence in the absence of target. Binding of the corresponding steroid target causes the aptamer strand to change conformation, which displaces the

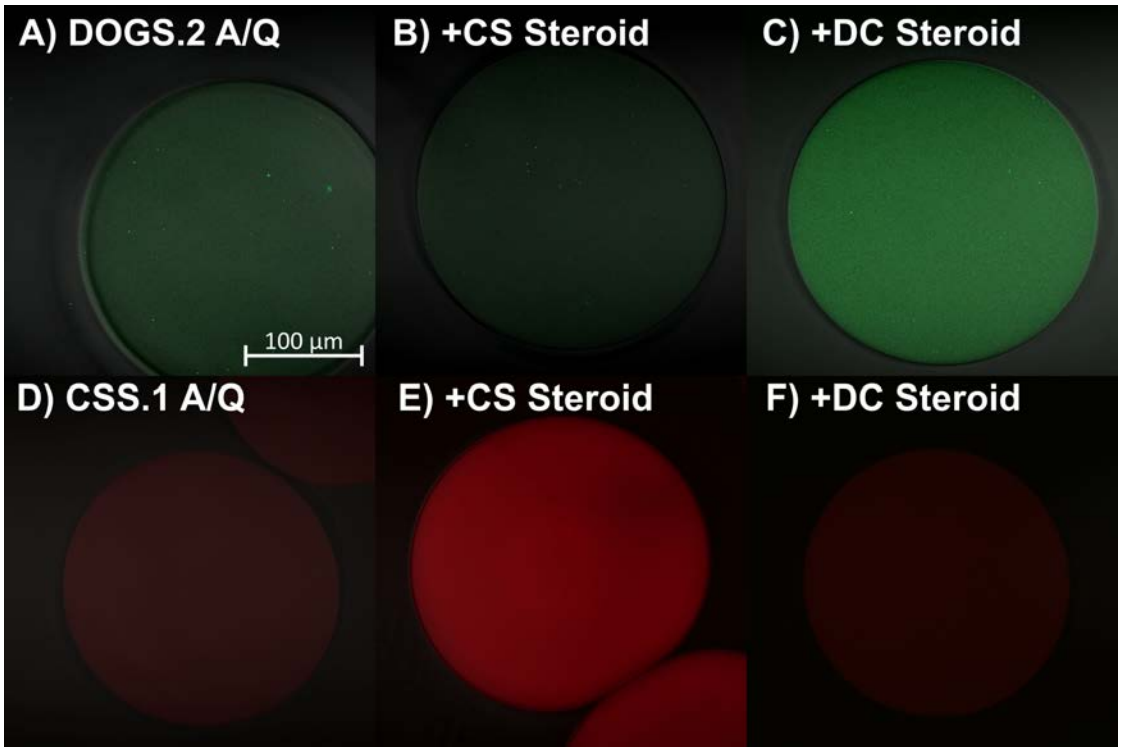

Figure 7.3 - GUV Response in the Presence of Various Steroid Inputs. A) DOGS.2 aptamer [500 nM]/quencher [550 nM] in the absence of input. **B)** DOGS.2 A/Q plus the non-specific CS steroid [500 µM]. **C)** DOGS.2 A/Q plus the specific DC steroid [500 µM]. Images A-C are composites of the FAM channel and a DIC image. **D)** CSS.1 aptamer [500 nM]/quencher [550 nM] in the absence of input. **E)** CSS.1 A/Q plus the specific CS steroid [500 µM]. **F)** CSS.1 A/Q in the presence of the non-specific DC steroid [500 µM]. Images D-F are a composite of the ATTO647 channel and a DIC image.

quencher strand. This leads to loss of FRET and hence increased fluorescence. We redesigned the stem region, which is not part of the conserved target binding aptamer sequence, of the published sequences so that the two aptamer/quencher pairs would not cross react when placed in the same GUV.

7.3.3 Responses of A/Q Pairs Encapsulated within GUVs

Aptamer function in 10 wt% PVA was first tested in solution, see Methods and Supporting Information for details. Having fully characterized the behaviors of both the DOGS.2 and the CSS.1 aptamers in the PVA solution, each A/Q pair was loaded into GUVs individually using our microfluidic platform. The loaded GUVs were incubated at room temperature for an hour, to allow dewetting of the oil phase solvents, at which point each steroid was added to a separate well containing ~100 GUVs loaded with one of the A/Q pairs and incubated at room temperature for one hour. **Figure 7.3A** shows confocal imagery of a GUV loaded with the DOGS.2 A/Q pair in the absence of steroid. **Figure 7.3B** shows the addition of the non-specific CS steroid [500 μM], and **Figure 7.3C** shows the addition of the target DC steroid

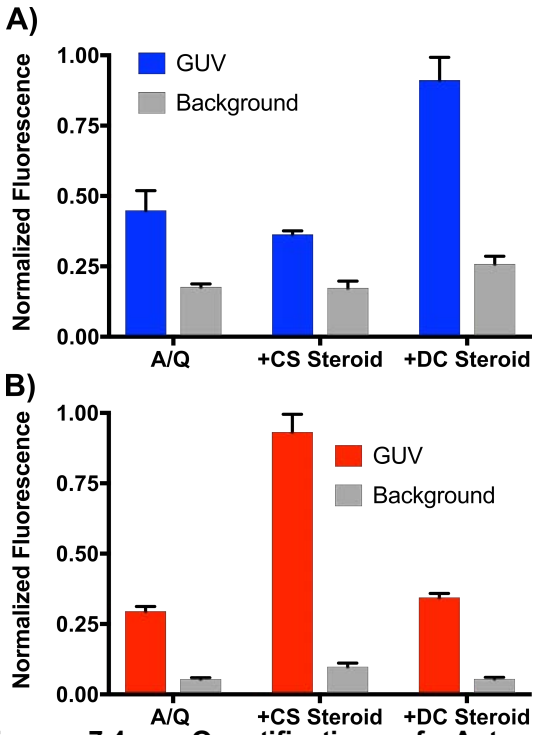

Figure 7.4 - Quantification of Aptamer Activation in GUVs, with Error Analysis. Five replicates (error bars are 95% CI) for the DOGS.2 and CSS.1 A/Q pairs. Both steroids were added at 500 μM. The FAM channel (488/520 nm) and ATTO647 channel (647/662 nm) values were calculated using an ROI that was identical for all replicates. The plots were normalized the mean of the A/Q pair as 0, and the mean of the target response as 1.

[500 μM]. The grayscales were standardized across all samples. **Figure 7.3D-F** shows the same for the CSS.1 A/Q pair, however the slower activation of the CSS.1 A/Q pair required an incubation period of 3 hours. As the binding kinetics between both aptamers and their respective targets are relatively equivalent in solution, we believe the slower activation may be related to the permeability of the CS steroid across the DOPC lipid bilayer. **Figure 7.4** show the results of a quantitative analysis of the intensity for 5 replicate GUVs. These results confirmed permeability of the steroid targets across the lipid bilayer and demonstrates signal

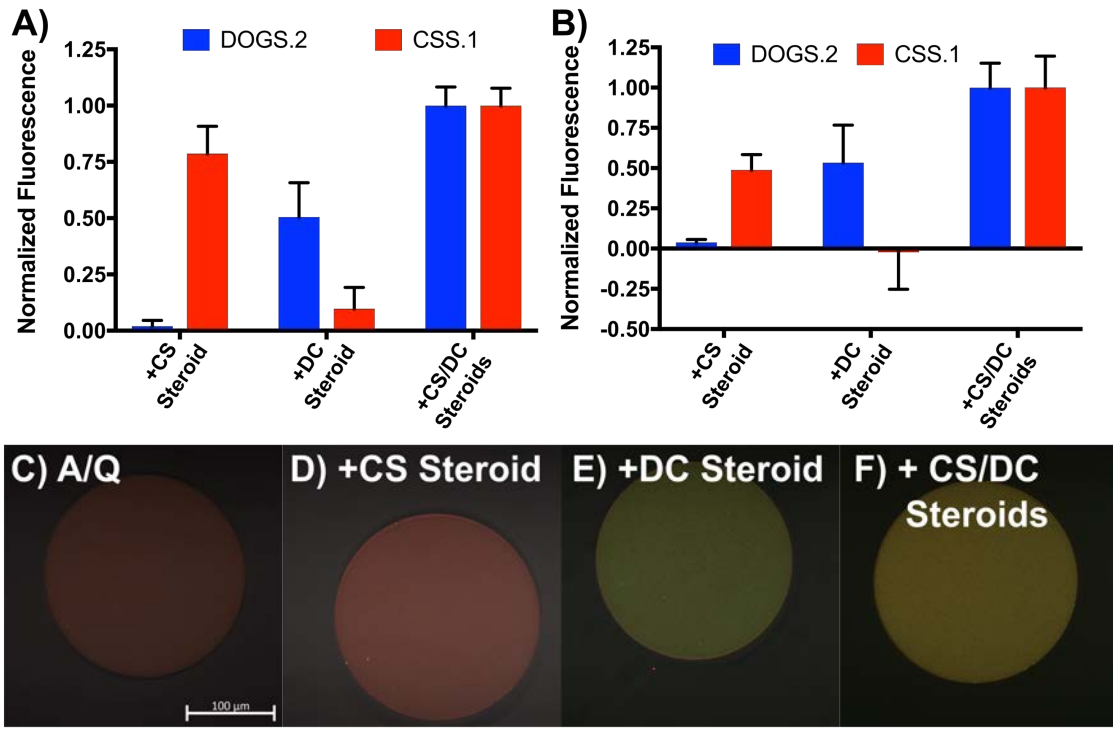

Figure 7.5 - Responses of Both Aptamers within a Single GUV. A) Solution phase experiment with both the DOGS.2 and CSS.1 A/Q present. Both aptamer strands are at 50 nM, and both quenchers at 55 nM. Both steroids were added at 150 μM, with a total steroid concentration of 300 μM for the +DC/CS steroids samples. **B)** Both the DOGS.2 and CSS.1 in the same GUV, in the presence of DC and CS steroids, and a combination of both steroid inputs. **C)** Composite image of both the FAM (488/520 nm) and the ATTO 647 (647/662 nm) channels, in the absence of all inputs. **D)** The same as C with the CS steroid [500 μM]. **E)** The same as C with the DC steroid [500 μM]. **F)** The same as C, with both steroids each at 500 μM, for a total steroid concentration of 1 mM.

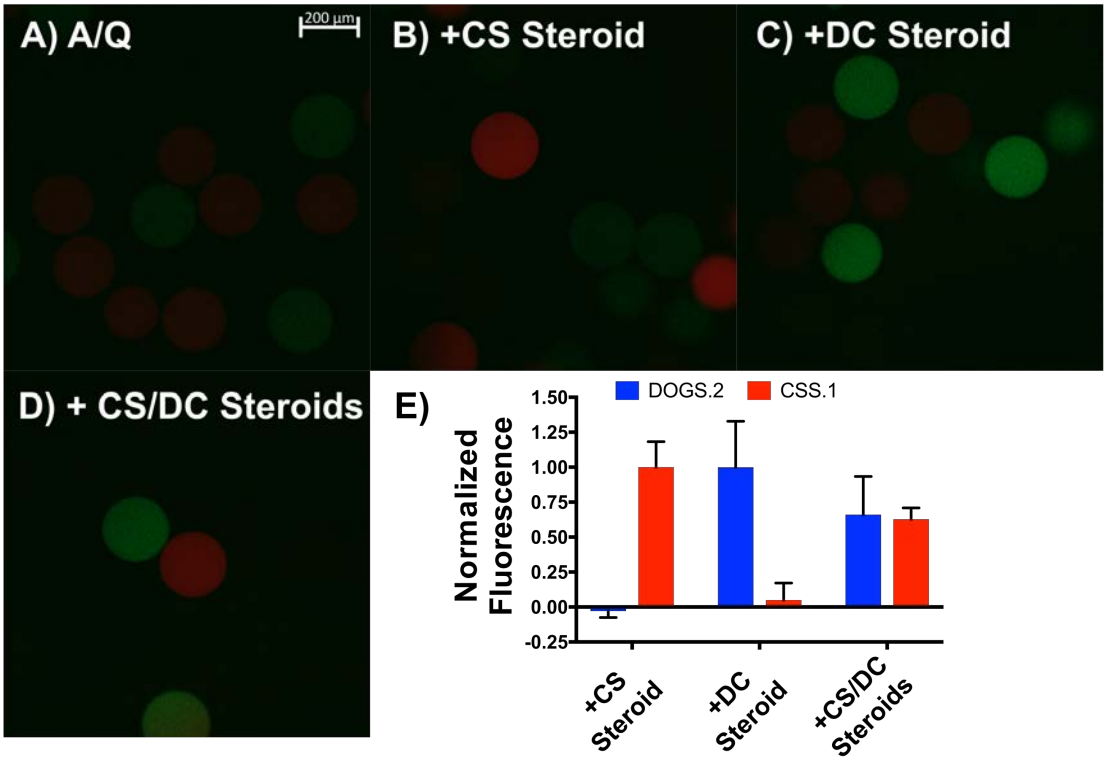

Figure 7.6 - Making Use of Separate Compartments. A) Two populations of GUVs loaded with individual aptamers, in same solution. In the absence of steroid inputs. **B)** Same as A, in the presence of CS steroid [500 µM]. **C)** Same as A, in the presence of DC steroid [500 µM]. **D)** Same as A, in the presence of both CS and DC steroids. **E)** Analysis of four replicates, error bars represent 95% CI, on the FAM (488/520 nm) ATTO647 (647/662 nm) channels.

transduction into a physically isolated membrane compartment using steroids. We next tested the behavior with both the DOGS.2 and CSS.1 A/Q pairs in the same solution. **Figure 7.5A**, shows the solution phase response of each aptamer in the presence of the DC steroid, the CS steroid and a combination of the DC and CS steroids. Having confirmed the function and specificity of the aptamers together in solution we loaded both A/Q pairs into the same GUV. **Figure 7.5B** shows the quantification of five replicate GUVs, an example of each shown in **Figure 7.5C-F**. As seen in solution, these aptamer-ligand sets are non-interfering and activation within the GUV is comparable to the experiments that contained individual A/Q pairs.

To make full use of the compartments, we created a solution with multiple populations of GUVs. Each GUV was loaded with the DOGS.2 A/Q pair or the CSS.1 A/Q pair. **Figure 7.6A** shows the two populations in solution, in the absence of steroid targets and although the aptamers are quenched it is still possible to determine which GUVs contain the FAM labeled DOGS.2 A/Q pair and which contain the ATTO647 labeled CSS.2 A/Q pair. In **Figure 7.6B**, with the CS steroid [500 μM] added, we only see increased fluorescence in the GUVs loaded with CSS.1. While in **Figure 7.6C**, with the addition of the DC steroid [500 μM], only the GUVs loaded with DOGS.2 brighten. Finally, in **Figure 7.6D**, with the addition of both the CS and the DC steroid targets, the fluorescence for all GUVs increases. **Figure 7.6E** shows the quantification of five replicate GUVs for each sample, further confirming the specificity of our aptamer-ligand sets. For this experiment we used non-interfering sequences, however, the same experiment would work very well if multiple aptamers, each with a standardized stem,[16] were loaded into separate GUVs in a single tube assay. Although others have used lipid bilayers to compartmentalization DNA-base molecular computing elements,[23-25] our high-throughput system provides a simple means of creating many compartments and does not require pores for signal transduction,[26] thereby maintaining a physical separation between the internal and external solutions.

7.3.4 Protection from Nucleases and Complementary Strands

To function *in vivo*, nucleic acid based molecular computing systems must be protected from nucleases. In a solution that lacks protection mechanisms, nucleic acids will be degraded by nucleases. As such, if a nuclease can access an A/Q pair it will completely degrade the individual strands and the fluorophore and

quencher will no longer be held in close proximity, resulting in an increase in fluorescence (**Figure 7.7A**). To test this hypothesis, we added DNAse I to the DOGS.2 A/Q pair in our 10 wt% PVA solution. DNAse I requires magnesium ions, and so we added Mg^{2+} [5 mM] to our solution. **Figure 7.7B** shows the anticipated increase in fluorescence in the presence of functional DNAse I, which is equivalent to that caused by the addition of the DC steroid target. To confirm that this was due to degradation by the DNAse and not via some other mechanism (e.g., aptamer binding to the nuclease protein itself), we exposed the A/Q pair to denatured DNAse (20 min at 95 ^{o}C) and observed a negligible increase in signal.

To demonstrate the ability of GUVs to protect DNA components from nucleases (**Figure 7.7C**), we loaded GUVs with the DOGS.2 A/Q pair, including Mg^{2+} [5 mM] in all aqueous solutions (the inner aqueous, continuous and collections solutions) for this experiment. We then added denatured DNAse I, functional DNAse I, functional DNAse I and the DC steroid target, and as an absolute positive control the DC steroid target on its own to GUV solutions (**Figure 7.7D**). We saw full protection from DNAse I when our A/Q pair was encapsulated in a GUV; the response was equivalent to the denatured DNAse I sample indicating full protection. We interpret this as the GUV membrane providing a physical barrier that prevents the DNAse from reaching the A/Q inside. To confirm DC steroid activation in the presence of the fully functional DNAse, we exposed the GUVs to both the DNAse and the DC steroid for 1 hour and saw an increase in fluorescence.

However, the increase in fluorescence for DC on its own was stronger and more consistent, possibly due to sequestration of the steroid by the DNAse.

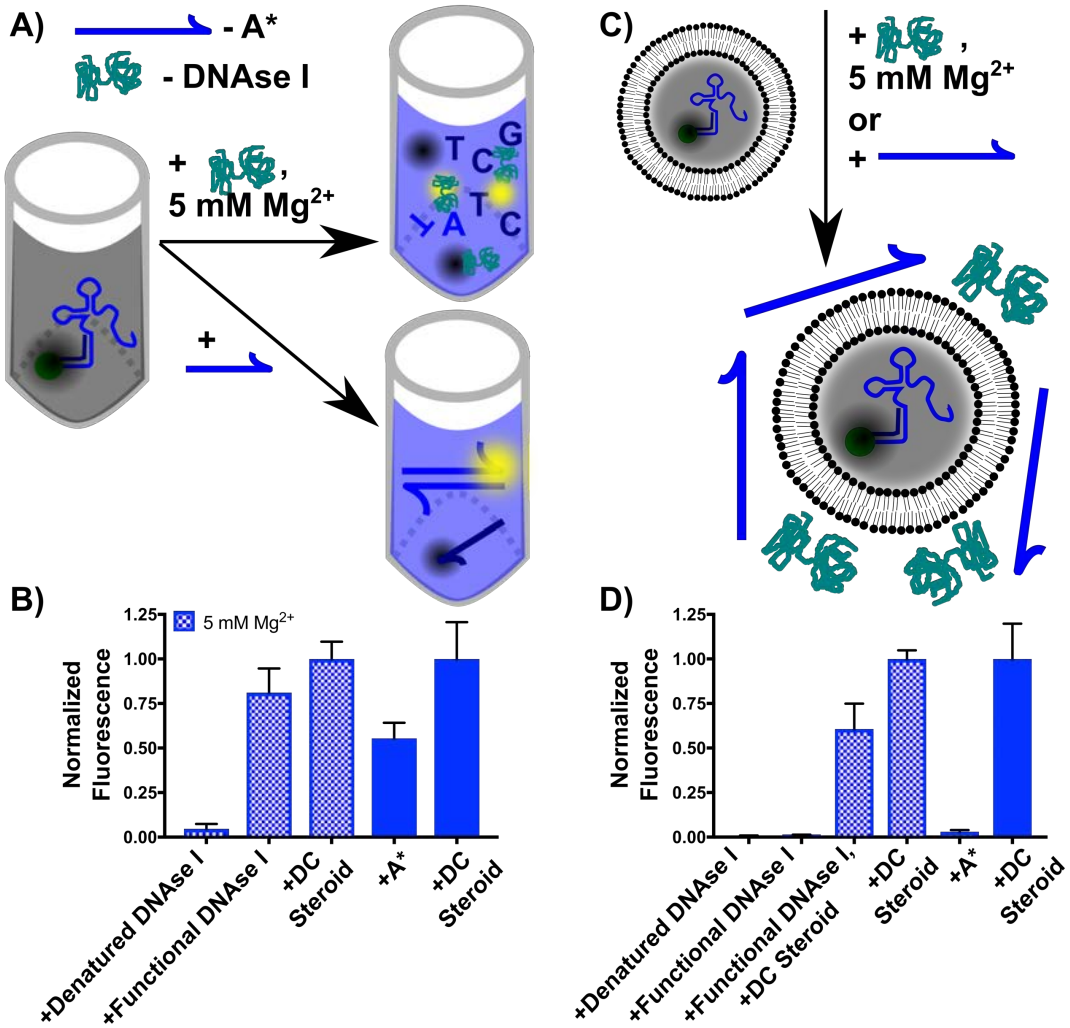

Figure 7.7 - Protection from Nucleases and Complementary Strands. A) Schematic illustrating solution phase experiments, with either the addition of DNAse I or a strand that is fully complementary to the DOGS.2 aptamer (A*). In this case all reactants are free to interact – DNAse I will degrade nucleic acids and complementary strands will for duplexes. **B)** Solution phase experiment with the DOGS.2 aptamer [100 nM]/quencher [110 nM] in the presence of denatured DNAse I [10 μM], functional DNAse I [10 μM], the DC steroid target [500 μM], in the presence of Mg^{2+}. On the same bar chart we have DOGS.2 aptamer [500 nM]/quencher [550 nM] in the presence of A* [600 nM], and the DC steroid target [500 μM] in the absence of Mg^{2+}. **C)** Schematic illustrating GUV experiments, where the lipid bilayer prevents both DNAse I and A* from interacting with the DOGS.2 A/Q pair. As illustrated in both A and C, the DNAse I experiments require 5 mM Mg^{2+}, which was added into all phases for the GUV experiment. The A* experiments do not have Mg^{2+}. Error bars represent 95% CI for five replicates. **D)** GUV experiment, with the DOGS.2 aptamer [500 nM]/quencher [550 nM] loaded into a GUV with 5 mM Mg^{2+} in all phases. The same denatured DNAse was added as a second negative control. For this experiment we added functional DNAse in the presence of the DC steroid target [500 μM]. As a true positive control, the DC steroid target was added at 500 μM. Error bars represent 95% CI for five replicates.

Another key advantage of physically isolating molecular circuits is that nucleotide sequences can be reused in different parts of the circuit without crosstalk. [12] To demonstrate that GUVs can protect internal components from undesired activation by partially complementary sequences, we introduced a strand (A*) that is fully complementary to the DOGS.2 aptamer strand. Our hypothesis was that the A* strand would interact with the A/Q pair when in bulk solution (**Figure 7.7A**) but would be prevented from doing so by a GUV membrane (**Figure 7.7C**). Our solution phase experiment studying the interactions of the DOGS.2 aptamer [500 nM]/quencher [550 nM] with the complementary A* strand [600 nM] (**Figure 7.7B**) shows activation of the fluorescent response, albeit slower and weaker activation than for the DC steroid input. This could be due to a kinetic trap that prevents the formation of the A/A* complex, which is predicted to be the most thermodynamically stable conformation. We demonstrated protection of the aptamers against the complementary strand by loading GUVs with the DOGS.2 A/Q and exposed them to an external solution containing A* (**Figure 7.7D**). The lack of response when A* is present in the external solution confirms protection of the A/Q pair from A* strand by the GUV and indicates that standardized strands (which in bulk solution would cause leakage) can be used in a solution containing separate compartments.

7.4 Conclusions

Using a previously reported high throughput microfluidic platform, DNA aptamers were encapsulated within GUVs. Initially, individual aptamers were encapsulated within GUVs. We then encapsulated two aptamers within the same GUV and finally we monitored behaviors with a mixture of two GUV populations,

each with a single A/Q pair, within the same solution. These aptamer-based molecular computing elements were activated by steroid inputs that passively diffused across a DOPC lipid bilayer, demonstrating signal transduction across lipid bilayers using steroids. To demonstrate spatial localization of sensing responses, we combined two populations of GUVs containing distinct aptamers and demonstrated target-specific activation in the presence of individual and multiple steroid inputs. Thus, our work introduces a mechanism for running standardized components in single-tube assay. Protecting DNA-based computing elements from nucleases that are found in living systems is an important problem, and we have shown that our system prevents degradation of encapsulated DNA components by DNAses. This system was also shown to decrease spurious interactions, by preventing fully complementary strands from meeting, and hence interacting with, the encapsulated A/Q pairs.

A fruitful avenue for future work will be to scale up the complexity of the computation performed within the compartments, in which the aptamer binding reactions monitored here would be just the first step of a multi-layer molecular computing cascade.[5] Our group previously demonstrated the use of an aptamer as the input layer of a cascade.[7] Furthermore, developing methods for signaling results back out of a compartment would enable the development of modular computational cascades assembled from reusable, vesicle-encapsulated subroutines.

7.5 Materials and Methods

7.5.1 Materials

All oligonucleotides were purchased from Integrated DNA Technologies (IDT, Coralville, IA). IDT purified unmodified strands by standard desalting, and the fluorophore/quencher tagged strands were purified by high performance liquid chromatography. Lipids were purchased from Avanti Polar Lipids (Alabaster, AL). Chloroform and hexanes were purchased from OmniSolv (Billerica, MA). PVA, PBS, $MgCl_2$, cortisol, deoxycorticosterone and DNAse I were purchased from Sigma Aldrich (St. Louis, MO). Square glass capillaries (OD 1.5 mm, ID 1.05 mm) were purchased from Atlantic International Technology (Rockaway, NJ). Round glass capillaries (OD 1.0 mm, ID 0.58 mm) were purchased from World Precision Instruments (Sarasota, FL). Devcon 5-minute epoxy must be used for device fabrication and was purchased from Scientific Commodities Inc. (Lake Havasu City, AZ).

7.5.2 Microfluidics to Generate GUVs

A micropipette puller (P-97, Sutter Instrument, Inc.) was used, at a heat setting of 500, a pull strength of 4, a velocity of 4 and a time setting of 150 for the injection, and collection capillaries. For the inner aqueous capillary, a heat setting of 600, a pull strength of 50, a velocity of 50 and a time setting of 150 was used. After pulling the capillaries a microforge (MF-830, Narishige) was used to determine ID dimensions, which were then adjusted use 2500 grit sandpaper from Home Depot. All PVA solutions were filtered with 5 μm filters (EMD Millipore) prior to use. The trimethoxy(octadecyl) silane was distilled prior to use, and devices were remade after each use to ensure efficient silane coats. The oil phase

consisted of pure 1,2-dioleyl-sn-glycero-3-phosphocholine (DOPC) at 5 mg/mL in a mixture of 36 vol% chloroform and 64 vol% hexane. To form ultrathin GUVs that were stable for up to 5 hours, we used a flow rate of 2500 μL/hr for both the inner aqueous and the oil phases and 10,000 μL/hr for the continuous phase.

7.5.3 Fluorimetry

Initial experiments were run to determine the optimal amount of quencher strand required for full quenching and strong ligand-dependent activation (see Supporting Information Figure A-IV.1). This was found to be 10 mol% above the aptamer strand concentration. To achieve consistent and maximal quenching, aptamer and quencher strands were incubated at room temperature for 15 minutes in a PBS solution and then diluted to the desired concentration in 10 wt% PVA in PBS (Supporting Information Figure A-IV.2). For the solution phase experiments the prehybridized aptamer [50 nM]/quencher [55 nM] complexes were added to 10 wt% PVA solution. Each steroid [150 μM] was added and the solution was incubated at room temperature for one hour (Figure A-IV.3). Each A/Q pair was activated by its ligand (i.e. the DOGS.2 A/Q pair was activated by the DC steroid target) and we saw a minimal increase in fluorescence for the non-specific steroid (i.e. the DOGS.2 A/Q pair in the presence of CS steroid). This non-specific activation was minimal when compared to the target steroid and was considered a negative response.

The DOGS.2 fluorimetry experiments were performed at room temperature (25 ^{0}C) on a Spectramax M2e fluorescent plate reader (Molecular Devices) in a 200 μL reaction volume (FAM: λ_{ex}=492 nm, λ_{em}=518 nm). The CSS.1 fluorimetry

experiments were performed on a Photon Technology International fluorimeter (ATTO647: λ_{ex}= 647 nm, λ_{em}= 662 nm).

7.5.4 Confocal Fluorescent Microscopy

All confocal experiments were performed on a Zeiss LSM800 confocal microscope, at the University of New Mexico's Cancer Center. Laser power for the FAM (λ_{ex}=488 nm, λ_{em}=520 nm) channel was held constant at 1%, with master gain set to 800 V. Laser power for the ATTO647 (λ_{ex}= 647 nm, λ_{em}= 662 nm) channel was held constant at 4%, with master gain set to 600 V. The pinhole for all experiments was set to 64 µm. A 40x oil emersion objective was used, with a scan speed of 6, and 0.5x magnification for individual GUVs. A 10x objective, with a scan speed of 6, was used when imaging multiple GUVs. A frame size of 2048x2048 was used, which corresponds to a pixel size of 0.16 µm with the above settings.

7.6 Associated Content

The Supporting Information is presented in Appendix IV. The Supporting Information document includes all supplementary figures as described in the main text. Movie A-IV.1 – To show device in operation.

7.7 Author Information

7.7.1 Corresponding Authors

*mlakin@cs.unm.edu (MRL), *ncarroll@unm.edu (NJC),
*graves@unm.edu (SWG)

7.7.2 Author Contributions

All authors contributed to writing the manuscript. NJC provided microfluidic training and expertise. NJC, AFW and AO fabricated the glass capillary microfluidics devices. AFW, MEF and AO conducted the fluorimetry experiments. AFW conducted all confocal experiments. MRL and AFW redesigned the CSS.1 aptamer stem sequence. MS, DS, MRL, SWG and NJC supervised the project.

7.7.3 Notes

The authors report no conflicts of interest.

7.8 Funding

This material is based upon work supported by the National Science Foundation under grants: 1525553, 1518861, and 1318833.

7.9 Acknowledgements

We kindly thank Andrew P. Shreve for discussion on lipid composition and membrane permeability experiments and Michael L. Paffett for his assistance with confocal experiments.

7.10 Rerences:

(1) Good, M. C.; Zalatan, J. G.; Lim, W. A. *Science* **2011**, *332*, 680.
(2) Yurke, B.; Turberfield, A. J.; Mills, A. P., Jr; Simmel, F. C.; Neumann, J. L. *Nature* **2000**, *406* (6796), 605.
(3) Stojanovic, M. N.; Mitchell, T. E.; Stefanovic, D. *J. Am. Chem. Soc.* **2002**, *124* (14), 3555.
(4) Qian, L.; Winfree, E. *Science* **2011**, *332* (6034), 1196.
(5) Brown, C. W., III; Lakin, M. R.; Horwitz, E. K.; Fanning, M. L.; West, H. E.; Stefanovic, D.; Graves, S. W. *Angew. Chem. Int. Ed.* **2014**, *53* (28), 7183.
(6) Seelig, G.; Soloveichik, D.; Zhang, D. Y.; Winfree, E. *Science* **2006**, *314* (5805), 1585.
(7) Brown, C. W., III; Lakin, M. R.; Fabry-Wood, A.; Horwitz, E. K.; Baker, N. A.; Stefanovic, D.; Graves, S. W. *ChemBioChem* **2015**, *16* (5), 725.
(8) Jiang, Y. S.; Bhadra, S.; Li, B.; Ellington, A. D. *Angewandte Chemie* **2014**, *126* (7), 1876.
(9) Thachuk, C.; Winfree, E.; Soloveichik, D. 2015; pp 133–153.
(10) Teichmann, M.; Kopperger, E.; Simmel, F. C. *ACS Nano* **2014**, *8* (8), 8487.
(11) Ruiz, I. M.; Arbona, J.-M.; Lad, A.; Mendoza, O.; Aimé, J.-P.; Elezgaray, J. *Nanoscale* **2015**, *7* (30), 12970.
(12) Chatterjee, G.; Dalchau, N.; Muscat, R. A.; Phillips, A.; Seelig, G. *bioRxiv* **2017**, 110965.
(13) Thubagere, A. J.; Li, W.; Johnson, R. F.; Chen, Z.; Doroudi, S.; Lee, Y. L.; Izatt, G.; Wittman, S.; Srinivas, N.; Woods, D.; Winfree, E.; Qian, L. *Science* **2017**, *357* (6356), eaan6558.
(14) Bui, H.; Shah, S.; Mokhtar, R.; Song, T.; Garg, S.; Reif, J. *ACS Nano* **2018**, *12* (2), 1146.

(15) Yang, N. J.; Hinner, M. J. In *Site-Specific Protein Labeling*; Methods in Molecular Biology; Springer New York: New York, NY, 2014; Vol. 1266, pp 29–53.
(16) Yang, K.-A.; Chun, H.; Zhang, Y.; Pecic, S.; Nakatsuka, N.; Andrews, A. M.; Worgall, T. S.; Stojanovic, M. N. *ACS Chem. Biol.* **2017**, *12* (12), 3103.
(17) Groves, B.; Chen, Y.-J.; Zurla, C.; Pochekailov, S.; Kirschman, J. L.; Santangelo, P. J.; Seelig, G. *Nat. Nanotechnol.* **2015**, *11* (3), 287.
(18) Mei, Q.; Wei, X.; Su, F.; Liu, Y.; Youngbull, C.; Johnson, R.; Lindsay, S.; Yan, H.; Meldrum, D. *Nano Lett.* **2011**, *11* (4), 1477.
(19) Chen, Y.-J.; Groves, B.; Muscat, R. A.; Seelig, G. *Nat. Nanotechnol.* **2015**, *10* (9), 748.
(20) Jiang, D.; Sun, Y.; Li, J.; Li, Q.; Lv, M.; Zhu, B.; Tian, T.; Cheng, D.; Xia, J.; Zhang, L.; Wang, L.; Huang, Q.; Shi, J.; Fan, C. *ACS Appl. Mater. Interfaces* **2016**, *8* (7), 4378.
(21) Arriaga, L. R.; Datta, S. S.; Kim, S.-H.; Amstad, E.; Kodger, T. E.; Monroy, F.; Weitz, D. A. *Small* **2013**, *10* (5), 950.
(22) Kim, S.-H.; Kim, J. W.; Cho, J.-C.; Weitz, D. A. *Lab Chip* **2011**, *11* (18), 3162.
(23) Yasuga, H.; Kawano, R.; Takinoue, M.; Tsuji, Y.; Osaki, T.; Kamiya, K.; Miki, N.; Takeuchi, S. 2013; pp 1221–1222.
(24) Yasuga, H.; Kawano, R.; Takinoue, M.; Tsuji, Y.; Osaki, T.; Kamiya, K.; Miki, N.; Takeuchi, S. *PLoS ONE* **2016**, *11* (2), e0149667.
(25) Langecker, M.; Arnaut, V.; List, J.; Simmel, F. C. *Acc. Chem. Res.* **2014**, *47* (6), 1807.
(26) Howorka, S. *Nat. Nanotechnol.* **2017**, *12* (7), 619.

CHAPTER 8 – CONCLUSIONS AND FUTURE DIRECTIONS

8.1 Conclusions

The work presented here represents initial steps towards developing easily adaptable, highly selective and rapid diagnostics tools. The first set of experiments presented solution phase TMSD and DNAzyme reactions, capable of dsDNA detection. Importantly, when multiple regions on the plasmid model were targeted an increase in response was seen. The implications of this will be further discussed in the next section. In the next set of experiments, a DENV diagnostic was demonstrated using TMSD reactions on multiplexed μSLBs. The limit of detection (LOD) for this system was 3 nM. Methods for further decreasing LODs will be proposed in the next section. In addition, buffer conditions were optimized to allow DNAzyme reactions to be run on zwitterionic lipid surfaces. This body of work, provides valuable methods for interfacing DNA and lipid bilayers. The design of a molecule capable of DNA-based transmembrane signal transduction was then presented. This molecule would allow communication into and potentially back out of compartments. Finally, DNA aptamers were encapsulated with GUVs using a glass capillary microfluidic platform. Signals were transduced across the bilayers using steroids. Importantly, we demonstrated protection from nucleases and from strands that would cause interference in a well-mixed solution. Preliminary experiments for increasing the complexity of these GUV compartments are presented in the next section.

8.2 Future Directions

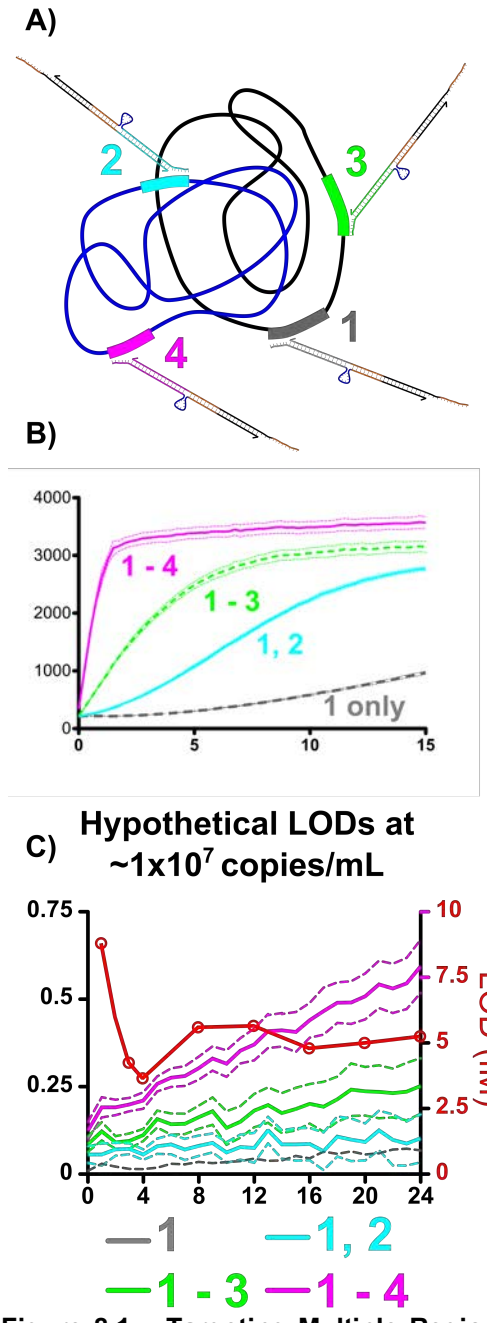

Figure 8.1 – Targeting Multiple Regions on Both Halves of a Genome to Decrease Limits of Detection. A) Logic gates targeting multiple regions on both halves of a genome. **B)** Hypothetical plot, showing an increase in response as the number of targets increases. The data presented in Figure 3.5 suggests that this is possible. **C)** Hypothetical plot, showing a decrease in the limit of detection.

Efforts to decrease the limit of detection using isothermal amplification techniques have proven difficult. As such, future efforts should focus on PCR readouts, as methods of analysis for PCR product do not currently use DNA-based molecular logic. Additionally, targeting multiple regions on a genome, and in the case of dsDNA genomes both halves of the genome should be targeted (**Figure 8.1A**). Figure 3.5 presented very promising data in this regard, suggesting that if we target multiple regions we can increase our response (**Figure 8.1B**) to levels comparable with simple ssDNA responses. This increase in response should translate to a decrease in LOD values (**Figure 8.1C**). The complexity of DNA-based molecular computation has the potential to contribute significant benefits to PCR readout and

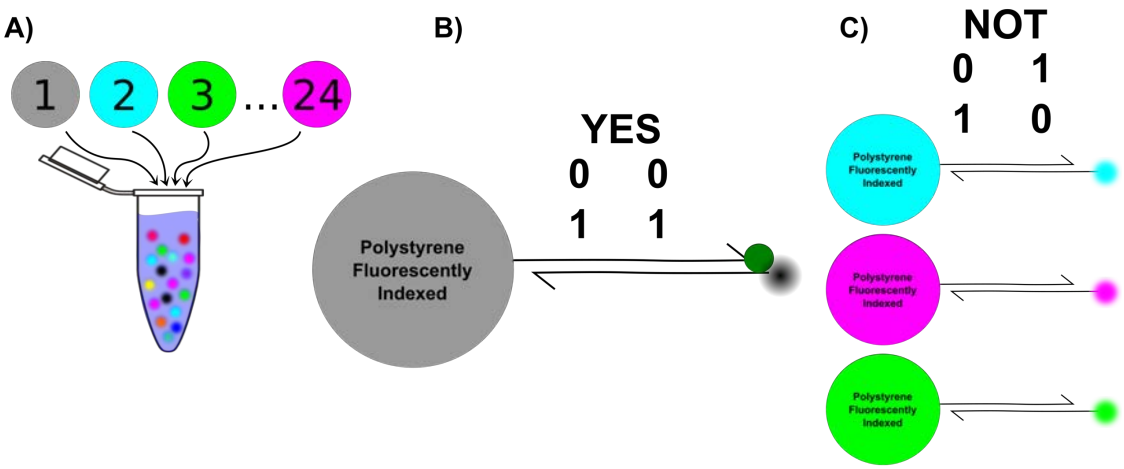

Figure 8.2 – Fluorescently Indexed Polystyrene Beads with both YES and NOT gates. A) A multiplex using fluorescently indexed polystyrene beads, with >9 populations (the largest multiplex achieved in Chapter 4 was 9 populations). Each bead set can be used to target multiple regions on DENV-1, for instance, using YES gates. While the other bead sets will have NOT gates, with sequences that would target the other DENV-2 - DENV-4.

diagnostics. Still, high throughput methods of analysis, such as flow cytometry, are needed.

One of the most powerful capabilities of flow cytometry is the ability to monitor multiplexed bead sets. **Figure 8.2**, presents a hypothetical method for detecting multiple regions on a genome, while simultaneously testing for other genomes. The multiplexed bead sets presented in Chapter 4 were achieved using lipid bilayers. However, as mentioned in Chapter 4, polystyrene beads are frequently used and much larger multiplexes can be achieved using these systems (**Figure 8.2A**). If TMSD gates were attached directly to the polystyrene beads multiple regions of a genome could be targeted using YES gates (**Figure 8.2B**), and NOT gates could be designed to target other genomes (**Figure 8.2C**). Analysis with flow cytometry could allow a limited number of fluorophores to be used and would produce highly qualitative and high dimensional data sets. This may seem

far-fetched but think of the DNA microarrays used for next generation sequencing, then put those arrays on polystyrene beads and analyze with flow cytometry.

Figure 8.3 presents images showing large unilamellar vesicles (LUVs), tagged with 0.5 mol% Liss Rhod PE (LRPE) and loaded with an Alexa Fluor 647 solution, within GUVs. The LUVs were prefabricated and loaded into the GUVs along with a FAM labeled oligonucleotide (DOGS.2 [500 nm]). The LUVs also contained 5 wt% PVA in PBS (pH 7.4), while the solution they were suspended in contained 10 wt% PVA, this ensured buoyancy of the LUVs within the GUV. The GUVs were collected in a 5 wt% PVA solution so they would settle on the cover

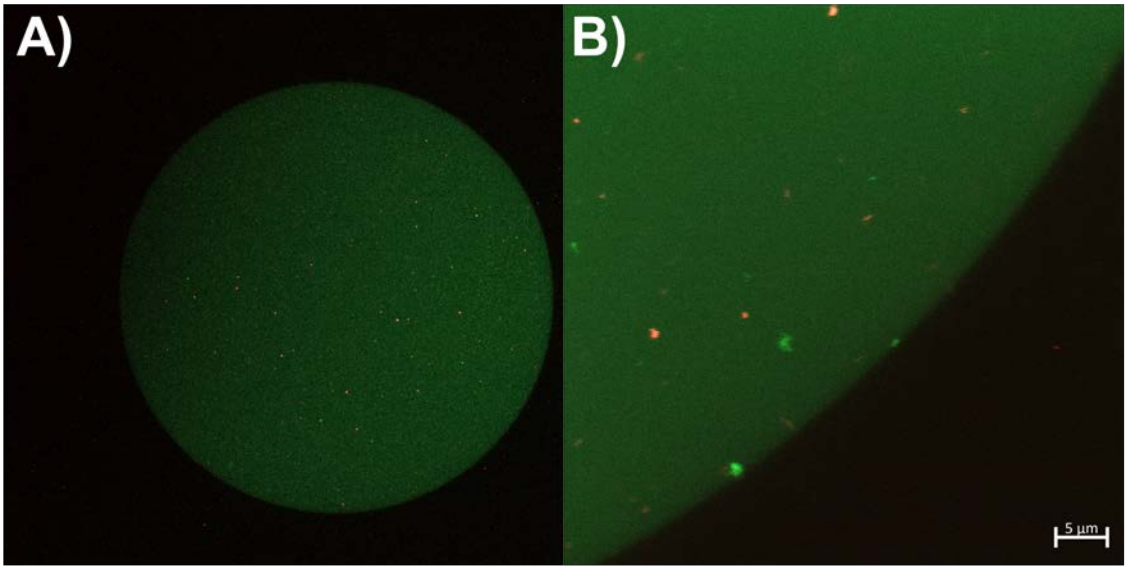

Figure 8.3 – Compartments within Compartments. A) Zeiss LSM 800 Airyscan confocal image of GUVs loaded with 0.2 µm large unilamellar vesicles (LUVs) and a fluorescently tagged oligonucleotide (LUT in green). **B)** Zoomed in image of A, showing the LUVs, which have a DOPC bilayer spiked with 0.5 mol% LRPE (LUT in red) and are loaded with a solution of Alexa Fluor 647 (LUT in white).

slip. The GUVs were then imaged on a Zeiss LSM 800 Airyscan confocal microscope with a 40x oil objective, and the LUVs were images with 63x oil objective. The esteemed Richard Feynman said the following – “What I cannot create, I do not understand.” Currently, there is a lot of interest in building cell like

structures, such as membranes within membranes, and the data from **Figure 8.3** offers a way to create, and thus understand hierarchical compartment systems. Additionally, being able to transduce signals into inner compartments would be very impactful. Although the LUVs presented here are smaller than desired, perhaps 10 μm polymersomes can be loaded into 100 μm polymersomes, at which point DNA could be used to receive signals that cross into the polymer capsule.

Speaking of polymersomes, encapsulation with polymersomes, as opposed to phospholipid bilayers, is a potentially fruitful avenue for future research. Polymersomes are considerably more stable than lipids, and they are more tunable. Eventually communication in and out of polymersomes could be achieved if the polymer membrane was permeable to ssDNA. Then, within the polymersome, logic gates could be linked to polystyrene beads, thereby preventing diffusion out of the polymersome in the absence of input signals. Alternatively, polymersomes could be used to create a membrane like region on the surface of a polystyrene bead, which provide an excellent platform for lipopolysaccharide presentation and detection.

The systems presented here use lipid bilayers to spatially organize, and in some regards physically isolate, DNA-base molecular computing elements. The complex spatial organization of biomolecular circuits contributes significantly to their function. I believe that mimicking the compartmentalized systems found in biology will improve the performance of engineered molecular computing systems. Thereby, allowing them to operate at high levels in diagnostics and *in vivo*.

APPENDIX I – SUPPORTING INFORMATION FOR CHAPTER 3

A Unified Sensor Architecture for Isothermal Detection of Double-Stranded DNA, Oligonucleotides, and Small Molecules

A-I.1 Supplementary Methods

In our experiments, we used a ~15% stoichiometric excess of inhibitor strands compared to DNAzymes at 2.5 uM when preparing the DNAzyme-inhibitor complex, to account for variation in concentrations between stocks and for pipetting errors. We aimed to minimize the complexity of circuit preparation by eliminating the need for purification of sensor complexes, therefore we left these excess inhibitors in the solution. This also helps to inhibit the DNAzymes more efficiently. However, the excess inhibitor may hinder circuit operation by binding to target strands, preventing them from activating the DNAzymes, and by rebinding activated DNAzyme strands to deactivate them. As a further step to suppress circuit leakage, we extended the inhibitor by 3 nt beyond the length of the fuel strand. This provided an additional toehold for rebinding of free DNAzymes to the fuel-inhibitor complex, which reduces leakage by allowing spuriously released DNAzymes to rebind to the inhibitor, at the price of also re-inhibiting DNAzymes that were released through a valid reaction mechanism. To counteract these effects, we used an excess of substrate relative to the DNAzyme concentration and relied on output signal amplification via multiple-turnover cleavage reactions to provide a higher maximum signal-to-background ratio.

A-I.1.1 Oligonucleotide sequences

Oligonucleotide sequences are presented in Tables A-I.1 – A-I.6. All sequences are listed 5' to 3'. Substrates are cleaved at the dinucleotide junction between the two bases highlighted in red, and the catalytic cores of DNAzymes are highlighted in boldface. The RNA base at the cleavage site in the substrate strand is represented as rA.

Fluorescein fluorophores and TAMRA quenchers are represented as /FAM/ and /TAM/ respectively.

A-I.1.2 Plasmid target selection

The full nucleotide sequence for the prSET emGFP plasmid was obtained from the manufacturer (Life Technologies catalog number V353-20). The full nucleotide sequence for the SNAP25 plasmid was obtained from previous work on this plasmid in our lab [1]. This plasmid is based on the commercially Pinpoint Xa-1 vector (Promega catalog number: V2031, Genbank accession number: U47626.2). Targets were identified from unique areas of each plasmid via a custom NUPACK design script [2], to determine optimized detection sequences. Each 18 nt target was selected to contain minimal secondary structure.

For optimal gate performance, it is important that the DNAzyme-inhibitor complex forms correctly and that the intermediate steps in the reaction mechanism do not lead to unwanted secondary structure formation. In particular, when the target binds to the detection module it displaces part of the DNAzyme strand, which is now single-stranded and positioned directly opposite the single-stranded toehold that was previously sequestered in the bulge. If there is any significant complementarity sequence between this part of the DNAzyme strand and the toehold on the inhibitor strand, it is highly likely that these two parts of the strands will hybridize. This would block the secondary toehold, preventing the fuel strand from binding and releasing the active DNAzyme from the complex. This issue can be addressed by choosing toehold sequences so that there is no possible interaction between the displaced target sequence and the toehold on the inhibitor strand. The results reported in the main text for the C1-3, E, and S sensors were obtained using a universal toehold sequence chosen from a restricted three-base alphabet (A,C,T). This minimized interactions between the inhibitor toehold and the G-poor target regions that we had selected from the plasmids. The data in Figures A-I.8 – A-I.11 show

that alternative toeholds may be used: in those Figures, a separate toehold was chosen for each sensor and similar behavior was observed.

A-I.2 Supplementary Figures

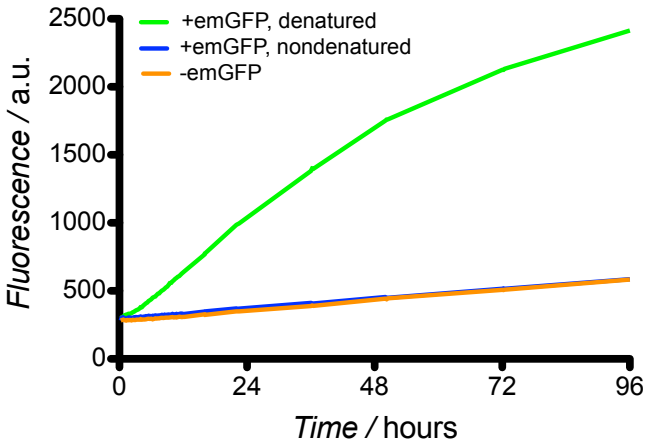

Figure A-I.1 - Plasmid Denaturation is Necessary for Target Detection. Fluorescent response with untreated emGFP (blue) is the same as without emGFP (orange), demonstrating the effect of pH cycling to expose the single-stranded domains of the plasmid. pH treatment of the plasmid (green) shows an immediate response. Concentrations: 40 nM DNAzyme, 50 nM inhibitor, 40 nM fuel, 40 nM emGFP, 250 nM substrate.

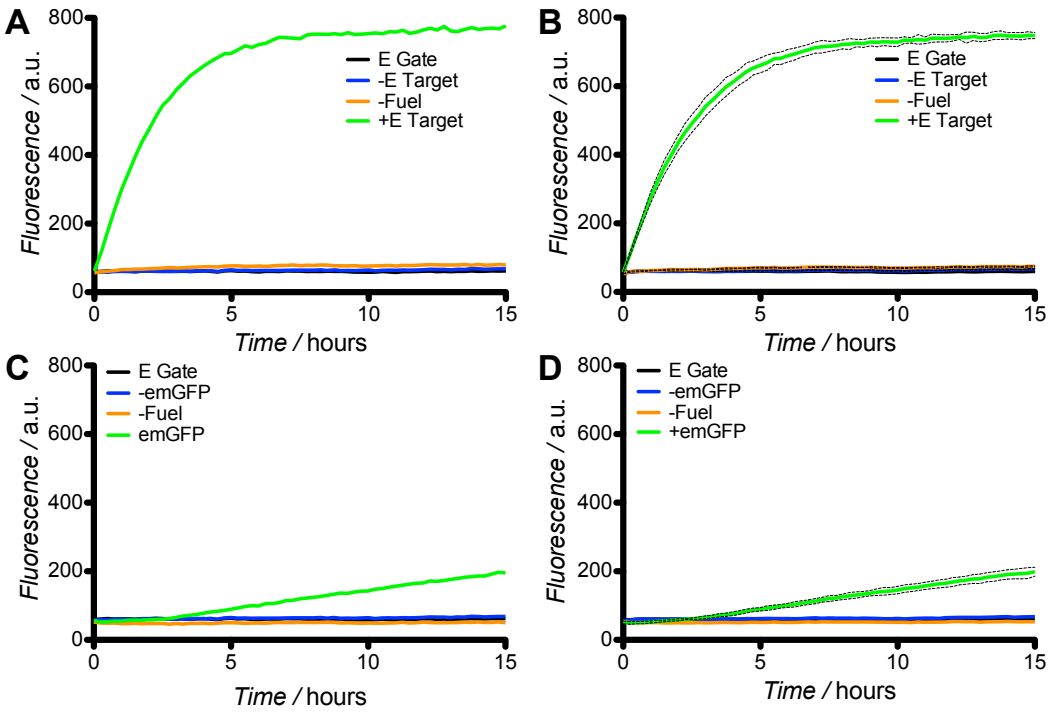

Figure A-I.2 - Sensor Performance in the Presence of Background DNA. Traces are gate only (black), gate with fuel only (blue), gate with target only (orange), and gate with both target and fuel. **A)** E gate performance with its corresponding target oligo **B)** E gate performance with its corresponding target oligo in the presence of background DNA. **C**) E gate performance with emGFP **D**) E gate performance with emGFP in the presence of background DNA. Background DNA was denatured herring sperm DNA (1ug/mL). Error bars (**B, D**) indicate one standard deviation of three replicates. Concentrations: 5 nM DNAzyme, 5.75 nM inhibitor, 5 nM fuel, 5 nM target, 25 nM emGFP, 50 nM substrate.

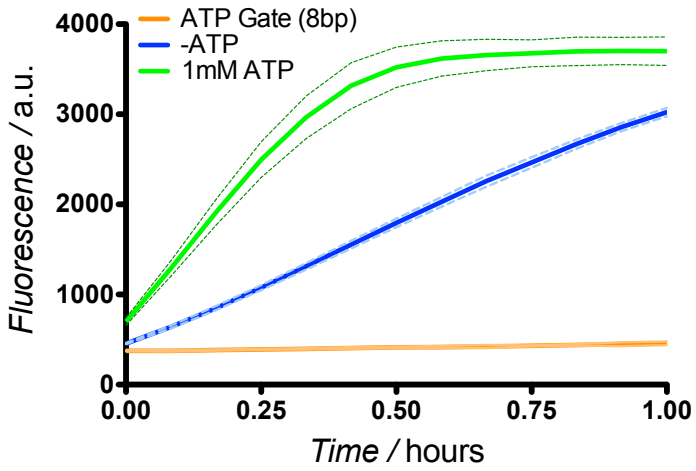

Figure A-I.3 - ATP Sensor Performance with Standard 8nt Loop Toehold. Addition of the fuel strand led to a higher than normal leakage in the gate compared to typical oligonucleotide or plasmid sensor responses. This is likely due to the shorter detection domain required for sufficient ATP aptamer activation (8 bp compared to 10 bp), that when coupled to an 8 nt loop enables a more productive invasion by the fuel strand. Error bars indicate one standard deviation of three replicates. Concentrations: 100 nM DNAzyme, 115 nM inhibitor, 100 nM fuel, 1 mM ATP, 250 nM substrate.

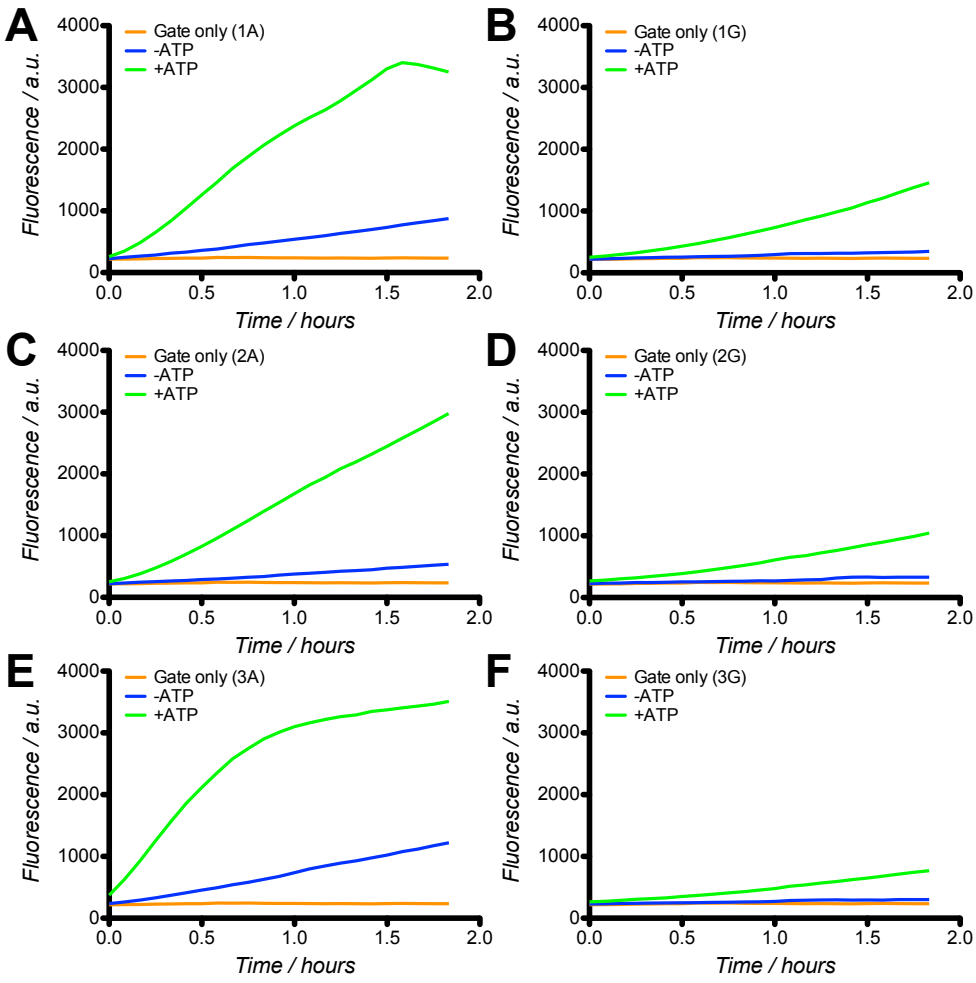

Figure A-I.4 - **Optimization of Toeholds for ATP Sensor.** 5 nt loop toeholds were tested for reduced gate leakage in the presence of fuel. Different mismatch base combinations were tested, varying the location of a single mismatch (base position 1, 2, or 3 from the reporter domain) and the presence or absence of a G-T wobble mismatch at the first base within the double-stranded reporter domain. Column 1 contains no G-T wobble, and a **A)** full mismatch in position 1, **C)** full mismatch in position 2, and **E)** full mismatch in position 3. Column 2 contains the G-T wobble, and a **B)** full mismatch in position 1, **D)** full mismatch in position 2, and **F)** full mismatch in position 3. Concentrations: 100 nM DNAzyme, 115 nM inhibitor, 100 nM fuel, 1 mM ATP, 250 nM substrate.

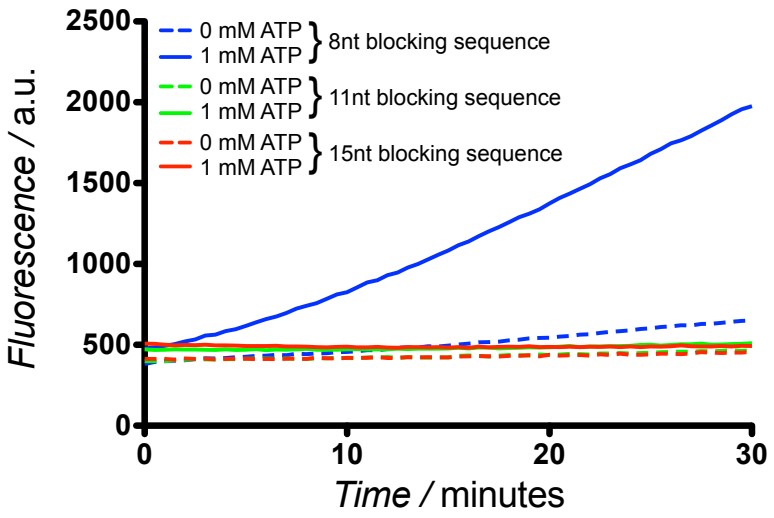

Figure A-I.5 - Effect of Longer Blocking Sequences on ATP Aptamer Activation. Only the 8bp blocking sequence is sufficient for activation (blue). Longer sequences, such as the 11bp (green) or 15 bp (red) lengths, blocked the ATP from displacing the detection domain, resulting in no gate activation. Fuel and loop toehold has a mismatched base in the 3rd position away from the reporter domain. Concentrations: 100 nM DNAzyme, 125 nM inhibitor, 100 nM fuel, 1 mM ATP, 250 nM substrate.

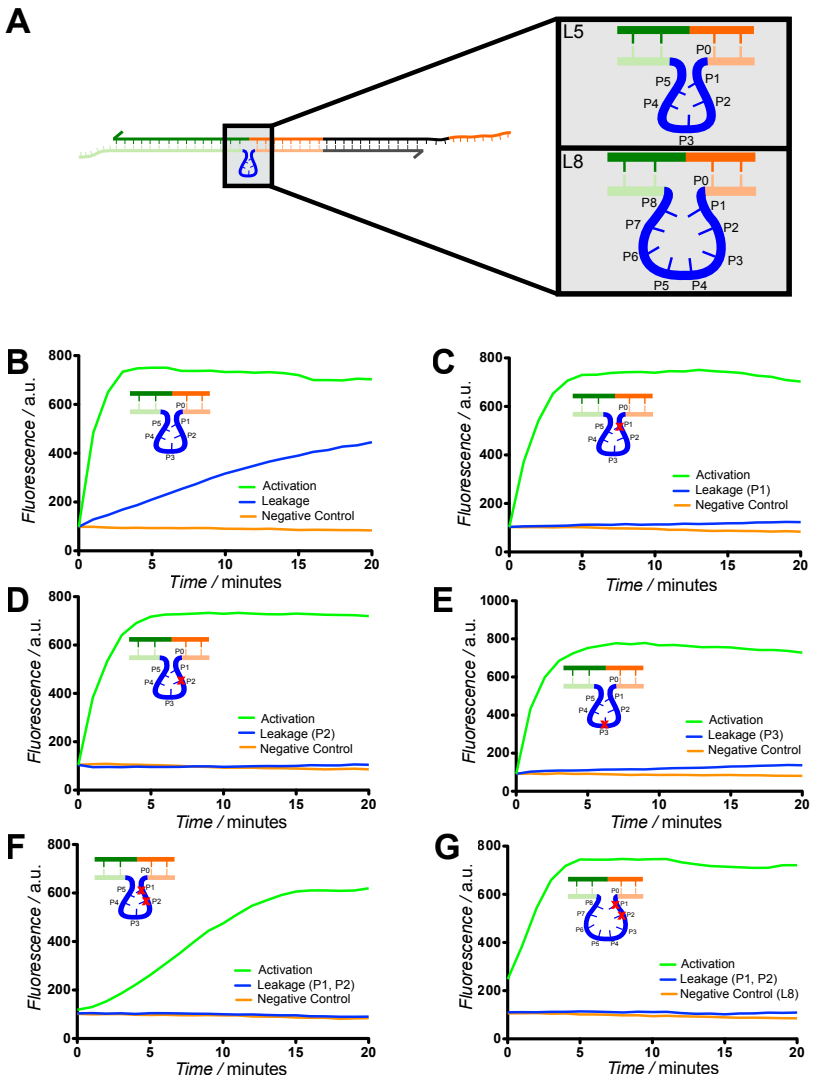

Figure A-I.6 - The effect of Mismatches on Sensor Performance. **A)** Rational mismatches were introduced to destabilize the binding of the free single-stranded fuel and the corresponding toehold on the inhibitor, sequestered in a loop. The position of the mismatch plays an important role in leakage and activation profiles. **B)** Sensor response with no mismatches results in high leakage. (**C-E**) The addition of a single mismatch significantly reduces this leakage. (**F**) The addition of two mismatches eliminates leakage, at the cost of activation rate. (**G**) Alternatively, activation rate can be increased through a larger loop, added more bases for the fuel to bind to the inhibitor. Insets for graphs depict the specific location for each mismatch. Concentrations: 100 nM DNAzyme, 125 nM inhibitor, 100 nM fuel, 100 nM target, 50 nM substrate.

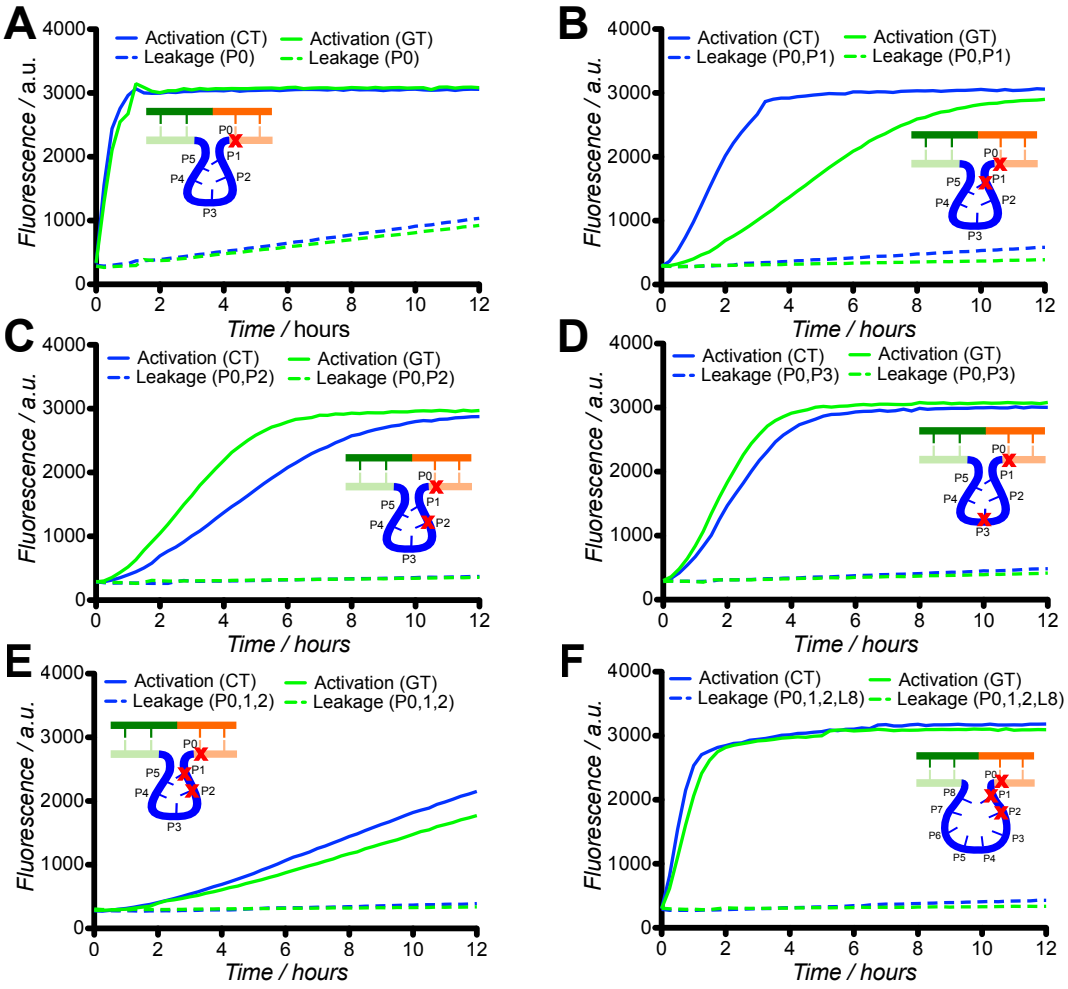

Figure A-I.7 - Effect of an Additional Mismatch, at the P0 Position. The mismatch was either a full mismatch (C-T) or a wobble mismatch (G-T). Each previously characterized gate was run with each new fuel containing either the CT or GT mismatch. (A) No mismatch gate (B) P1 gate (C) P2 gate (D) P3 gate (E) P1, P2 gate and (F) P1, P2, L8 gate. Concentrations: 40 nM DNAzyme, 50 nM inhibitor, 40 nM fuel, 40 nM target, 250 nM substrate.

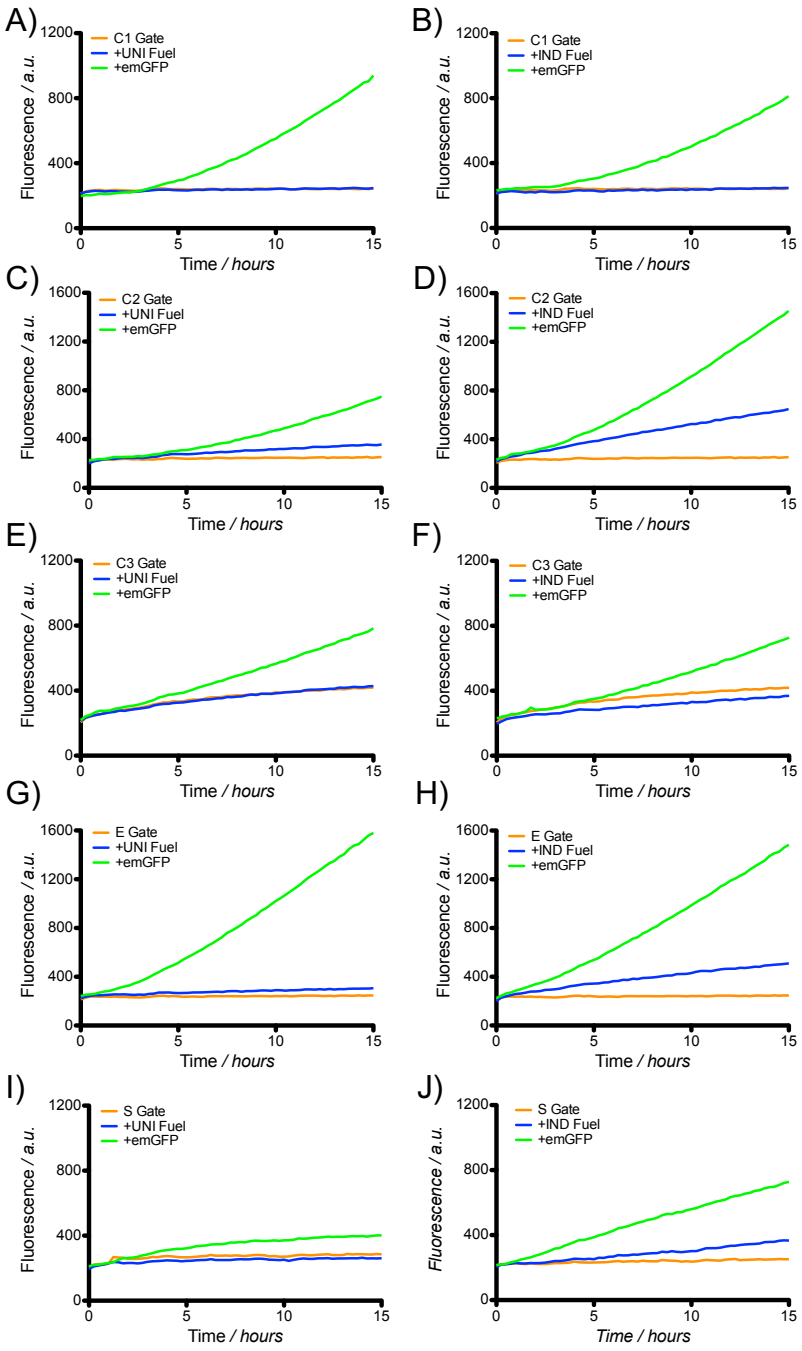

Figure A-I.8 - Response of Each Individual Gate in the Presence of emGFP Plasmid. A significantly higher fluorescent response was observed under these conditions. The response of using individual fuels compared to a universal fuel was similar, with some variations in signal and leakage (most notably in gate C2), indicating the viability of either approach. Column 1 indicates gate response with the universal fuel, column 2 contains individual fuels. (**A-B**) Gate C1, (**C-D**) Gate C2, (**E-F**) Gate C3, (**G-H**) Gate E, (**I-J**) Gate S. Concentrations: 5 nM DNAzyme, 5.75 nM inhibitor, 5 nM fuel, 25 nM emGFP, 250 nM substrate.

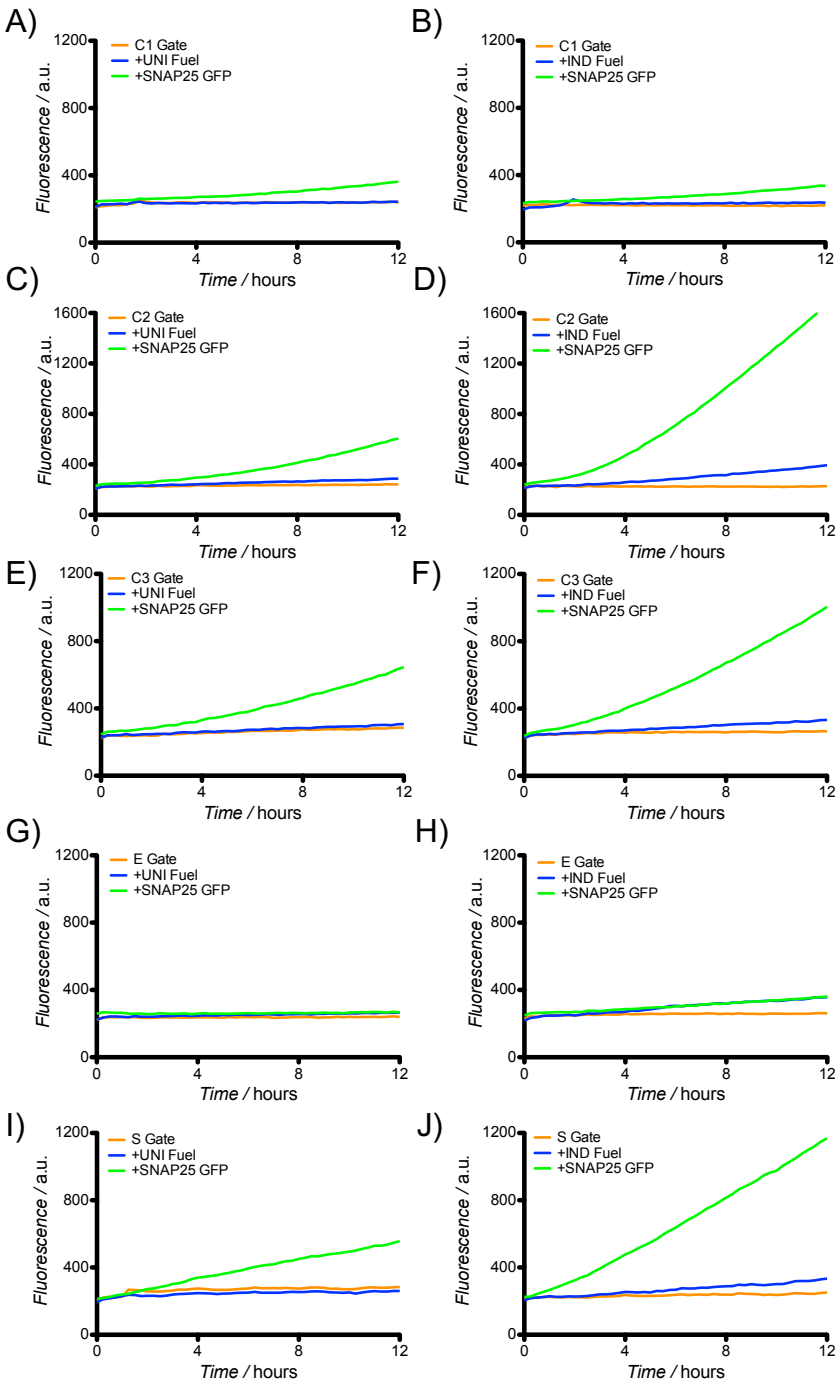

Figure A-I.9 - Response of each Individual Gate in the Presence of SNAP25 Plasmid. A significantly higher fluorescent response was observed under these conditions. The response of using individual fuels compared to a universal fuel was similar, with some variations in signal and leakage, indicating the viability of either approach. Column 1 indicates gate response with the universal fuel, column 2 contains individual fuels. (**A-B**) Gate C1, (**C-D**) Gate C2, (**E-F**) Gate C3, (**G-H**) Gate E, (**I-J**) Gate S. Concentrations: 5 nM DNAzyme, 5.75 nM inhibitor, 5 nM fuel, 25 nM SNAP25, 250 nM substrate.

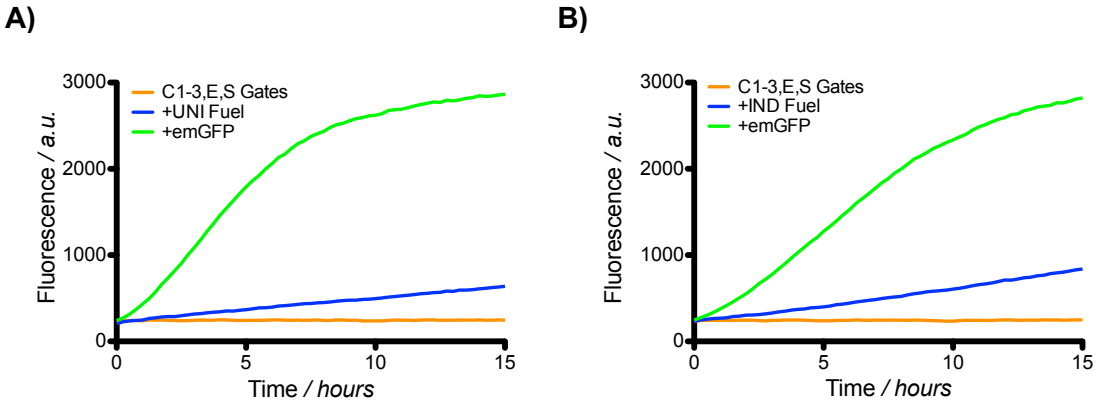

Figure A-I.10 - Response of all Five Sensors Combined in the Presence of emGFP Plasmid. Comparing the effect of using a **A)** universal fuel strand versus **B)** individualized fuel strands. A significantly higher fluorescent response was observed under these conditions. The response of using individual fuels compared to a universal fuel was similar, with the universal fuel yielding a slight increase in positive fluorescence, indicating the viability of either approach. Concentrations: 5 nM DNAzyme/sensor, 5.75 nM inhibitor/sensor, 25 nM universal fuel or 5 nM individual fuel/sensor, 25 nM emGFP, 250 nM substrate.

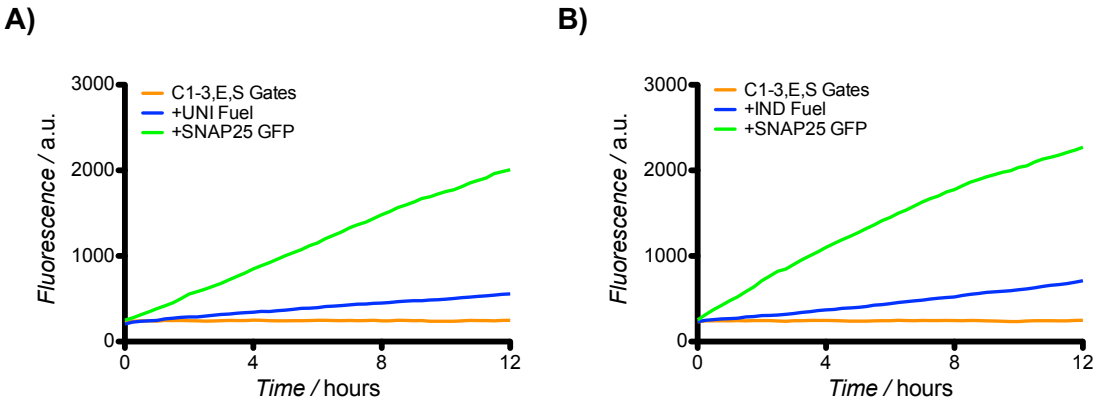

Figure A-I.11 - Response of all Five Sensors Combined in the Presence of SNAP25 Plasmid. Comparing the effect of using **A)** a universal fuel strand versus **B)** individualized fuel strands. A significantly higher fluorescent response was observed with all five sensors compared to a single gate. The response of using individual fuels compared to a universal fuel was similar, indicating the viability of either approach. Concentrations: 5 nM DNAzyme/sensor, 5.75 nM inhibitor/sensor, 25 nM universal fuel or 5 nM individual fuel/sensor, 25 nM SNAP25, 250 nM substrate.

A-I.3 Supplementary Tables

Table A-I.1 - Biosensor sequences. Target sequences reflect the entirety of the target oligonucleotide sequences as well as the sequence contained within the respective plasmid (Figures 2-6, S2, S8-S11).

Strand	Sequence
Substrate	FAM-TCTTAGTTrAGTCTATCCAAT-TAM
Universal Fuel	GGTCGAAAACTAAGGCATGTTGG
C1 DNAzyme	TGGATAGATCCGAGCCGGTCGAAAACTAAGAAACTACAACA
C1 inhibitor	CTTGTGGCTGTTGTAGTTCCAACACCTCTTAGTTTTCGACCGGC
C1 target	AACTACAACAGCCACAAG
C2 DNAzyme	TGGATAGATCCGAGCCGGTCGAAAACTAAGAAACTATTAAC
C2 inhibitor	GTTCGCCAGTTAATAGTTCCCAACCCTCTTAGTTTTCGACCGGC
C2 target	AACTATTAACTGGCGAAC
C3 DNAzyme	TGGATAGATCCGAGCCGGTCGAAAACTAAGAACCAAATACT
C3 inhibitor	AGAAGAACAGTATTTGGTCAAACCCCTCTTAGTTTTCGACCGGC
C3 target	ACCAAATACTGTTCTTCT
E DNAzyme	TGGATAGATCCGAGCCGGTCGAAAACTAAGACTCATCATCA
E inhibitor	GATGATGATGATGATGAGCAACACCCTCTTAGTTTTCGACCGGC
E target	CTCATCATCATCATCATC
S DNAzyme	TGGATAGATCCGAGCCGGTCGAAAACTAAGAAACCATATCA
S inhibitor	GTCTTGGTTGATATGGTTCCACCACCTCTTAGTTTTCGACCGGC
S target	AACCATATCAACCAAGAC
ATP DNAzyme	ACCTGGGGGAGTATGTGCGGAGGAAGGTACACCTCTTAGTTTTCGACCGGC
ATP inhibitor	GGTCGAAAACTAAGAGATGT
ATP target	ATP, GTP

Table A-I.2 - Sequences for Plasmid Denaturation Controls (Figure S1).

Strand	Sequence
Dz	GAACTATCTCCGAGCCGGTCGAAAACTAAGAAACAACACTC
INH (P1,2,L8)	ATAGGGTTGAGTGTTGTT CATCTCGC TCTTAGTT TTCGACCGGC
GT Fuel (L8)	GGTCGAAAACTAAGGTGGAGATG
Target	pRSET emGFP
Substrate	FAM-TCTTAGTTrAGGATAGTTCAT-TAM

Table A-I.3 - Sequences from ATP Sensor Toehold Optimization (Figures S3,S4). Sequences correspond to toehold length (5nt vs 8nt). Sequence in bold were used for the ATP sensor demonstration (Figure 6).

Strand	Sequence
Substrate (8nt)	FAM-TCTTAGTTrAGGATAGTTCAT-TAM
ATP DNAzyme (8nt)	GAACTATCTCCGAGCCGGTCGAAAACTAAGAACCTTCCT
ATP inhibitor (8nt)	ACCTGGGGGAGTATGTGCGGAGGAAGGTCCAACACCTCTTAGTTTTCGACC GGC
ATP fuel (8nt)	GGTCGAAAACTAAGGCATGTTGG
Substrate (5b)	FAM-TCTTAGTTrAGTCTATCCAAT-TAM
ATP DNAzyme (5nt)	TGGATAGATCCGAGCCGGTCGAAAACTAAGAACCTTCCT
ATP inhibitor (5nt)	ACCTGGGGGAGTATGTGCGGAGGAAGGTACACCTCTTAGTTTTCGACCGGC
ATP Fuel (5nt-1A)	GGTCGAAAACTAAGAGGCGT
ATP Fuel (5nt-1G)	GGTCGAAAACTAAGGGGCGT
ATP Fuel (5nt-2A)	**GGTCGAAAACTAAGAGATGT**
ATP Fuel (5nt-2G)	GGTCGAAAACTAAGGGATGT
ATP Fuel (5nt-3A)	GGTCGAAAACTAAGATGTGT
ATP Fuel (5nt-3G)	GGTCGAAAACTAAGGTGTGT

Table A-I.4 - Sequences from ATP Sensor Inhibitor Length Experiments (Figure S5).

Strand	Sequence
Substrate (8nt)	FAM-TCTTAGTTrAGGATAGTTCAT-TAM
ATP DNAzyme-Apt8	GAACTATCTCCGAGCCGGTCGAAAACTAAGAACCTTCCT
ATP DNAzyme-Apt11	GAACTATCTCCGAGCCGGTCGAAAACTAAGAACCTTCCTCCG
ATP DNAzyme-Apt15	GAACTATCTCCGAGCCGGTCGAAAACTAAGAACCTTCCTCCGCACA
ATP inhibitor	ACCTGGGGGAGTATGTGCGGAGGAAGGTCTCCATCTTAGTTTTCGACCGG C
ATP Fuel	GGTCGAAAACTAAGATGCAG

Table A-I.5 - Sequences for Toehold Optimization (Figure S6,S7).

Strand	Sequence
Dz	GAACTATCTCCGAGCCGGTCGAAAACTAAGAAACAACACTC
INH	ATAGGGTTGAGTGTTGTT CTCCA TCTTAGTT TTCGACCGGC
INH (P1)	ATAGGGTTGAGTGTTGTT CTCCT TCTTAGTT TTCGACCGGC
INH (P2)	ATAGGGTTGAGTGTTGTT CTCGA TCTTAGTT TTCGACCGGC
INH (P3)	ATAGGGTTGAGTGTTGTT CTGCA TCTTAGTT TTCGACCGGC
INH (P1,2)	ATAGGGTTGAGTGTTGTT CTCGC TCTTAGTT TTCGACCGGC
INH (P1,2,L8)	ATAGGGTTGAGTGTTGTTCATCTCGCTCTTAGTTTTCGACCGGC
Fuel	GGTCGAAAACTAAGATGGAG
Fuel (L8)	GGTCGAAAACTAAGATGGAGATG
Target	AACAACACTCAACCCTAT
Substrate	FAM-TCTTAGTTrAGGATAGTTCAT-TAM

Table A-I.6 - Sequences From Experiments Using Individual Toeholds (Figures A-1.8-A-I.11).

Strand	Sequence
Substrate	FAM-TCTTAGTTrAGTCTATCCAAT-TAM
C1 DNAzyme	TGGATAGATCCGAGCCGGTCGAAAACTAAGAAACTACAACA
C1 ind inhibitor	CTTGTGGCTGTTGTAGTTCCAACACCTCTTAGTTTTCGACCGGC
C1 fuel	AACTACAACAGCCACAAG
C2 DNAzyme	TGGATAGATCCGAGCCGGTCGAAAACTAAGAAACTATTAAC
C2 ind inhibitor	GTTCGCCAGTTAATAGTTCCCAACCCTCTTAGTTTTCGACCGGC
C2 fuel	GGTCGAAAACTAAGGCAGTTGGG
C3 DNAzyme	TGGATAGATCCGAGCCGGTCGAAAACTAAGAACCAAATACT
C3 ind inhibitor	AGAAGAACAGTATTTGGTCAAACCCCTCTTAGTTTTCGACCGGC
C3 fuel	GGTCGAAAACTAAGGCAGGTTTG
E DNAzyme	TGGATAGATCCGAGCCGGTCGAAAACTAAGACTCATCATCA
E ind inhibitor	GATGATGATGATGATGAGCAACACCCTCTTAGTTTTCGACCGGC
E fuel	GGTCGAAAACTAAGGCAGTGTTG
S DNAzyme	TGGATAGATCCGAGCCGGTCGAAAACTAAGAAACCATATCA
S ind inhibitor	GTCTTGGTTGATATGGTTACACCACCTCTTAGTTTTCGACCGGC
S fuel	GGTCGAAAACTAAGGCATGGTGT

A-I.4 References

1. Saunders, M.J., et al., *Microsphere-based flow cytometry protease assays for use in protease activity detection and high-throughput screening.* Curr Protoc Cytom, 2010. **54**(13.12): p. 13.12.1-13.12.17.
2. Zadeh, J.N., B.R. Wolfe, and N.A. Pierce, *Nucleic acid sequence design via efficient ensemble defect optimization.* J Comput Chem, 2011. **32**(3): p. 439-52.

APPENDIX II – SUPPORTING INFORMATION FOR CHAPTER 4

Supporting Information

A Microsphere-Supported Lipid Bilayer Platform for DNA Reactions on a Fluid Surface

Aurora Fabry-Wood[1], Madalyn E. Fetrow[1], Carl W. Brown III[1†], Nicholas A. Baker[1, 2], Nadiezda Fernandez Oropeza[1], Andrew P. Shreve[1, 2], Gabriel A. Montaño[4], Darko Stefanovic[1, 3], Matthew R. Lakin[1, 2, 3*], Steven W. Graves[1, 2*]*

1. Center for Biomedical Engineering, University of New Mexico
2. Department of Chemical and Biological Engineering, University of New Mexico
3. Department of Computer Science, University of New Mexico
4. Los Alamos National Laboratory

Corresponding Authors

*graves@unm.edu, *darko@cs.unm.edu, *mlakin@cs.unm.edu

A-II.1 Strand Design

Table A-II.1 - TMSD Sequences

Name	Sequence (5' -> 3')
Standardized Thiol	/5ThioMC6-D/ TTTTTTTTTTTTATGTATCTTAGTTTTCGACCGGT ATGAGTGTAGATGTGAAGTTTG
Sero1 incumbent	/5ATTO647NN/TCTTCCCTTTATGCAAACTTCACATCTACACTCATA CCG
Sero1 template	CATAAAGGGAAGAGAGAT/3IAbRQSp/
Sero1 target	ATCTCTCTTCCCTTTATG
Sero2 incumbent	/5ATTO647NN/CTCTTAACATCCTCAAACTTCACATCTACACTCATA CCG
Sero2 template	AGGATGTTAAGAGCAGTG/3IAbRQSp/
Sero2 target	CACTGCTCTTAACATCCT
Sero3 incumbent	/5ATTO647NN/TACCCGCAACATTCAAACTTCACATCTACACTCAT ACCG
Sero3 template	AATGTTGCGGGTATGGAG/3IAbRQSp/
Sero3 target	CTCCATACCCGCAACATT
Sero4 incumbent	/5ATTO647NN/CTTTGTCCTAATGCAAACTTCACATCTACACTCATA CCG
Sero4 template	CATTAGGACAAAGAAGAC/3IAbRQSp/
Sero4 target	GTCTTCTTTGTCCTAATG

Table A-II.2 - DNAzyme Sequences:

Thiol Strand DNAzyme (TSD)	CAAACTTCACATCTACACTCAAAAA/3ThioMC3-D/
DNAzyme_TSD	GAGTGTAGATGTGAAGTTTGAAAAAGAACTATCTCCGAGCCGGTCG AAAACTAAGA
Thiol Strand Substrate (TSS)	/5ThioMC6-D/AAA AAGAATAGAACAAGACAGAAAC
Substrate_TSS	/5ATTO647NN/TCTTAGTT rAG GATAGTTCAT AAAAA GTTTCTGTCTTGTTCTATTC
FRET Substrate	/56-FAM/TCTTAGTT rAG GATAGTTCAT /36-TAMSp/
Cy5_Substrate_no_r_TSS	/5Cy5/TCTTAGTTAGGATAGTTCATAAAAAGTTTCTGTCTTGTTCTATTC
Thiol Strand Filler (TSF)	CCATACCATCAACTCAACCTAAAAA/3ThioMC3-D/
Blocking strand_TSF	AGGTTGAGTTGATGGTATGG

A-II.2 Non-Specific Interaction Controls

To confirm conjugation specificity controls lacking MPB PE were run, Figure S-7. These controls were exposed to the fluorescently labeled incumbent strand.

For the non-specific interaction experiments in the presence of Zn^{2+} an oligo complementary to TSS and tagged with Cy5 (Cy5_Substrate_no_r_TSS), instead of the expensive ATTO647 labeled chimeric substrate (Substrate_TSS), was used.

A-II.3 Limit of Detection

To determine the limit of detection a single μSLB population was used. Five replicates of each sample were run, and each sample set was exposed to 5 target concentrations (5 nM, 1 nM, 500 pM, 100 pM and 50 pM). The samples were gated on forward versus side scatter, and then median fluorescence values were calculated for the incumbent strand. The baseline (no target added) was subtracted from all samples and a linear regression was calculated. To calculate the limit of detection the IUPAC equation[1] (1) was used, where s_B is standard

deviation of the background, s_i is error of the y-intercept of a linear regression of concentration plotted against response, i is the y-intercept of a linear regression of concentration plotted against response, m is the slope of a linear regression of concentration plotted against response, and s_m is the error of the slope.

$$(1)\ \text{Limit of Detection} = \frac{3\sqrt{{s_B}^2+{s_i}^2+\left(\left(\frac{i}{m}\right)^2 {s_m}^2\right)}}{m}$$

A-II.4 Confocal Microscopy

Confocal stack images were used to confirm even coating of the SiMSs. See Movie S2, which shows the DNA-lipid conjugate (here, there is 1 mol% MPB PE, the Standardized Thiol strand was conjugated and this is on the Cy5 channel), there are 19 steps at 1 μm/step. Movie S3 is the same bead, showing the lipid (PECF) channel.

A-II.5 Merging

Merging of individual populations does occur over time. This merging can be mitigated by coating the particles with bovine serum albumin (BSA), and by rotating the particles. Figure S-4 shows the samples at 4 hours.

A-II.6 Supporting Figures

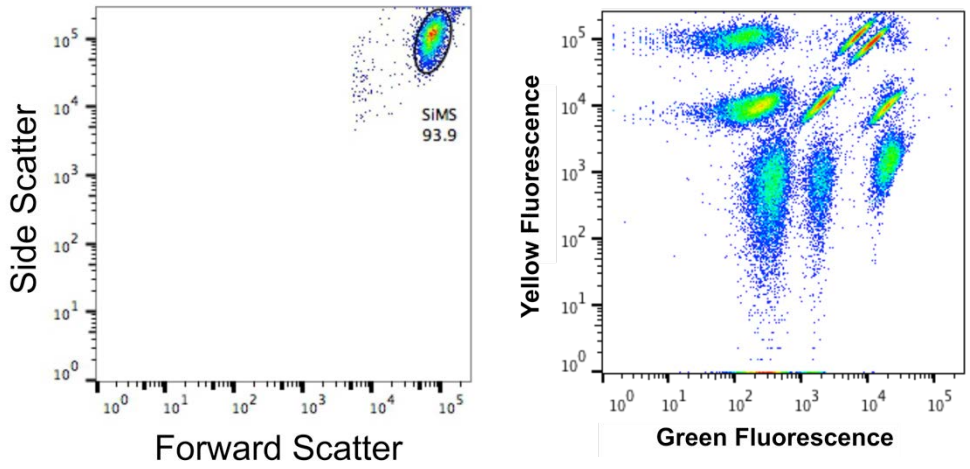

Figure A-II.1 – SiMS Gating and 9-Plex. a) Initially the μSLBs were gated on FSC vs. SSC. **b)** A multiplex of nine populations, using green (PECF) and yellow (PELR) fluorophores. Four of the populations have the same concentrations as described in Figure 1; the other 5 populations have intermediate concentrations of green and yellow fluorophores.

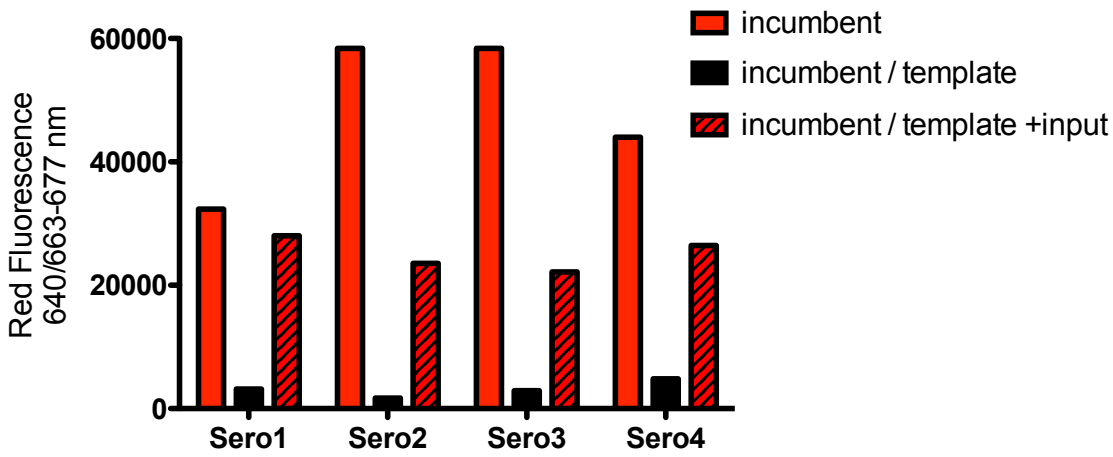

Figure A-II.2 - Individual TMSD Functionality Test. A positive control was established by hybridizing the fluorescently labeled incumbent strand. Next the incumbent and template strand, which comprised the complete TMSD gate, were hybridized to the corresponding μSLB set. Finally the corresponding target sequences were added to the μSLB population with the complete TMSD gate hybridized.

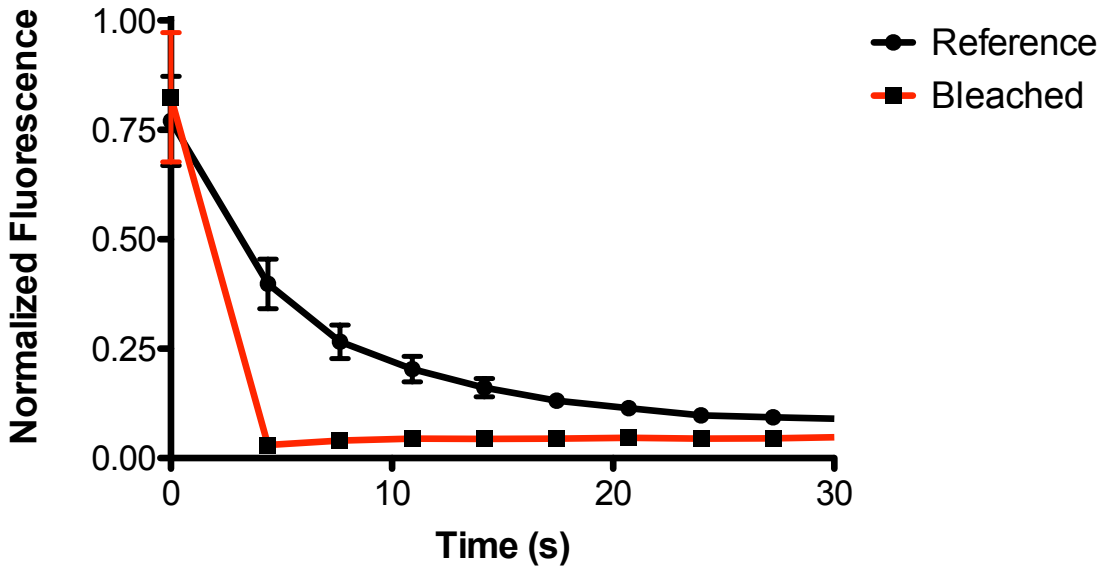

Figure A-II.3 - Second Data Set, Representing the Same Experimental Setup as Figure 4.2C. 0.5 mol% MPB PE, which represents ~2.25×10^6 DNA-lipid conjugates/μSLB. The error bars represent standard error of mean for 7 replicates.

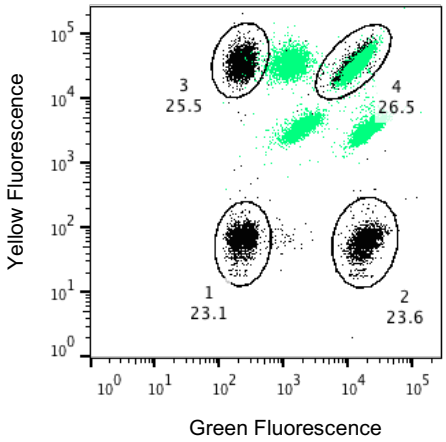

Figure A-II.4 – Merging with BSA Coat and Rotation. Multiplexed μSLBs, coated with BSA and rotated for 4 hours at room temperature (shown in green), remain discretely separated. The initial readings are shown in black.

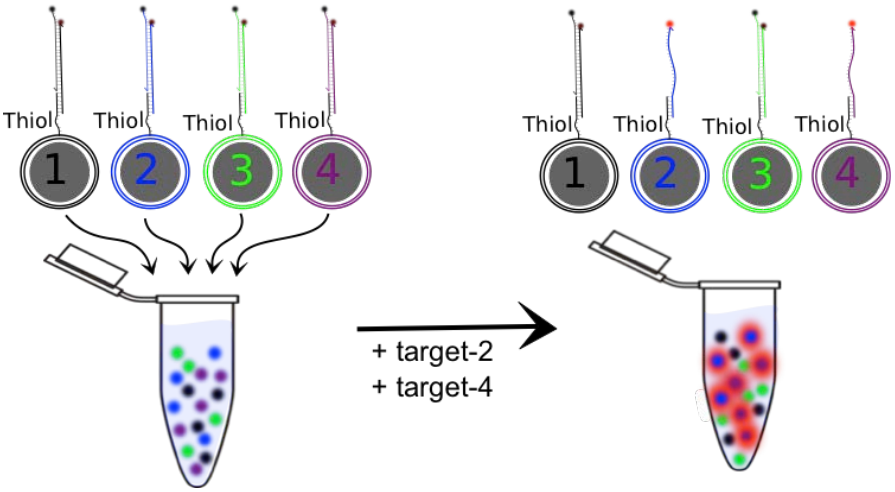

Figure A-II.5 - TMSD Gates and Multiplex Formation. Four μSLB populations (1-4) were generated separately. Each population was identified by a spectral address that corresponds to a specific TMSD gate. These populations were then combined in a single tube to form a multiplex. Addition of target strands (2 and 4 in this case) resulted in a TMSD reaction and an increase in the incumbent strand fluorescence.

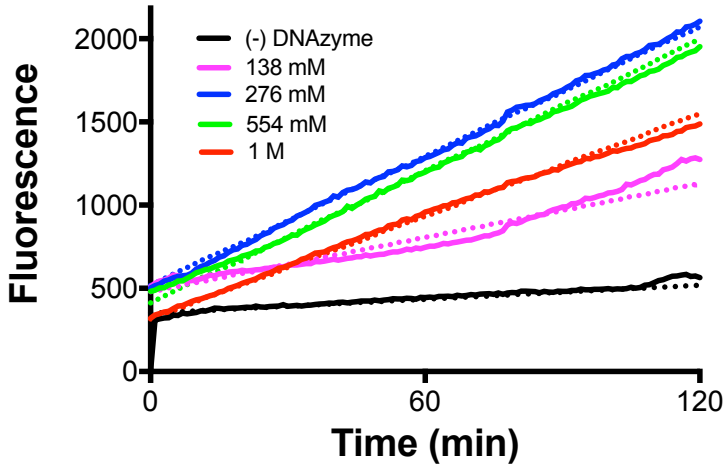

Figure A-II.6 - Solution Phase DNAzyme and Solution phase Substrate Reaction in the Presence of Decreasing Na^+ Concentrations. DNAzyme [100 nM], substrate [250nM], with 25 μM Zn^{2+} and 50 mM HEPES.

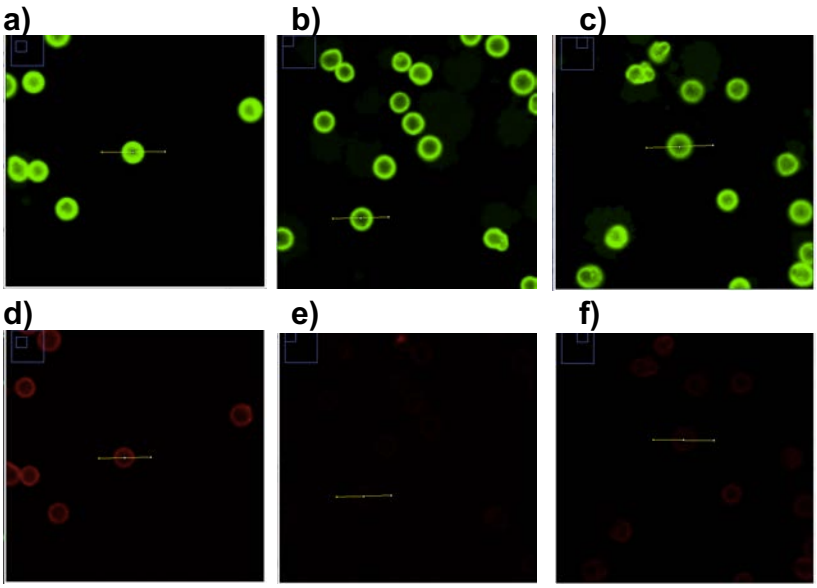

Figure A-II.7 – Non-Specific Interaction Controls. a), b) and **c)** All bilayers contain 0.5 mol% PECF, and show equal fluorescence for the 488/520 nm filter. **d)** The positive control contains 1 mol% MPB PE, and the Standardized Thiol strand is conjugated. This is the 647/670 nm filter. See Movie S2. **e)** This hybridization control is a μSLB population with TSF conjugated to the bilayer, which is not complementary to the fluorescently labeled incumbent strand. This is the 647/670 nm filter. **f)** This conjugation control contains no MPB PE. This is the 647/670 nm filter.

A-II.7 References

(1) Long, G. L.; Winefordner, J. D. Limit of Detection. *Anal. Chem.* **1983**, *55*, 712–724.

APPENDIX III – SUPPORTING INFORMATION FOR CHAPTER 6

DNA Functionalized Oligophenylenevinylenes for Transmembrane Signal Transduction

A-III.1 Synthesis of SP-III-163C

A-III.1.1 Synthesis of Intermediate SP-III-131C

This procedure was adopted from Garner et al.,[1] and began with the preparation of (*E*)-1,2-bis(4-(chloromethyl)phenyl)ethene (SP-III-130C). A 250 mL round-bottom flask was placed under an Argon atmosphere and flame dried. To the flask was added 40 mg of 2nd generation Grubbs catalyst (0.047 mmol, 1 eq.) dissolved in anhydrous CH_2Cl_2 and this solution was degassed. To the reaction flask was added 1.34 mL (202 eq., 9.5 mmol) dry 4-vinylbenzyl chloride. The solution was slowly refluxed under Ar at 50 °C for 24 hours. The reaction solution was then allowed to cool slowly and concentrated up to ~10 mL. The product crystallized out of the reaction solution and the crude (off-white needle crystals) was collected via filtration and washed with cold hexanes. Following silica gel chromatography using 1:1 (CH_2Cl_2:hexane) solvent system, the pure product was afforded as a white solid 920 mg (35% yield). MP: 160-163 °C. ^{1}H NMR (500 MHz, $CDCl_3$): δ 7.51 (d, *J*= 8.4 Hz, 4H), 7.38 (d, *J*= 7.6 Hz, 4H), 7.11 (s, 2H), 4.60 (s, 4H). ^{13}C (125 MHz, $CDCl_3$): δ 137.47, 137.03, 129.16, 128.77, 127.00, 46.20.

Figure A-III.1 - Synthesis of SP-III-163C. Shown in the next page. The synthesis begins with the metathesis condensation of 4-vinylbenzyl chloride to yield SP-III-130C. This is followed by an Arbuzov reaction to yield **SP-III-131C**. Synthesis of the intermediate **SP-III-159C** begins with replacing aniline's protons with two hexanol moiety. The electron rich aromatic **SP-III-149C** is converted to **SP-III-159C** via a Vilsmeier-Haack formulation. A Horner-Wadsworth-Emmons reaction yields **SP-III-161C**, by dropwise addition of **SP-III-159C** to a solution containing **SP-III-131C**. From here the terminal chlorine groups are replaced by iodine with a Finkelstein reaction, which is an equilibrium reaction that is pushed to completion because one of the side products, NaCl, is not soluble in acetone. Finally, a nucleophilic substitution (S_N2) replaces the alkyl iodide with an azide, to yield the final compound, **SP-III-163C**.

Figure A-III.1

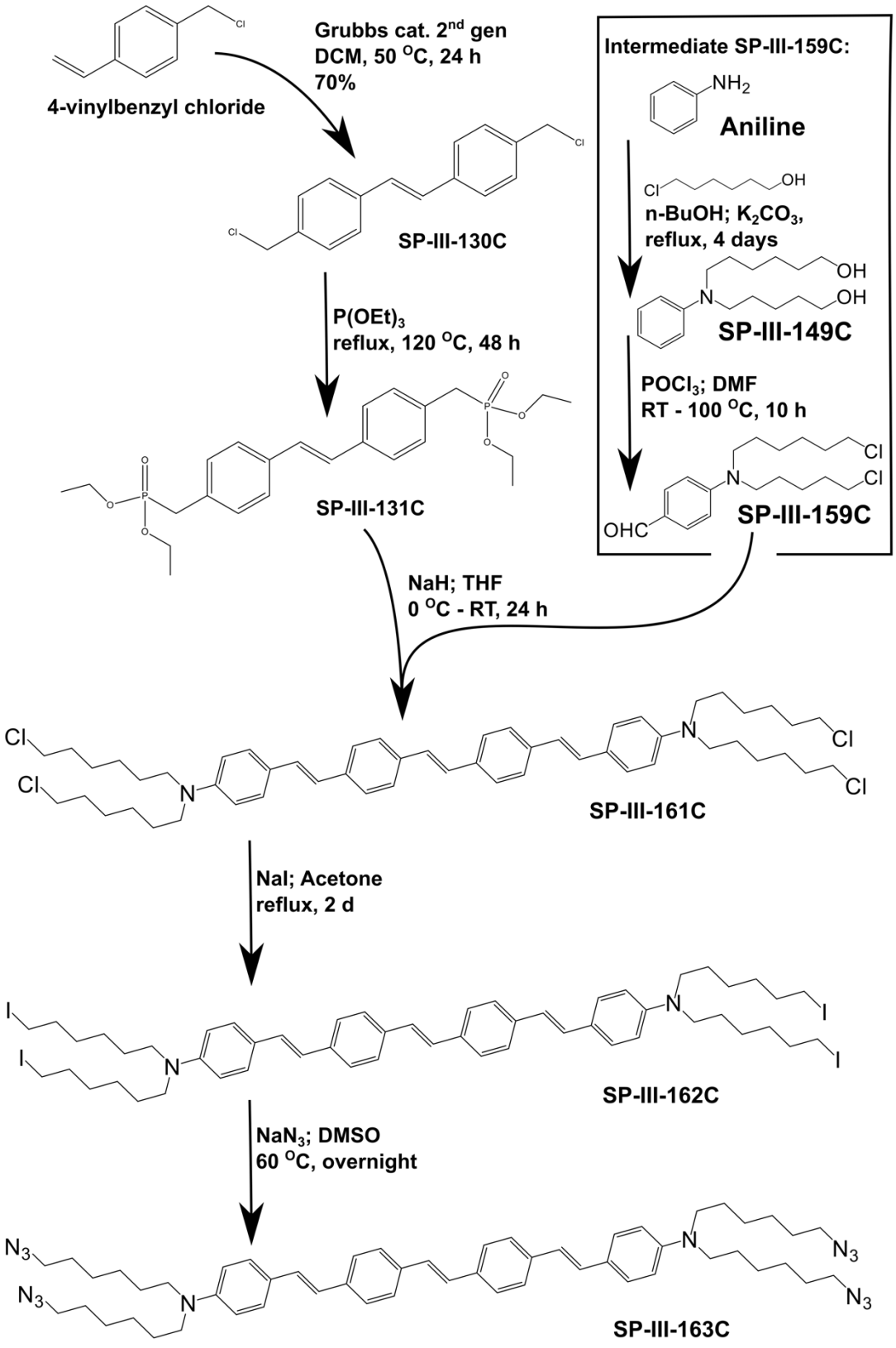

To prepare (*E)*-4,4'-bis(diethylphosphonatemethyl)stilbene (SP-III-131C), 500 mg of **SP-III-130C** (1 eq., 1.8 mmol) and 10 mL of neat triethylphosphite was combined in a 100 mL round bottom flask equipped with a reflux condenser. This solution was allowed to reflux at 120 °C for 48 hours. Upon completion of the reaction, solution was allowed to cool and the off-white solid crude product was isolated via removal of excess $P(OEt)_3$ by vacuum distillation. Pure **3** was obtained as white crystals in 35 % yield by recrystallization from diethyl ether.^{1}H NMR (500 MHz, $CDCl_3$): δ 7.42 (d, *J*= 7.6 Hz, 4H), 7.25 (d, *J*= 14 Hz, 4H), 7.03 (s, 2H), 3.99 (t, (d, *J*= 7.6 Hz, 8H), 3.13 (d, (d, *J*= 22 Hz, 4H), 1.22 (t, (d, *J*= 6.8 Hz, 12H). ^{13}C (125 MHz, $CDCl_3$): δ 136.14, 136.10, 131.14, 131.05, 130.27, 130.20, 128.28, 126.78, 126.75, 62.37, 62.31, 34.41, 33.04, 16.55, 16.49.

A-III.1.2 Synthesis of Intermediate SP-III-159C

To synthesize *N,N*-Bis(6-hydroxyhexyl)aniline (SP-III-149C), a procedure adopted from Woo et al. was used.[2] A mixture of 1.14 mL g (12.5 mmol, 1 eq) of aniline, 3.66 mL (27.5 mmol, 2.2 eq) of 6-chloro-1-hexanol, and 3.8 g (27.5 mmol, 2.2 eq) potassium carbonate was heated in 25 mL of *n*-butanol under reflux for 4 days. After cooling, the remaining solids were filtered off, and the solvent was removed under reduced pressure to afford the crude product. Purification by silica gel chromatography (2:1 ethyl acetate/hexane) yielded 1.2 g (32% yield) of **SP-III-149C** as a yellow thick oil. ^{1}H NMR (500 MHz, $CDCl_3$): δ 7.19 (t, *J*= 7.2 Hz, 2H), 6.63 (d, *J*= 8 Hz, 3H), 3.64 (t, *J*= 6.4 Hz, 4H), 3.25 (t, *J*= 7.6 Hz, 4H), 1.61-1.56 (m, 8H), 1.43-1.35 (m, 8H).^{13}C (125 MHz, $CDCl_3$): δ 148.24, 129.31, 115.38, 111.91, 62.98, 51.08, 32.85, 27.33, 27.06, 25.77.

To synthesize *N,N*-Bis(6`-chlorohexyl)-4-aminobenzaldehyde (SP-III-159C), phosphorus oxychloride (0.83 mL, 9 mmol, 3.5 eq) was added dropwise to 5 mL of dry DMF at 0 °C. After 30 min, 0.75 g (2.6 mmol, 1 eq) of **SP-III-149C** in 3 mL of DMF was added to the above solution. The resulting mixture was heated to 100 °C for 3 h. After cooling to room temperature, 50 mL of ice water was poured into reaction mixture. The pH of the mixture was adjusted to 7 by addition of saturated potassium acetate aqueous solution. The mixture was extracted with dichloromethane, and the combined organic phase was washed with water and dried over Na_2SO_4. The solvent was evaporated and the crude product was purified by silica gel chromatography (starting with 10% hexane:ethyl acetate and increased to 40% hexane:ethyl acetate) to afford **SP-III-159C** (0.3 mg, 33%) as a light yellow oil. ^{1}H NMR (500 MHz, $CDCl_3$): δ 9.70 (s, 1H), 7.69 (d, *J*= 8.4 Hz, 2H), 6.63 (d, *J*= 9.2 Hz, 2H), 3.54 (t, *J*= 6.8 Hz, 4H), 3.35 (t, *J*= 7.2 Hz, 4H), 1.83-1.76 (m, 4H), 1.67-1.59 (m, 4H), 1.54-1.46 (m, 4H), 1.41-1.35 (m, 4H). ^{13}C (125 MHz, $CDCl_3$): δ 190.04, 152.56, 132.32, 124.87, 110.83, 51.04, 45.01, 32.58, 27.15, 26.78, 26.43.

A-III.1.3 Synthesis of the final compound

To synthesize 4,4'-((1E,1'E)-(((E)-ethene-1,2-diyl)bis(4,1-phenylene))bis(ethene-2,1-diyl))bis(N,N-bis(6-chlorohexyl)aniline) SP-III-161C, NaH (42 mg, 1.04 mmol, 60% in oil, 5 eq) was suspended in 5 mL anhydrous THF at 0 °C under argon atmosphere with stirring. **SP-III-131C** dissolved in THH was added dropwise, followed by addition of **SP-III-159C** (186 mg, 0.52 mmol, 2.5 eq) dissolved in THF. The stirring was continued at room temperature overnight. The

reaction mixture was cooled to 0 °C then water (2 mL) was added dropwise under argon with stirring. 2N Hydrochloric acid (5 mL) was added dropwise to the reaction mixture then it was extracted with diethyl ether. The organic layers were collected, dried ($MgSO_4$), filtered and the solvent removed under reduced pressure to give the crude product, which was applied to a silica gel column chromatography using 1:1 dichloromethane:hexane solvent system. Fractions containing the required product were collected and the solvent removed under reduced pressure. Yellowish crystals (0.11 g, 54%). MP: 123-126 °C. ^{1}H NMR (500 MHz, $CDCl_3$): δ 7.45 (d, *J*= 10.4 Hz, 4H), 7.40 (d, *J*= 4.8 Hz, 4H), 7.36 (t, *J*= 4 Hz, 4H), 7.09-7.00 (m, 4H), 6.87 (t, *J*= 12.8 Hz, 2H), 6.60 (t, *J*= 12.4 Hz, 4H), 3.53 (t, *J*= 13.2 Hz, 8H), 3.27 (d, *J*= 6 Hz, 8H), 1.81-1.73 (m, 8H), 1.67-1.59 (m, 4H), 1.60-1.34 (m, 28H). ^{13}C (125 MHz, $CDCl_3$): δ 147.78, 137.75, 135.95, 128.82, 127.95, 127.87, 126.84, 126.36, 124.96, 123.64, 111.90, 51.07, 45.13, 32.69, 27.34, 26.89, 26.56.

To synthesize 4,4'-((1E,1'E)-(((E)-ethene-1,2-diyl)bis(4,1-phenylene))bis(ethene-2,1-diyl))bis(N,N-bis(6-iodohexyl)aniline) SP-III-162C, to a flame dried round bottom flask was added sodium iodide (168 mg, 1.12 mmol, 10 eq) and under argon atmosphere was added **SP-III-161C** (100 mg, 0.112 mmol, 1 eq) dissolved in 5 mL anhydrous acetone. Reaction mixture was refluxed for 48 hours under argon atmosphere. Upon cooling down to room temperature, acetone was evaporated and reaction mixture dissolved in 50 mL CH_2Cl_2, washed twice with water (to remove excess NaI) and dried over $MgSO_4$. Yellow solid obtained after recrystallization in diethyl ether. ^{1}H NMR (500 MHz, $CDCl_3$): δ 7.46 (t, *J*= 1.6 Hz, 8H), 7.38 (d, *J*= 8.4 Hz, 4H), 7.08 (t, *J*= 7.6 Hz, 4H), 7.03 (s, 2H), 6.88 (d, *J*=

16 Hz, 2H), 6.62 (d, *J*= 8.4 Hz, 4H), 3.29 (t, *J*= 6.8 Hz, 8H), 3.20 (t, *J*= 6.8 Hz, 8H), 1.88-1.81 (m, 8H), 1.65-1.57 (m, 8H), 1.53-1.46 (m, 8H), 1.44-1.36 (m, 8H). ^{13}C (125 MHz, $CDCl_3$): δ 147.78, 137.73, 135.95, 128.82, 127.96, 127.85, 126.85, 126.38, 124.99, 123.65, 111.92, 51.07, 33.56, 30.49, 27.30, 26.22, 7.13.

4,4'-((1E,1'E)-(((E)-ethene-1,2-diyl)bis(4,1-phenylene))bis(ethene-2,1-diyl))bis(N,N-bis(6-azidohexyl)aniline) SP-III-163C. SP-III-162C (50 mg, 0.04 mmol) were dissolved in 2 mL DMF, followed by addition of sodium azide (72 mg, 1.12 mmol). Reaction mixture was heated for 2 hours at 60 °C and stirred overnight at room temperature. Water was added (50 mL) and product was extracted with 35 mL ethyl acetate. Organic layer was washed twice with water (25 mL each), dried over $MgSO_4$ and concentrated under vacuum. Recrystallization in diethyl ether yielded yellow solid compound. **Figure A-III.2** shows the emission spectrum of this comound in chloroform. ^1H NMR (500 MHz, $CDCl_3$): δ 7.47 (t, *J*= 9.6 Hz, 8H), 7.39 (d, *J*= 8 Hz, 4H), 7.08 (d, *J*= 7.2 Hz, 2H), 7.03 (s, 2H), 6.88 (d, *J*= 16 Hz, 2H), 6.62 (d, *J*= 8.4 Hz, 4H), 3.31-3.26 (m, 14H), 3.20 (t, *J*= 6.8 Hz, 2H), 1.86-1.83 (m, 4H), 1.63-1.37 (m, 28H). ^{13}C (125 MHz, $CDCl_3$): δ 147.77, 137.73, 135.95, 128.82, 127.96, 127.85, 126.84, 126.37, 124.99, 123.65, 111.91, 51.49, 51.07, 33.55, 30.48, 28.98, 27.37, 27.29, 26.84, 26.79, 26.22, 7.12.

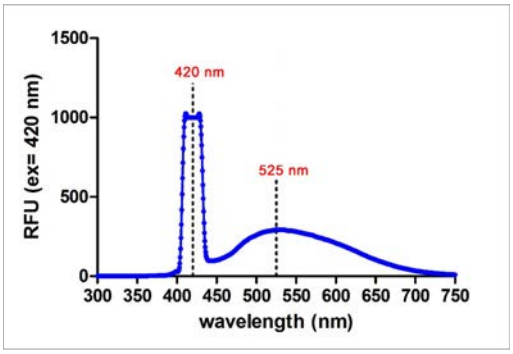

Figure A-III.2 - Emission Spectrum of SP-III-163C in Chloroform. The emission spectrum of SP-III-163C, with excitation at 420 nm, shows maximal emission at 525 nm.

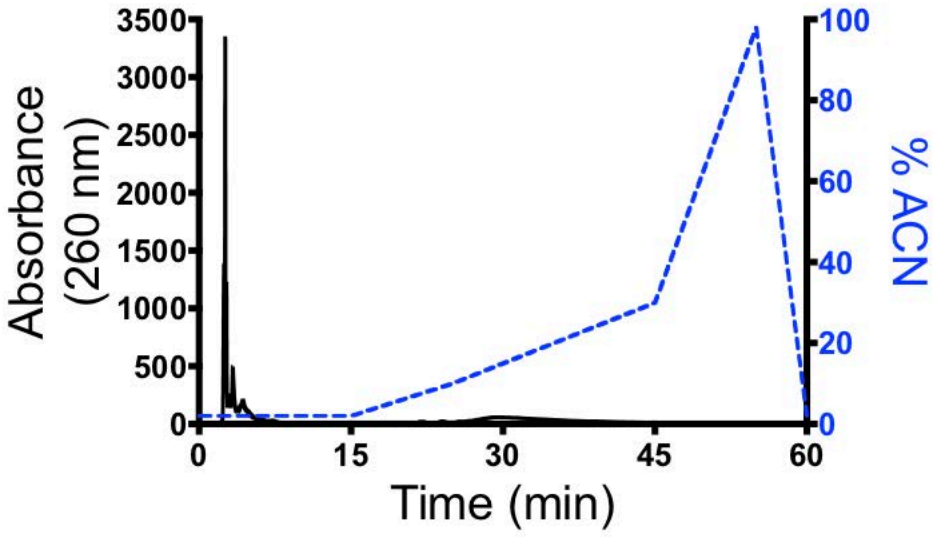

Figure A-III.3 – HPLC of SP-III-163C-Enz1. We were able to narrow the 30-minute peak by increasing to 20% ACN immediately, instead of the linear increase, from 2% - 30%, shown here. However, the yield was always around 0.1% no matter how much we optimized the system.

A-III.2 Strand Design

Table A-III.1 - Strand Sequences

Name	Sequence
Enz1	5' - T GAACTATC **TCCGAGC** AAAAA /35OctdU/ - 3'
Enz1_tagged	5' - /5ATTO647NN/ T GAACTATC **TCCGAGC** AAAAA /35OctdU/ - 3'
Enz2_tagged	5' /55OctdU/ AAAAA **CGGTCGAA** AACTAAGA /3ATTO565N/ - 3'
Tether Strand	5'- TCTTAGTT AG GATAGTTC AT – 3'
U2 Substrate	5' - /56FAM/ TCT TAG TTrA GGA TAG TTC AT /36-TAMSp/ - 3'

A-III.3 Effects of THF

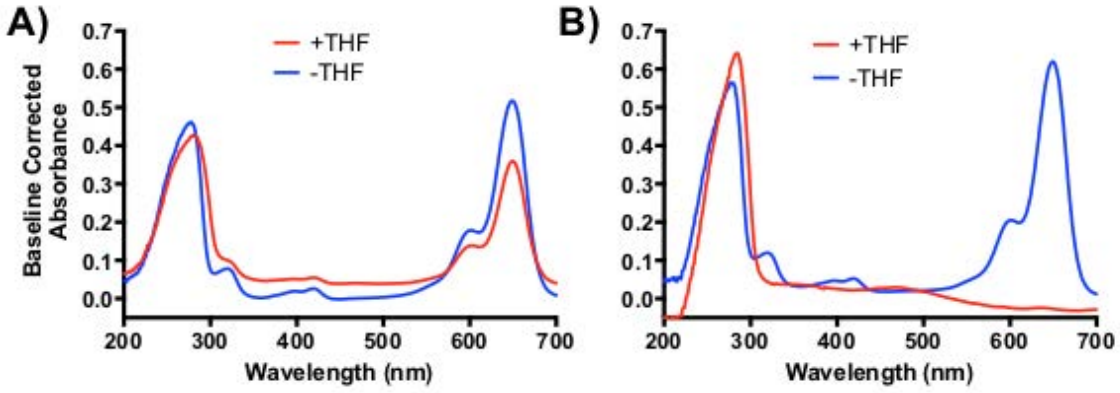

Figure A-III.4 - Effects of THF on DNA and ATTO647. A) Initial UV-Vis spectrum. **B)** UV-Vis spectrum at 1 week.

A-IIII.4 References

1. Garner, L. E. *et al.* Modification of the Optoelectronic Properties of Membranes via Insertion of Amphiphilic Phenylenevinylene Oligoelectrolytes. *J. Am. Chem. Soc.* **132,** 10042–10052 (2010).
2. Han Young Woo *et al. Solvent Effects on the Two-Photon Absorption of Distyrylbenzene Chromophores*. *Journal of the American Chemical Society* **127,** 14721–14729 (American Chemical Society, 2005).
3. Mokany, E., Bone, S. M., Young, P. E., Doan, T. B. & Todd, A. V. MNAzymes, a Versatile New Class of Nucleic Acid Enzymes That Can Function as Biosensors and Molecular Switches. *J. Am. Chem. Soc.* **132,** 1051–1059 (2010).

APPENDIX IV – SUPPORTING INFORMATION FOR CHAPTER 7

Physical Isolation and Protection of Molecular Computing Elements in Giant Unilamellar Vesicles

Aurora Fabry-Wood,[†] Madalyn Elise Fetrow,[†] Ayomide Oloyede,[†] Kyung-Ae Yang,[#] Milan Stojanovic,[#,⊥] Darko Stefanovic,[†,§] Steven W. Graves,[†,‡,*] Nick J. Carroll,[†,‡,*] Matthew R. Lakin[§,†,*]

[†]Center for Biomedical Engineering, [‡]Department of Chemical and Biological Engineering, and [§]Department of Computer Science, University of New Mexico, Albuquerque, New Mexico 87131, United States

[#]Division of Experimental Therapeutics, Department of Medicine, [⊥]Departments of Biomedical Engineering and Systems Biology, Columbia University Medical Center, New York, New York 10032, United States

Supporting Information

Table A-IV.1 - Strand Sequences

Name	Sequence
DOGS.2 aptamer	/56-FAM/CTCTCGGGACGACCCGGATTTTCCGAGTGGAACTAGCTGTGGCGGTCGTCCC
DOGS.2 quencher	GTCGTCCCGAGAG/3IABkFQ/
CSS.1 aptamer	CTTCAACCGCCCGCATGTTCCATGGATAGTCTTGACTAGGTTGAAGTTGGA/3ATTO647NN/
CSS.1 quencher	/5IAbRQ/TCCAACTTCAACC
DOGS.2 aptamer complement (A*)	GGGACGACCGCCACAGCTAGTTCCACTCGGAAAATCCGGGTCGTCCCGAGAG

A-IV.1 Supporting Figures

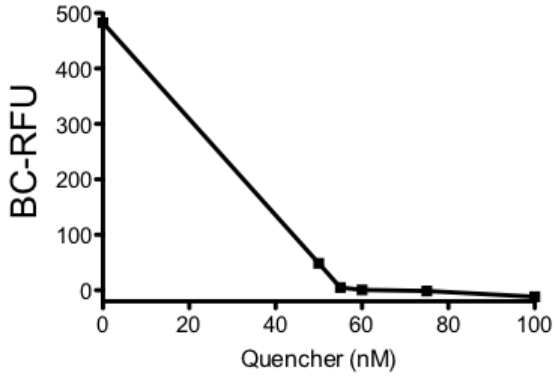

Figure A-IV.1 – Optimizing the Amount of Excess Quencher. To determine the amount of excess quencher required for efficient quenching and strong ligand-dependent activation. The DOGS.2 quencher at 0, 50, 55, 60, 75 and 100 nM was added to DOGS.2 aptamer [50 nM], in 10 wt% PVA, in PBS pH 7.4. At a 1:1 ration (50 nM aptamer:50 nM quencher) nearly complete quenching was achieved. With 10 mol% excess quencher (50 nm aptamer:55 nM quencher) full quenching was achieved, with minimal improvement at higher quencher concentrations. The FAM channel (488/520 nm) was baseline corrected to remove autofluorescence of the PVA solution.

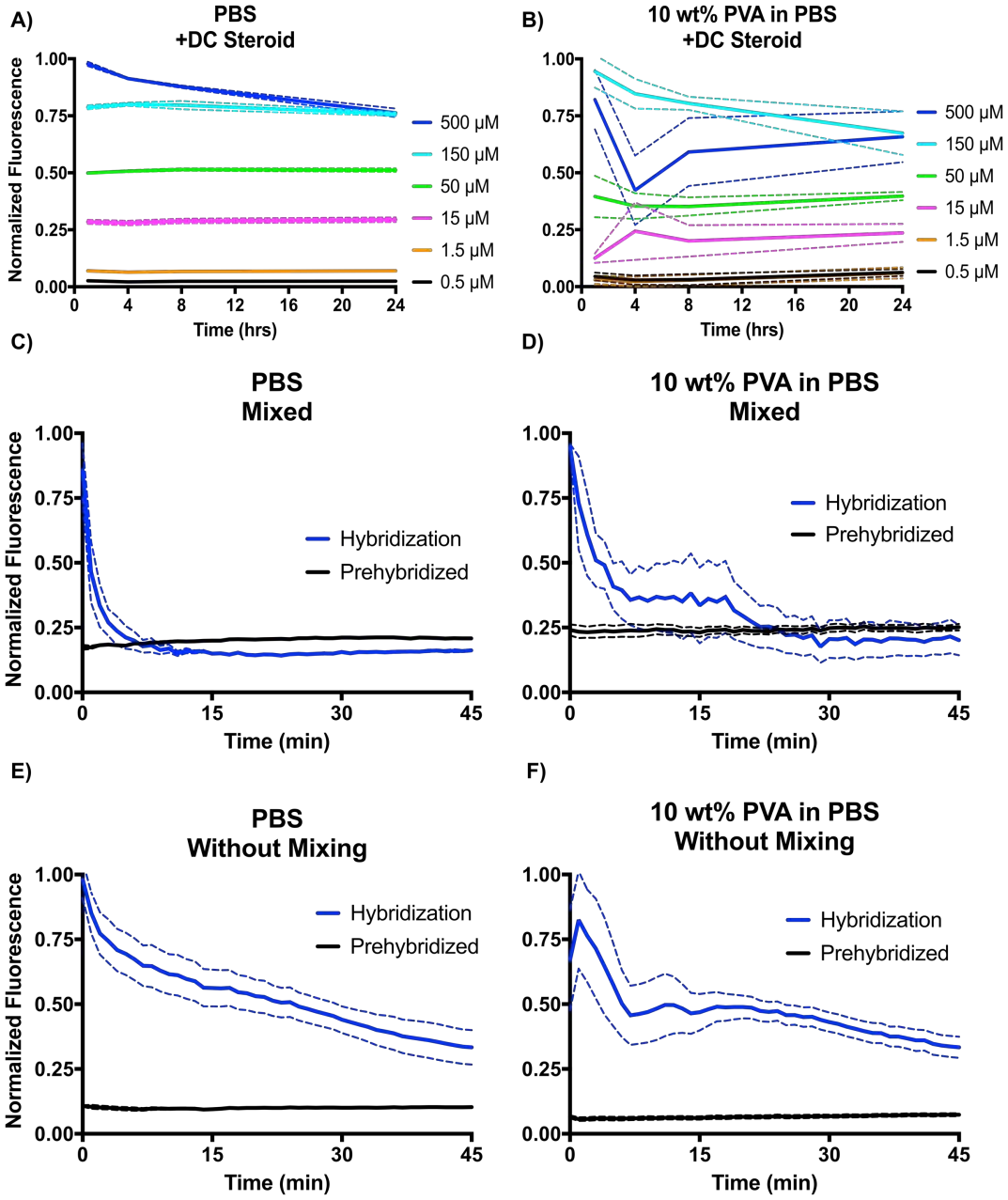

Figure A-IV.2 - The Need for Prehybridization. A) Various concentration of the DC steroid added to the DOGS.2 aptamer/quencher in PBS over time, showing minimal variation across replicates and time. **B)** The same as panel A in the presence of 10 wt% PVA, showing significantly more variation across both replicates and time. **C)** Prehybridized vs Hybridization over time in PBS of the DOGS.2 aptamer and quencher. **D)** The same as panel C in the presence of 10 wt% PVA, showing more variation across replicates and a decreased rate of hybridization. **E)** The same as panel C without mixing, showing a decreased rate of hybridization. **F)** The same as panel E in the presence of 10 wt% PVA, showing increased variation across replicates and a decreased rate of hybridization. Error bars for all plots represent SEM for 3 replicates.

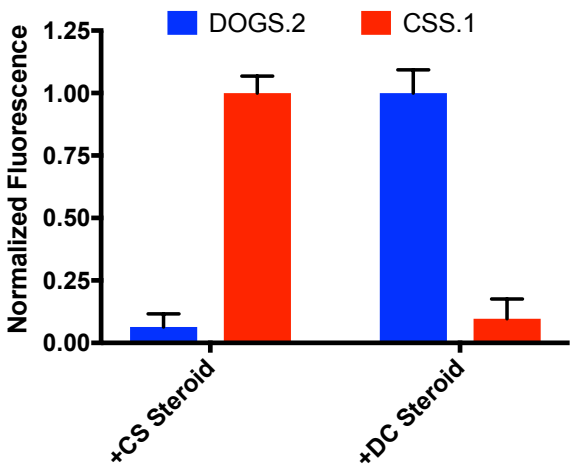

Figure A-IV.3 - Aptamer Responses in Solution. A) DOGS.2 and CSS.1 aptamer [50 nM]/quencher [55 nM] in the in the presence of the CS steroid [150 μM], and in the presence of the DC steroid [150 μM]. The fluorescence (488/520 nm) and (647/662 nm) was normalized and error bars represent 95% confidence interval (95% CI) for five replicates.

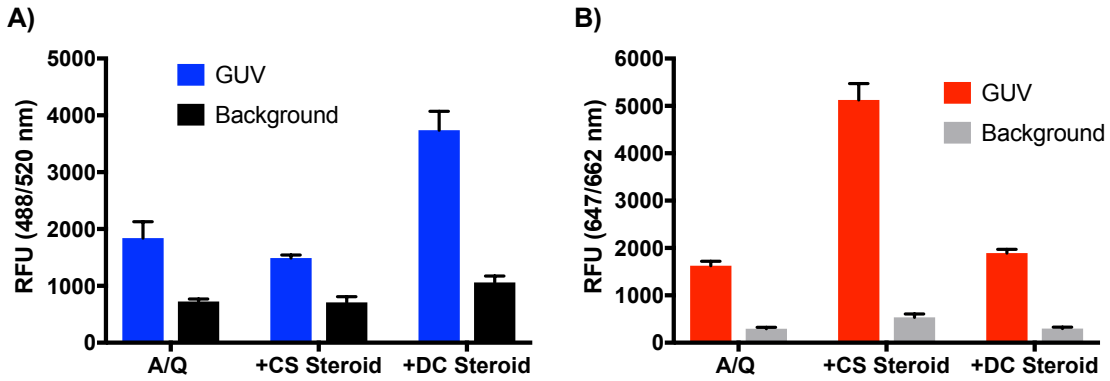

Figure A-IV.4 - Raw Data for Figure 7.4. Five replicates (error bars are 95% CI) for the DOGS.2 and CSS.1 A/Q pairs. Both steroids were added at 500 μM. The FAM channel (488/520 nm) and ATTO647 channel (647/662 nm) values were calculated using an ROI that was identical for all replicates. The GUV ROI was a circular region that comprised the majority of all GUVs, while the Background ROI was a circular region taken outside the GUV.

APPENDIX V – LATERAL DIFFUSION OF DNAZYMES USING CHOLESTEROL FOR INCORPORATION INTO THE LIPID BILAYER

A-V.1 Cholesterol Incorporation was Stable and Quantifiable

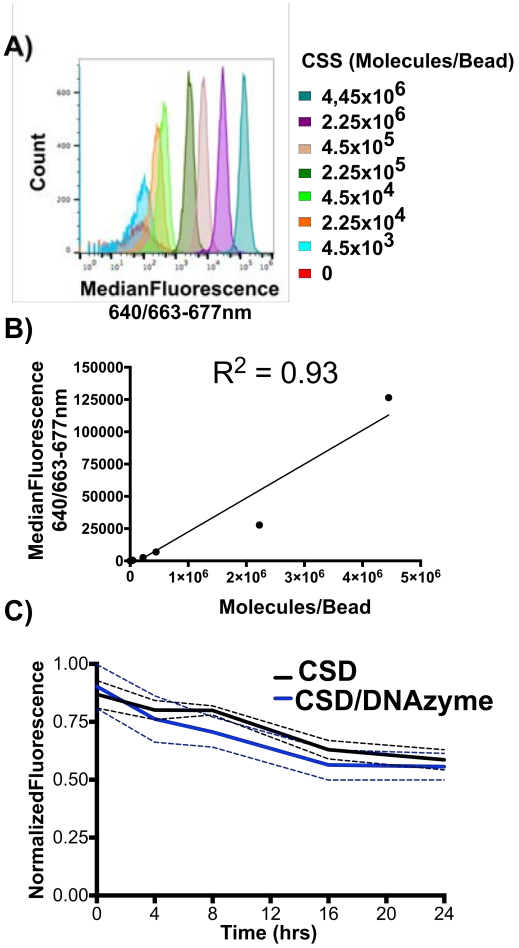

Figure A-V.1 – DNA-Cholesterol in µSLBs. A) ATTO647 tagged CSS incorporated at increasing concentrations (molecules/bead). **B)** Linear regression of the median fluorescent values from A. **C)** Twenty-four hour stability test with CSD and CSD hybridized to U2_Enzyme_CSD (CSD/DNAzyme).

As a continuation of Chapter 4 we moved away from maleimide-thiol linkages, as the conjugation efficiency was low and quantifying the number of strands per bead was desirable. Oligonucleotides modified with cholesterol are commercially available and cholesterol readily inserts into lipid bilayers, so we used the same µSLB system and left out the MPB PE. From here, cholesterol tagged versions of TSD (CSD) and TSS (CSS) could easily be incorporated into the µSLBs (**Figure A-V.1A**, and a linear regression of this data **Figure A-V.1B**). These systems were stable for up to 24 hours (**Figure A-V.2C**), which was an improvement over the previous system. Additionally, the number of strands could be quantified using Bang Laboratory calibration beads. As such, we were able to incorporate a specific

number of different strands into a μSLB and this system was stable for periods of time that were relevant for DNAzyme reactions.

A-V.2 The DNAzyme did not Release the Substrate Post Cleavage

The preferable behavior for the DNAzyme reactions presented in Chapter 4 would be cleavage of all substrate molecules on the μSLB. Hypothetically, once the first substrate was cleaved the DNAzyme and the cleaved substrate would dissociate, allowing the DNAzyme to diffuse away and hybridize to another substrate (**Figure A-V.2A**). However, we observed a much lower cleavage rate, an explanation for which is illustrated in **Figure A-V.2B**. Here, the DNAzyme remains bound to the lower portion, proximal to the μSLB, of the substrate molecule. This could due to a stabilizing effect that arises due to both strands being restricted to the μSLB.

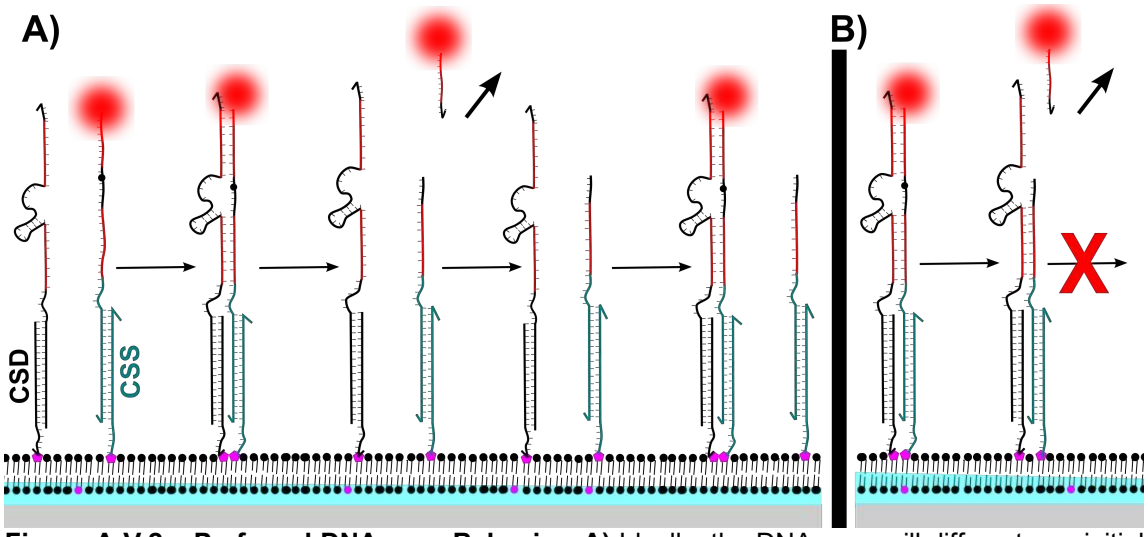

Figure A-V.2 – Preferred DNAzyme Behavior. A) Ideally, the DNAzyme will diffuse to an initial substrate molecule, which will be cleaved and the binding arms will dissociate. The upper binding arm, with the fluorophore, will move into solution and the lower binding arm will be released allowing the DNAzyme to diffuse to the next uncleaved substrate molecule. **B)** However, if restriction of strands to the bilayer confers stability, the lower binding arm will never dissociate from the DNAzyme. Thereby, preventing cleavage of additional substrate molecules.

A-V.3 Destabilizing the Lower Substrate Binding Arm

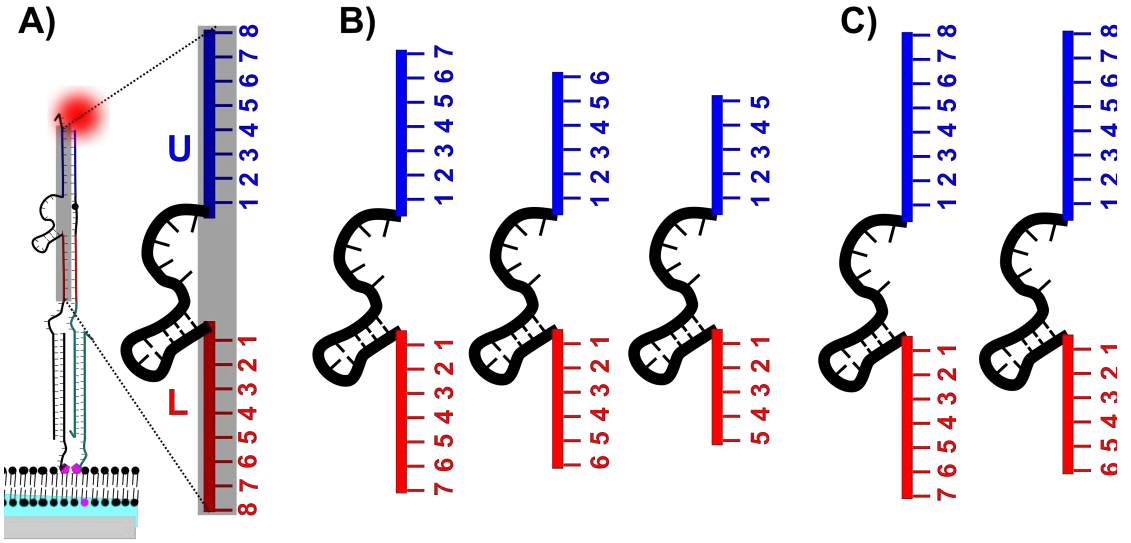

Figure A-V.3 – DNAzyme Redesign to Achieve Preferred Behavior. A) The original U2_Enzyme_TSD contained 8 base pairs on both the upper (U) and lower (L) binding arms. **B).** To destabilize the post-cleavage interaction, we reduced the number of base pairs on each binding arm to 7 (U2_7_Enzyme_CSD), 6 (U2_6_Enzyme_CSD) and 5 (U2_5_Enzyme_CSD). **C)** We then held the upper binding arm constant and decreased only the lower binding are to 7 (U2_78_Enzyme_CSD) and 6 (U2_68_Enzyme_CSD).

In order to achieve the preferable DNAzyme behavior, we redesign the DNAzyme sequence to destabilize the post-cleavage interaction (**Figure A-V.3**). The original DNAzyme contain 8 base pairs on both the upper and lower binding arms (**Figure A-V.3A**). To destabilize the interaction 3 version of the DNAzyme were designed, each with one less base pair on both the upper and lower binding arms (**Figure A-V.3B**). When the first set of strands were tested in solution we saw a decreased function (**Figure A-V.4**) as the number of base pairs in the binding arms decreased. For the second round of DNAzyme designs we did not order a version with 5 base pairs on the lower binding arm, as 5 base pairs on both arms resulted in minimal DNAzyme function. We then tested U2_7_Enzyme_CSD and U2_6_Enzyme_CSD on bead, but did not observe the desired dissociation, which would have resulted in increased DNAzyme turnover and thus a stronger decrease

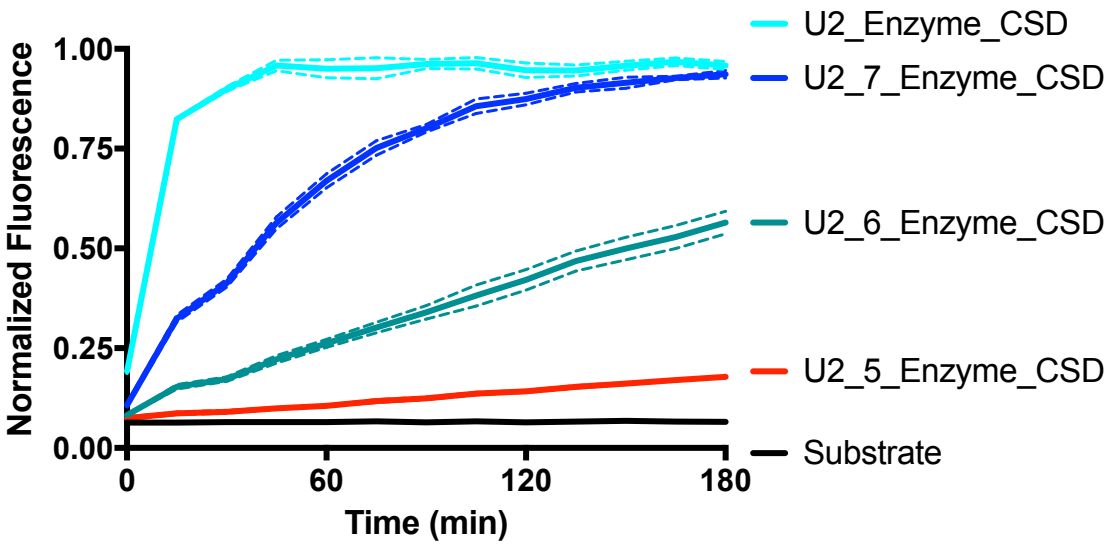

Figure A-V.4 – Solution Phase Reactions with Redesigned DNAzymes. Solution phase experiment in E6-276-1000 (50 mM HEPES, 276 mM NaCl, 1000 μM $ZnAc_2$). With the various DNAzymes at 8 nM, and the solution phase U2 substrate is at 40 nM. The normalized fluorescence is tracking the substrate tagged with FAM (492/518 nM).

in bead fluorescence. Next, a set of DNAzymes where the number of base pairs on the upper binding arm were held constant, while the number of base pairs on the lower binding were decreased by one, was designed (**Figure A-V.3C**). These strands have not yet been tested, future work should investigate their behavior in solution and then on bead surfaces. Sequences for all version are presented in Table A-V.1.

Table A-V.1 – Strand Sequences

Name	Sequence
CSD	/56-FAM/CAAACTTCACATCTACACTCAAAAA/3CholTE/
CSS	/5Alex647N/AGAATAGAACAAGACAGAAACAAAAA/3CholTEG/
U2 Substrate	/56-FAM/TCTTAGTTrAGGATAGTTCAT/36-TAMSp/
U2_Enzyme_CSD	5'-GAGTGTAGATGTGAAGTTTGAAAAAGAAC TATCTCCGAGCCGGTCGAAAACTAAGA-3'
U2_7_Enzyme_CSD	5'-GAGTGTAGATGTGAAGTTTGAAAAAAACTA TCTCCGAGCCGGTCGAAAACTAAG-3'
U2_6_Enzyme_CSD	5'-GAGTGTAGATGTGAAGTTTGAAAAAACTAT CTCCGAGCCGGTCGAAAACTAA-3'
U2_5_Enzyme_CSD	5'-GAGTGTAGATGTGAAGTTTGAAAAACTATCT CCGAGCCGGTCGAAAACTA-3'
U2_78_Enzyme_CSD	5'-GAGTGTAGATGTGAAGTTTGAAAAAAACTAT CTCCGAGCCGGTCGAAAACTAAGA-3'
U2_68_Enzyme_CSD	5'-GAGTGTAGATGTGAAGTTTGAAAAAACTATC TCCGAGCCGGTCGAAAACTAAGA-3'